

POLITECNICO DI TORINO



Corso di Laurea Magistrale in Ingegneria Civile

Tesi di Laurea Magistrale

*Masonry arches in fire conditions*

Relatore:

**Prof. Ing. A. P. Fantilli**

Candidato:

**Elisa Canevari**

Anno Accademico 2019/20



# *Table of Contents*

---

<i>Abstract</i> .....	7
<i>Chapter 1</i> .....	10
<i>Introduction</i> .....	10
<i>Chapter 2</i> .....	14
<i>Masonry arches modeling in fire conditions</i> .....	14
2.1 Codes prescriptions .....	14
2.2 Heat transfer: hypothesis and effects .....	23
2.3 Constitutive laws and failure mechanism .....	31
<i>Chapter 3</i> .....	40
<i>Experimental project</i> .....	40
3.1 Project description .....	40
3.2 Compressive tests .....	51
<i>Chapter 4</i> .....	58
<i>Tests procedure and results</i> .....	58
4.1 Experimental and design temperature curves .....	58
4.2 Tests 1 .....	61
4.2.1 Test 1A: temperatures .....	61
4.2.2 Test 1A: displacements .....	66

<i>4.2.3 Test 1B: temperatures</i> .....	71
<i>4.2.4 Test 1B: displacements</i> .....	73
<i>4.3 Test 2</i> .....	75
<i>4.3.1 Test 2: temperatures</i> .....	75
<i>4.3.2 Test 2: displacements</i> .....	77
<i>4.4 Results comparison</i> .....	80
<b><i>Chapter 5</i></b> .....	<b>82</b>
<b><i>Model validation</i></b> .....	<b>82</b>
<i>5.1 How the model works</i> .....	82
<i>5.2 Validation procedure</i> .....	89
<i>5.3 Experimental and numerical comparison</i> .....	104
<b><i>Chapter 6</i></b> .....	<b>107</b>
<b><i>Conclusions</i></b> .....	<b>107</b>
<b><i>References</i></b> .....	<b>110</b>
<b><i>List of Figures</i></b> .....	<b>112</b>
<b><i>List of Tables</i></b> .....	<b>117</b>
<b><i>Attachments</i></b> .....	<b>120</b>
<b><i>Ringraziamenti</i></b> .....	<b>129</b>





## *Abstract*

Main goal of my experimental thesis is to validate and improve a numerical model, previously developed, which describes the mechanical behavior of curvilinear structures, such as arches and vaults, in fire conditions. The aim is of paramount importance considering that current Italian and European Standards use tabular and graphical methods, related to vertical elements as walls or columns, which are actually inconsistent with arches and vaults behavior. Rules prescribe these methods because of lack of experimentation on curvilinear elements.

Results analysis of two experimental tests, performed at Vigili del Fuoco Laboratory in Roma Capannelle, is the starting point of my work. Two masonry arches in different loading conditions are considered, in order to easily describe many real behaviors. The heart of the paper is focused on model responses: the goal is to understand strengths and weaknesses of the numerical procedure. Considering results obtained, some improvements of the model are presented in order to fill current gaps.

## *Abstract*

La tesi sperimentale che presento si pone l'obiettivo di validare e migliorare il modello numerico, elaborato in precedenza, che descrive il comportamento meccanico di strutture ad asse curvilineo, come archi e volte, sottoposte ad incendio. L'obiettivo assume primaria importanza se si considera che le Normative vigenti italiana ed europea, prescrivono metodi tabellari o grafici, relativi a elementi verticali come muri o pilastri, che spesso si rivelano inconsistenti con il comportamento di archi e volte. Le Normative infatti non contemplano metodi di calcolo che derivano da prove sperimentali appositamente eseguite su strutture curvilinee.

L'analisi dei risultati di due prove sperimentali, effettuate presso il Laboratorio dei Vigili del Fuoco a Roma Capannelle, costituisce la base da cui parte questo lavoro. Le prove sono svolte su due archi in muratura sottoposti a diverse condizioni di carico. Nella parte centrale della tesi i dati sono sfruttati per capire punti di forza e di debolezza del modello numerico. Alla luce dei risultati ottenuti, sono proposti miglioramenti ed estensioni, al fine di avvicinare il modello alla realtà.



# *Chapter 1*

## *Introduction*

---

Motivations, aims and main steps of the analysis process are presented.

---

Goal of the thesis is to describe the behavior of horizontal structural elements with curvilinear longitudinal axis, such as masonry arches and vaults, in fire conditions. The study will be carried out using a numerical model, calibrated through observation of experimental tests performed on real structures built at Vigili del Fuoco laboratory in Roma Capannelle. The final result will be presented in terms of temperatures, stresses, strains, displacements, coactions and bearing capacity in function of time.

Although masonry technique is not the most used nowadays, it is widespread in existing structures especially in Italian country, where a great number of masonry buildings belongs to the artistic heritage. The important presence of historical structures in our territory makes the problem close to us.

The whole issue is placed in current Codes prescriptions. Are considered both the Italian Code *Normativa Tecnica per le Costruzioni*, NTC 2018 and the European one, *Eurocode 6* regarding masonry structures. This paper wants to fill the gap existing in these Codes: they do not say how to deal with the problem of fire in curvilinear structural elements. In the

first part Code prescriptions are presented, the most relevant is the annex D of *Eurocode 6*. It suggests a method to compute thermal variation in vertical structural elements and a model to forecast mechanical behavior in time. This annex is the starting point for the implementation of the numerical code, which has been previously developed in “Archi in muratura soggetti ad elevati gradienti termici” master thesis by Nicholas Sergio Burello. Therefore heat transfer modes are described and main hypothesis assumed in the problem are fixed. Most important aspects studied are how temperature can be computed within the arch and how the loss of strength due to fire can be considered in the numerical procedure, taking into account different constitutive laws. Then collapse mechanism associated to masonry arches in fire conditions is described.

In chapter 3 the experimental part begins: an accurate description of tests carried out in laboratory is introduced, focusing on loading conditions, mechanical characteristics of the material and devices positioning. Two configurations are tested: first one is the most critical since the minimum load is applied on the arch, therefore the minimum stabilizing effect will be obtained; second one is performed using loads related to the normal usage of the structure in order to understand how much the increased weight influences arch behavior in fire. Mechanical properties of the material are computed through three compressive tests performed on masonry samples, results are expressed in terms of compressive strength and elastic modulus. During the arches construction, devices are located in strategic points within cross section and along longitudinal axis with the purpose to properly collect temperatures and displacements in time.

Results obtained in laboratory are pointed out in graphs and tables, hence some observations are provided. Temperatures applied during tests are compared to design curve

prescribed by Codes in order to verify the accuracy of the experimental procedure and devices records are considered in function of the expected results, qualitatively known by the literature, hence discarded when unreliable.

On the other hand numerical results are computed by running FireArM model, starting from some inputs, as problem geometry, experimental temperature curve in time, loading conditions, constitutive law, initial mechanical strength and thermal parameters of the material.

Comparison between experimental and numerical results allows model validation. In this part a great role is played by the choice of some inputs: constitutive law, both in terms of stress-strain relationship and in terms of thermal strains in time, tensile strength and Young Modulus of the masonry. In fact these parameters are prone to variability related to manufacturing process and working conditions of units. The aim of this part is to find proper law and parameters which allow to describe the real behavior of the structure.

Validation results are evaluated considering the proximity of numerical results to experimental ones and the ability of the model to reach the convergence in function of inputs and load increments set. This is the case of the first test, which cannot be represented by the model because of the peculiar behavior shown by the arch under minimum loads. The change of compatibility linked to the opening of the fracture at the crown prevents the model to reach the convergence for high load increments, hence many numerical results are not available. In order to overcome this limit, results of the second test are useful to carry out the validation.

At the end of the validation process some improvements are suggested where great differences between experimental and numerical results are shown and some extensions of

## Chapter 1 - Introduction

the model are proposed in order to represent a greater number of cases. Hence significant conclusions are drawn.

## *Chapter 2*

# *Masonry arches modeling in fire conditions*

---

Main assumptions made in the numerical procedure are presented, taking into account current Codes prescriptions, heat transfer modes, arch mechanical behavior and failure criterion in fire conditions.

---

## *2.1 Codes prescriptions*

Third chapter, section 6 of NTC 2018 is dedicated to the evaluations of requirements which should be satisfied by generic structures during some exceptional events such as fire, explosion and impact. Now only fire is considered. Requirements are function of the intended use of the building, stated in “performance levels” explained in the table 3.5.IV of the Code (Table 1). They are evaluated in terms of load bearing function, limiting fire spread and separating function (REI).

Classification is based on minutes (15, 20, 30, 45, 60, 90, 120, 180, 240, 360) during which load bearing capacity, thermal insulation and integrity properties must be guaranteed.

Minutes are referred to curves of conventional fire described by fire nominal curves, function of the material which is burning (Figure 1).

*Tab. 3.5.IV - Livelli di prestazione in caso di incendi*

Livello I	Nessun requisito specifico di resistenza al fuoco dove le conseguenze del crollo delle strutture siano accettabili o dove il rischio di incendio sia trascurabile;
Livello II	Mantenimento dei requisiti di resistenza al fuoco delle strutture per un periodo sufficiente a garantire l'evacuazione degli occupanti in luogo sicuro all'esterno della costruzione;
Livello III	Mantenimento dei requisiti di resistenza al fuoco delle strutture per un periodo congruo con la gestione dell'emergenza;
Livello IV	Requisiti di resistenza al fuoco delle strutture per garantire, dopo la fine dell'incendio, un limitato danneggiamento delle strutture stesse;
Livello V	Requisiti di resistenza al fuoco delle strutture per garantire, dopo la fine dell'incendio, il mantenimento della totale funzionalità delle strutture stesse.

Table 1 - Performance levels of buildings in fire.

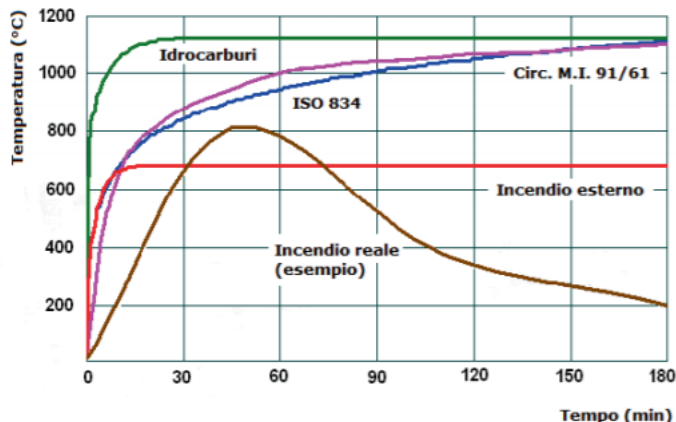


Figure 1 - Nominal and natural (real) fire curves.

The procedure of evaluation of fire resistance can be summed up as follows:

- Selection of the appropriate fire for the building design
- Description of the temperature profile in structural elements during fire
- Mechanical behavior analysis of the building in fire
- Safety assessments.

*Selection of the appropriate fire for the building design* – The Code suggests graphs where temperature in function of time is described for different burning materials such as

hydrocarbons and cellulosic origin compounds or fires grown outside the structure. Among this curves the ISO 834, which is the standard curve, is generally adopted in structural assessments.

*Temperature profile in structural elements during fire* – The problem of heat transmission is solved in terms of thermal radiation and gas convection, considering protective materials, if present.

*Mechanical behavior analysis* – The loss of strength in damaged elements due to temperature increasing is studied for the time considered in the analysis of temperature changing. Moreover also permanent and variable loads must be accounted through the formula for exceptional loads combination. Other exceptional loads such as wind and seismic actions are not considered as the combination coefficient is null. Since in statically indeterminate frames prevented strains give rise to coactions, these should be considered in the analysis. However they can be ignored in few cases: when they are favorable or negligible, when they are already considered in the simplified model used or when fire resistance classes and nominal fire curves are used to assess the structure.

*Safety assessments* – Mechanical strength of the structure must be adequate during the entire period guaranteed by the fire resistance or, if the fire curve is considered, for the time the fire lasts, including also the cooling phase.

In section 4.5.11 the Italian Rule addresses to Eurocode 6, the European Code which deals with masonry structures. Part 1-2 applies to masonry structures which, “for reasons of general fire safety, are required to fulfill certain functions when exposed to fire, in terms of avoiding premature collapse of the structure (load bearing function) and limiting fire spread (flames, hot gases, excessive heat) beyond designated areas (separating function)”.

It suggests three different methods to model and solve the problem of masonry structures in fire, Figure 2 is a summary of design procedures. UNI EN 1996-1-2:2005 is considered.

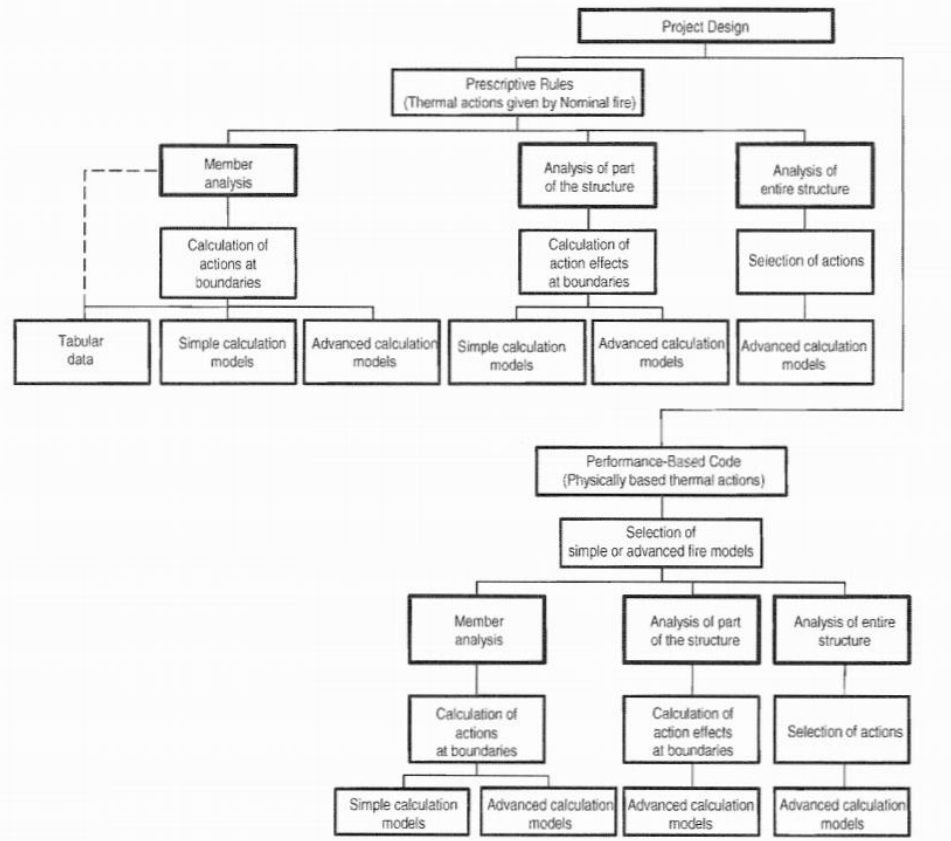


Figure 2 - Figure 0.1: Design procedures. (Source Eurocode 6, part 1-2 pag 8).

The first method is introduced in *EC 6 part 1-2, Annex B* – It is called “Tabulated fire resistance of masonry walls” and provides tabular data which allows to assess the fire resistance in function of materials, wall type and loading conditions. Different tables are presented for different types of bricks, cement mortar in function of thickness, strength, density and non-load bearing or load bearing capacity walls. By knowing the period of fire resistance, we can obtain the minimum thickness or the length which ensures the performance required. Only partition walls are considered (Table 2), no prescriptions regarding arches or vaults are present.

row number	material properties: unit strength $f_b$ [N/mm <sup>2</sup> ] gross dry density $\rho$ [kg/m <sup>3</sup> ] combined thickness $ct$ % of wall thickness	Minimum wall thickness (mm) $t_f$ for fire resistance classification REI for time (minutes)						
		$t_{f,d}$						
		30	45	60	90	120	180	240
IS	<b>Group IS units</b>							
IS.I	5 ≤ $f_b$ ≤ 75 general purpose mortar 5 ≤ $f_b$ ≤ 50 thin layer mortar 1 000 ≤ $\rho$ ≤ 2 400							
IS.I.1	$\alpha \leq 1,0$	90 (70/90)	90 (70/90)	90 (70/90)	100 (70/90)	100/140 (90/140)	170/190 (110/140)	170/190 (170/190)
IS.I.2								
IS.I.3	$\alpha \leq 0,6$	90 (70/90)	90 (70/90)	90 (70/90)	100 (70/90)	100/140 (100/140)	170 (110/140)	170 (140/170)
IS.I.4								

Table 2 - Part of Table N.B.1.2 Minimum thickness of loadbearing partition walls (criteria REI) for fire resistance classification. (Source Eurocode 6, part 1-2, annex B, p32).

In *EC 6 part 1-2, Annex C* – It is the “simplified calculation model” which is based on the following procedure. First the temperature profile inside the element must be determined. It is function of the material type, in the paper only clay units are considered (Figure 3). Then two temperature values are computed: one value refers to the complete loss of bearing capacity ( $\theta_2$ ), the other to the beginning of this process ( $\theta_1$ ). Therefore the element is divided in three areas: a inner part where the temperature is under the second limit  $\theta_1$ , the bearing capacity is unchanged; the middle part where temperature is higher than  $\theta_1$  but lower than  $\theta_2$ , the bearing capacity is gradually decreasing as temperature increases; the outer part which is at a temperature higher than the first limit  $\theta_2$ , becomes ineffective (Figure 4, Figure 5). Temperature limits which divide the areas are function of the material type. For clay units  $\theta_1 = 100^\circ\text{C}$ ,  $\theta_2 = 600^\circ\text{C}$  (Table 3). In order to assess the structure at ULS, the following formula should be verified:

$$N_{Ed} \leq N_{Rd,fi\theta_2}$$

where  $N_{Ed}$  is the design value of vertical load,  $N_{Rd,fi\theta_2}$  is the design value of the resistance in fire, it depends on resistant cross section, masonry design strength in function of temperature.

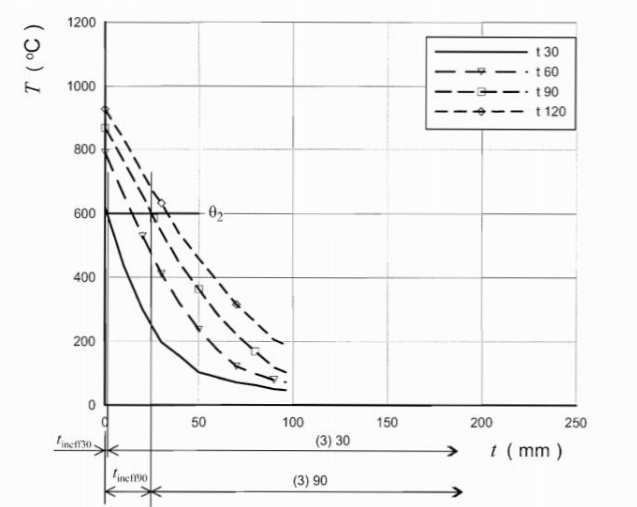


Figure C.3(a): Clay masonry, gross  $\overline{\text{AC}_1}$  dry  $\overline{\text{AC}_1}$  density 1 000 – 2000 kg/m<sup>3</sup>

Figure 3 - Temperature in function of time, thickness and units type. (Source Eurocode 6, part 1-2, p68).

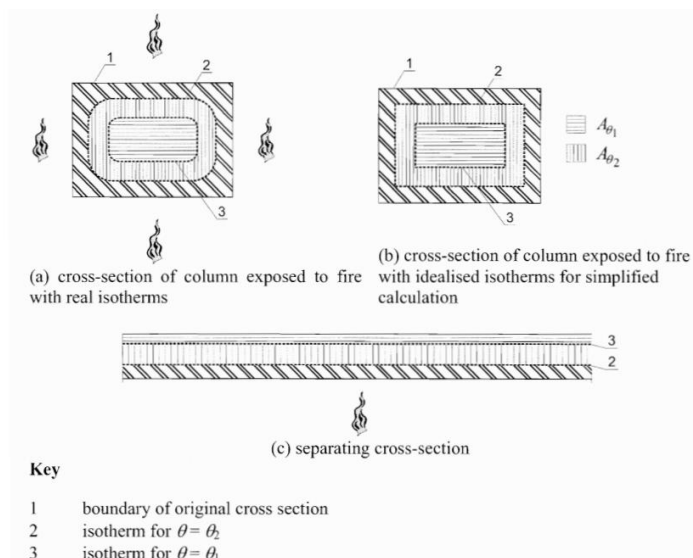


Figure 4 - Areas of masonry element divided in function of temperature profile. (Source Eurocode 6, part 1-2, annex C p66).

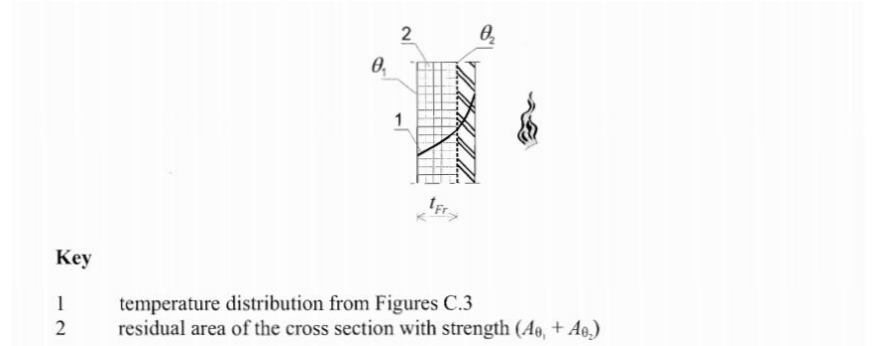


Figure 5 - Temperature distribution in different areas. (Source Eurocode 6, part 1-2, annex C, p67).

Masonry units and mortar (surface unprotected) according to 1.1 (2)	Values of constant $c$	Temperature °C	
		$\theta_2$	$\theta_1$
Clay units with general purpose mortar	$c_{cl}$	600	100
Calcium silicate units with thin layer mortar	$c_{cs}$	500	100
Lightweight aggregate units (pumice) with general purpose mortar	$c_{la}$	400	100
Dense aggregate units with general purpose mortar	$c_{da}$	500	100
Autoclaved aerated units with thin layer mortar	$c_{aac}$	700	200

Table 3 - Values of temperatures linked to a change of performance under fire for clay masonry blocks and constant  $c$  obtained from stress strain tests at high temperatures. (Source Eurocode 6, part 1-2, p67).

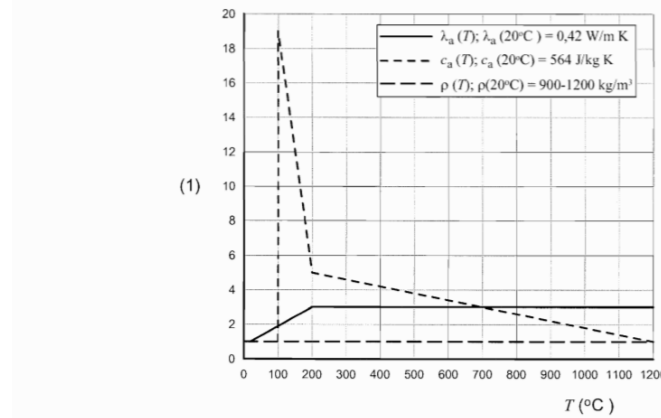
Moreover it should be considered that due to the random distribution of temperature, the bearing cross section is no more symmetric and some eccentricity may arise. This value must be limited and checked using another formula suggested by the Code which is function of temperature, height of the wall and coefficient of thermal expansion. Once again prescriptions are referred to walls and columns only.

The last method described in *EC 6 part 1-2, Annex D* – it is the “Advanced calculation method”. Therefore a more strict evaluation of development in time of temperature, of mechanical behavior of the generic structure is expected. Advance calculation methods can be used in association with any heating curve. This is the method following chapters refer to. Main ingredients are:

- *Temperature distribution in the element:* map  $T(x, t)$  should be built.
- *Mechanical behavior modeling:* study how properties change in time in function of temperatures. Most relevant are: thermal parameters, thermal stresses and strains, constitutive laws.

Thermal parameters such as thermal conductivity ( $\lambda_a$ ), gross dry density ( $\rho$ ) and specific heat capacity ( $c_a$ ) are to be evaluated in order to obtain the temperature distribution, as they govern heat conduction according to Fourier second order differential equation. Rule suggests some graphs describing how these parameters change in function of the temperature. Following graphs are normalized with respect to the value assumed by the parameter at room temperature (20°C).

$$f_{(1)}(T = x [^{\circ}\text{C}]) = \frac{f(T = x [^{\circ}\text{C}])}{f(20^{\circ}\text{C})}$$



**[AC]** Figure D.1(a): calculation values of temperature-dependant material properties of clay units with a density range of 900 – 1 200 kg/m<sup>3</sup> **[AC]**

Figure 6 - Normalized parameters on respective room temperature values for temperatures from 0°C to 1200°C. (Source Eurocode 6, part 1-2, p73).

Thermal map within the masonry element can be built on the basis of these parameters therefore it can be linked to thermal strains  $\varepsilon_T$ , and through constitutive laws to  $\sigma_T$  (Figure 7).

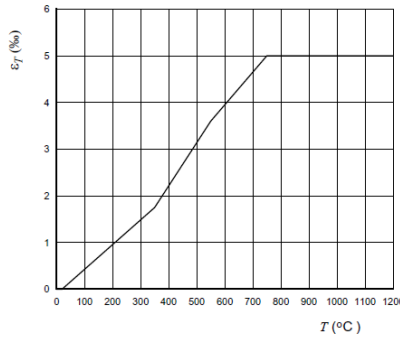


Figure D.2(a): Calculation values of thermal strain  $\varepsilon_T$  of clay units (group 1) with unit strength  $12 - 20 \text{ N/mm}^2$  and units with a density range  $900 - 1200 \text{ kg/m}^3$

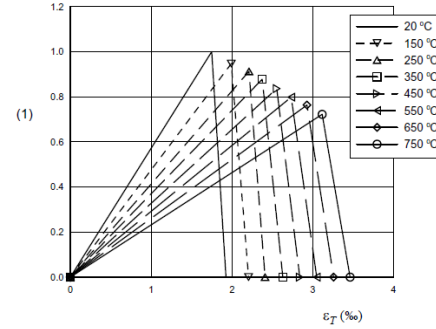


Figure D.2(b): Calculation values of temperature-dependant stress-strain diagrams of clay units (group 1) with unit strength  $12 - 20 \text{ N/mm}^2$  and with a density range  $900 - 1200 \text{ kg/m}^3$

Figure 7 - Thermal strains (on the left) and stress-strain constitutive laws (on the right) in function of temperature for clay units with a normalized compressive strength range  $12-20 \text{ N/mm}^2$ , gross dry density  $900-1200 \text{ kg/m}^3$  (Source Eurocode 6, part 1-2, p76).

Considering clay units, thermal strains are almost linear till  $750^\circ\text{C}$  and remain constant as temperature increases. Constitutive laws are function of temperature and denotes a brittle behavior. As temperature increases elastic modulus describing the first branch ( $E_{\text{pre-pick}}$ ) decreases and maximum strain  $\varepsilon_{\text{max}}$  increases.

In conclusion annex D suggests more detailed procedures to face fire problem. However nothing addresses to curvilinear structures. Therefore advanced calculation method is used to fix hypothesis and laws of the numerical model, since no prescriptions are currently stated for curvilinear elements. Anyway all hypothesis are validated through comparison with experimental results.

## 2.2 Heat transfer: hypothesis and effects

Heat transfer concerns generation and exchange of thermal energy between physical systems. It is classified into various mechanisms, such as thermal conduction, convection, radiation and transfer of energy by phase changes. The latter is not considered in this paper. While these mechanisms have distinct characteristics, they often occur simultaneously in the same system.

- Heat conduction is the direct exchange of energy through the boundary between two systems. When an object is at a different temperature from another body or its surroundings, heat flows, so that the body and the surroundings reach the same temperature, therefore they are in thermal equilibrium.
- Heat convection happens between an object and its environment, due to motion of fluids, as gas or liquid. The flow may be forced by external processes, or sometimes (in gravitational fields) by buoyancy forces caused when thermal energy expands the fluid (for example in a fire plume), thus influencing its own transfer. The latter process is often called "natural convection".
- Thermal radiation occurs through a vacuum or any transparent medium (solid, fluid or gas). It is the transfer of energy by means of photons in electromagnetic waves.

All spontaneous heat transfer always occurs from a region of high temperature to another region of lower temperature, as described in the second law of thermodynamics.

During fire all these modes are involved. Thermal convection and radiation on the inner and the exterior surfaces, thermal conduction within the medium, thermal radiation in medium voids.

As soon as fire starts, four are the main stages of its development suggested by most standards (Figure 8).

The first stage begins when heat, oxygen and a fuel source combine and have a chemical reaction resulting in fire. This is also known as “ignition” or “incipient” and is usually represented by a very small fire which often goes out on its own, before the following stages are reached. The second stage, called growth stage, is where the structures fire load and oxygen are used as fuel for the fire. There are numerous factors affecting the growth stage including where the fire started, what combustibles are near it, ceiling height and the potential for “thermal layering”. It is during this shortest of the 4 stages when “flashover” can occur; when the growth stage has reached its maximum and all combustible materials have been ignited, a fire is considered fully developed, the third stage begins. This is the hottest phase of a fire and the most dangerous (Figure 9). The last stage of a fire, usually the longest, called the decay stage is characterized by a significant decrease in oxygen or fuel, putting an end to the fire. During this stage the existence of non-flaming combustibles can potentially start a new fire if not fully extinguished.

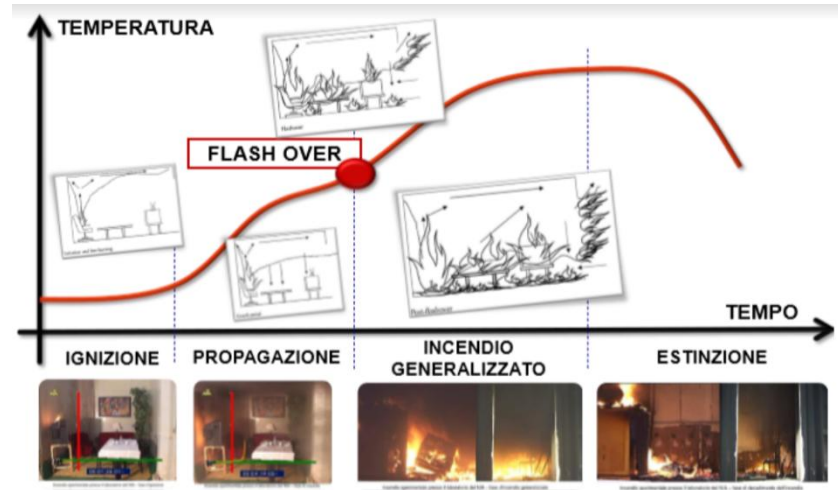


Figure 8 - Fire development stages in time-temperature graph: ignition, growth stage, fully developed, decay.

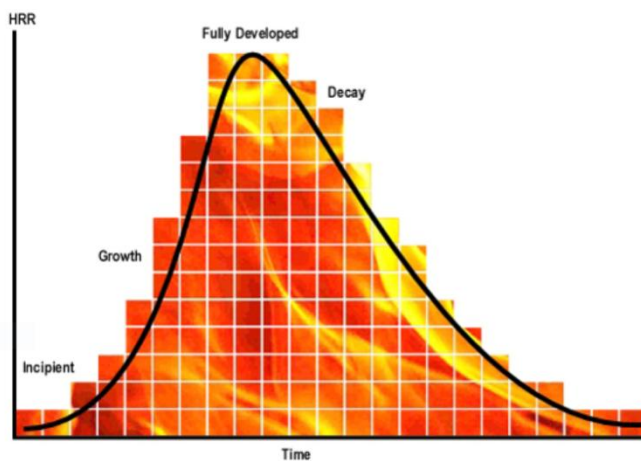


Figure 9 - Heat release rate (HRR) during fire development stages.

Natural temperature curves are referred to values recorded in the room involved in fire. Current Rules do not use natural curves in the analysis, but nominal curves which are simplified description of the event where cooling phase is not included. Latter curves (such as ISO 834, Figure 1) are directly applied on the surface of the structural element, which is a safer assumption, since temperatures describe fire in the room, not at the element surface.

Once temperature at one boundary is fixed, heat transfer within the element should be defined. Following lines suggest a possible method to describe temperature variation in structural elements, inspired by Eurocode 6, Annex D. The method is implemented in the numerical model.

Starting from normal conditions, room temperature as boundary condition is linked to constant temperature values in the medium studied. Therefore temperature profile is described by a single value assumed equal to 20°C through the whole element. Then temperature profile changes during fire according to Fourier second order differential equation:

$$\frac{\partial T(x, y, z, t)}{\partial t} = \alpha^2 \frac{\partial^2 T(x, y, z, t)}{\partial x^2}$$

$$\alpha(T) = \frac{\lambda_a}{\rho c_a}$$

where:

- $T(x, y, z, t)$  is the function which describes temperature [°C] in space [mm] and time [s];
  - $\alpha$  is function of thermo physical parameters of the medium: thermal conductivity ( $\lambda_a$ ), [W/(m °C)], gross dry density ( $\rho$ ), [kg/m<sup>3</sup>] and specific heat capacity ( $c_a$ ), [J/(kg K)];
- Figure 6 is considered.

For sake of simplicity heat propagation is considered radial as arch transversal sections axis (Figure 10). In this way heat vertical and horizontal components should not be considered. As already said temperature values in time of the ISO 834 curve are imposed on the inner surface (intrados) of the arch.

$$T(t)_{ISO\ 834} = 20 + 345 \log (1 + 8t)$$

where time t is expressed in minutes, T is computed in °C.

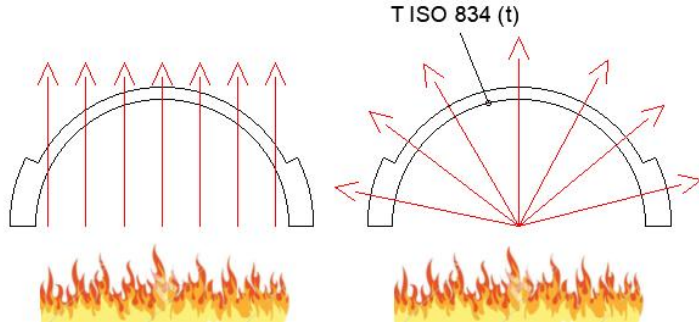


Figure 10 - Actual and considered heat transfer.

Anyway both boundary conditions must be known in order to solve the problem. Considering the exterior surface of the arch (extrados), two are possible options. Experimental results can be used, according to measurements given by thermometers applied. However, when these data are not available, a numerical procedure able to build a realistic temperature profile should be considered. The approach is based on the discretization of the arch cross section in infinitesimal parts and the description of heat transfer through the Euler forward method (Figure 11).

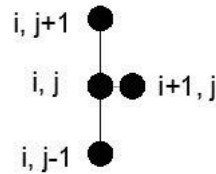


Figure 11 - Euler forward method example. Points involved in the calculation of temperature in point (i+1, j): temperatures at the previous instant in nearest fibers.

For example the thermal map in Figure 12 describes temperatures in time in 6 fibers equally spaced of the cross section. It represents the temperature profile in arch cross sections as time passes. In order to obtain a proper evaluation, transversal sections are divided in a number of stripes function of the time the fire lasts. The following relationship must be verified:

$$\Delta t \leq \frac{1}{2} \Delta x^2$$

Where  $\Delta t$  is the sampling time of the fire therefore of the temperature,  $\Delta x$  is the sampling space of the section.

Looking at Figure 12, each circle on the vertical axis at  $t = 0$  represents a fiber, which are described at six instants (horizontal lines). In this example six fibers are studied. Axis  $x = 0$  tells temperature values in time, of the fiber at the intrados, according to ISO 834 curve (gradient colored circles, black circled). The six fibers on axis  $t = 0$  are at room temperature (blank circles), since fire is not happened yet. Fiber on the extrados is at the same temperature of the previous fiber  $\Delta x$  at the previous instant  $\Delta t$  (points linked with the arrow). This is an intuitive assumption called hypothesis “a”, based on principles of natural heat transfer. Once that boundary conditions are defined, all temperatures of the six fibers within the cross section are known by using the Euler forward method (inner circles, uniformly colored). Between the six fibers considered, linear interpolations are allowed. Now the thermal map is filled up and the function  $T(t, x)$  is known in each fiber of the arch at each instant of the fire. The example shows how temperature changes in six fibers during six instants, however it can be extended for more fibers and instants.

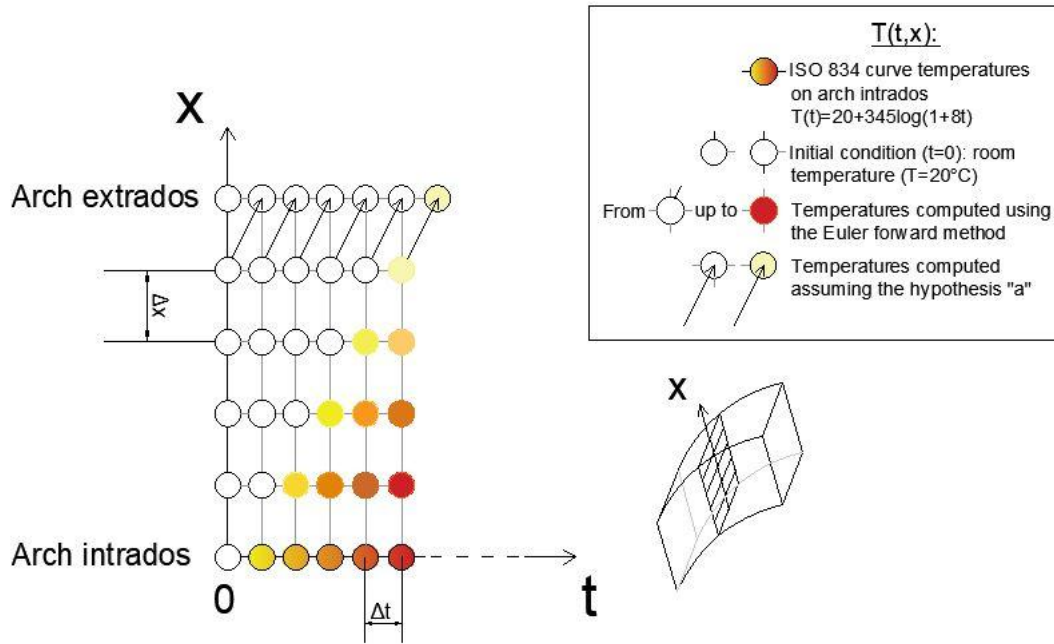
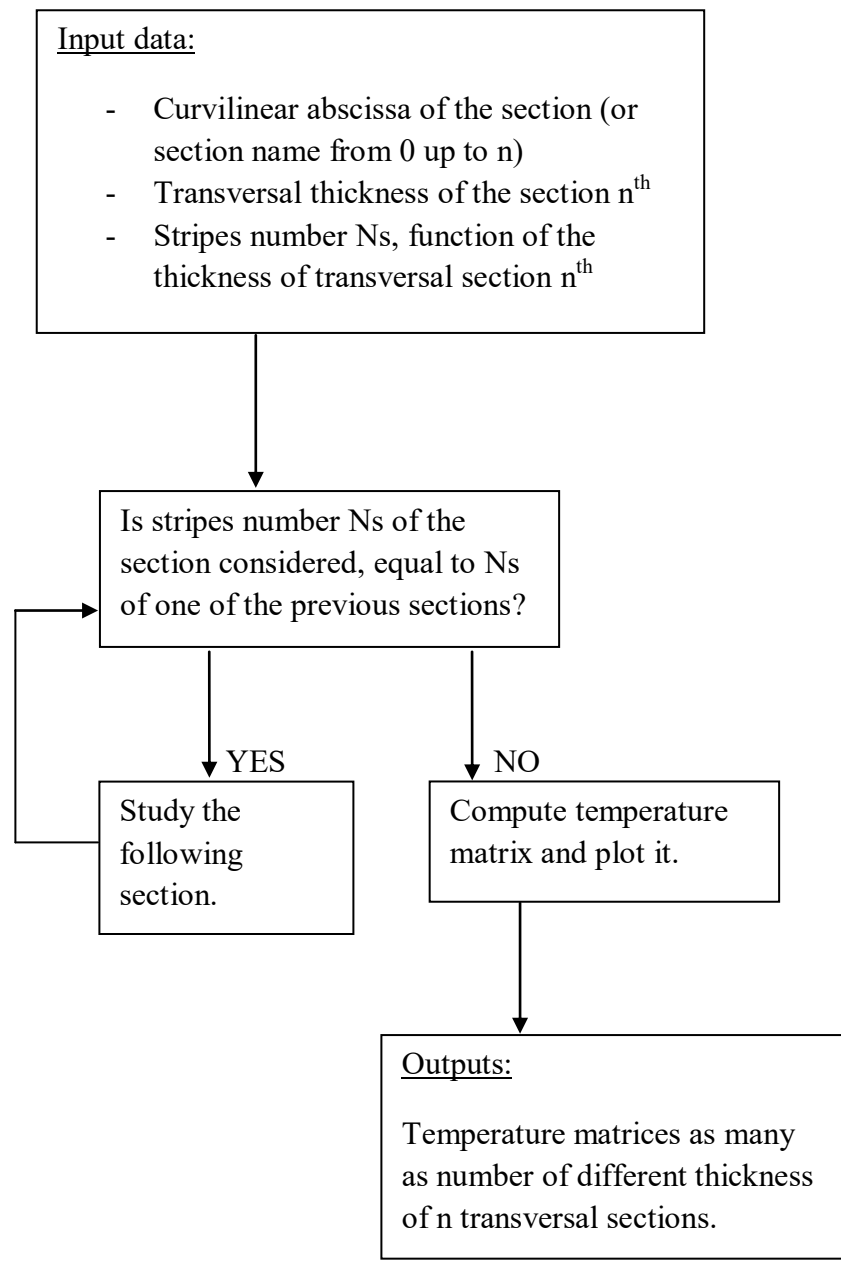


Figure 12 - Thermal map  $T(t,x)$  of six fibers of a generic cross section.

Considering hypothesis assumed in the procedure, it follows that each cross section is characterized by the same thermal map, wherever it is along the arch longitudinal axis. Moreover temperature is uniform on each fiber since the radial axis is only direction considered. Although this is not the actual thermal distribution, it allows to obtain a simplified representation of the reality, on the safe side. At the moment model has been implemented only for constant cross sections arches. However since springings have usually thicker sections than keystone's due to the increase in internal actions, the model could be extended through steps listed below. It is the flow diagram which computes thermal maps in cross sections characterized by different thicknesses.



## 2.3 Constitutive laws and failure mechanism

As temperature increases, mechanical behaviours of material, voussoirs cross sections and structural element change: loss of strength and thermal stresses growth are main immediate consequences.

In order to take into account material progressive degradation, the constitutive law is described in function of temperature (Figure 13), therefore of time (Figure 1). Strength is studied in terms of elastic modulus  $E_{pre pick}$ ,  $E_{post pick}$  and yield stress  $\sigma_y$ . The first branch shows a linear elastic behavior till the yield stress, than a brittle failure occurs.  $E_{pre pick}$ ,  $E_{post pick}$ ,  $\sigma_y$  decrease as temperature increases and both  $\varepsilon_{pick}$ ,  $\varepsilon_{max}$  increases as temperature increases, according to degradation process. Figure 13 shows values normalized on the maximum yield stress, achievable only at room temperature.

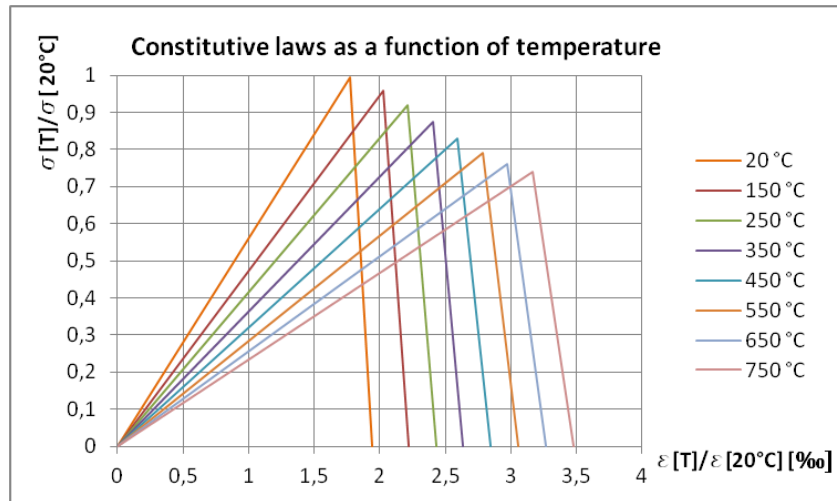


Figure 13 - Constitutive laws as a function of temperature. Gross dry density range 900-1200 kg/m<sup>3</sup> (clay units) is considered. (Source: Nicholas Sergio Burello master thesis, 2018, p79).

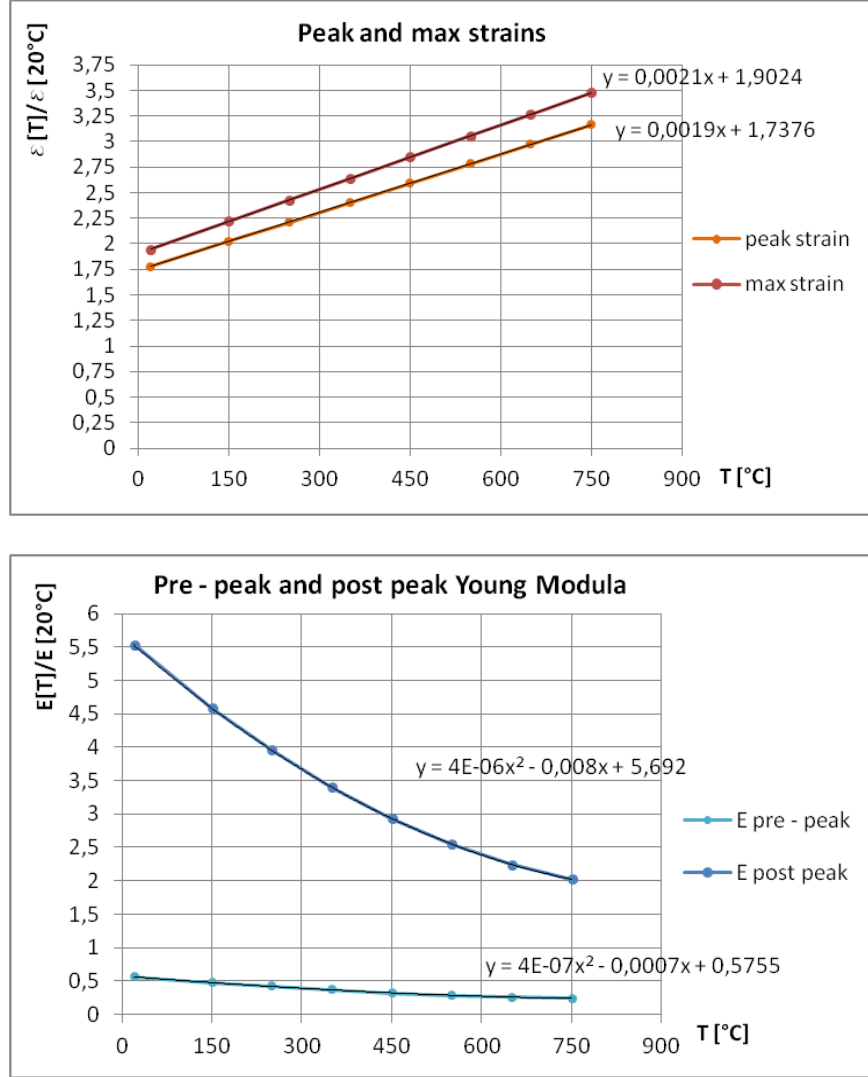


Figure 14 - Peak and maximum strains, pre-peak and post-peak Young Modula as functions of temperature (Source: Nicholas Sergio Burello master thesis, 2018).

Equations shown in Figure 14 are useful to describe material behavior in the numerical procedure. Therefore mechanical response is known at each temperature during each instant of the fire. Considering that the medium analyzed is composed by clay units and masonry mortar, the global behavior will be affected by the heterogeneous nature. Thermal parameters depends on temperature as described in Figure 6, however in the numerical analysis have been assumed constant intermediate values, neglecting peak ones. Beside

heat conductivity ( $\lambda_a$ ), gross dry density ( $\rho$ ) and specific heat capacity ( $c_a$ ), another useful parameter is thermal expansion coefficient  $\alpha_T$  which represents the change in volume of the material when subject to temperature variation. It is involved in computation of normal strains  $\varepsilon_z(z)$ ,  $\varepsilon_z(x, z)$  and stresses  $\sigma_z(z)$ ,  $\sigma_z(x, z)$  which are assumed constant along the y axis since one – dimensional problem is assumed. Reference system considered is shown in Figure 15.

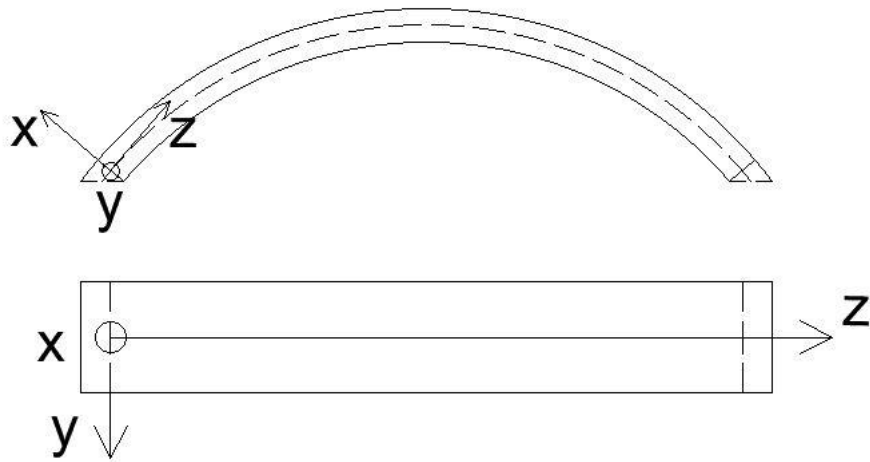


Figure 15 - Reference system. One-dimensional model.

In usual conditions, at room temperature normal stresses described by constitutive laws in function of temperature in Figure 13 are linked to the working principle of the arch: self-supportive, compressive structure which carries no tensile stresses, higher is the difference between internal loads resultant (pressure curve) and the arch longitudinal axis (z) higher is the bending moment acting, hence tensile stresses related. When temperature changes take place, this distance can increase: in a fixed arch translations and rotations are prevented at both supports, hence it is three times statically indeterminate element. This static configuration restrains thermal expansion and significant internal forces occur leading to plasticization and cracking with the consequent redistribution of internal forces.

Considering experimental tests carried out, only one surface is exposed to fire, hence temperature distribution is described by Figure 16.

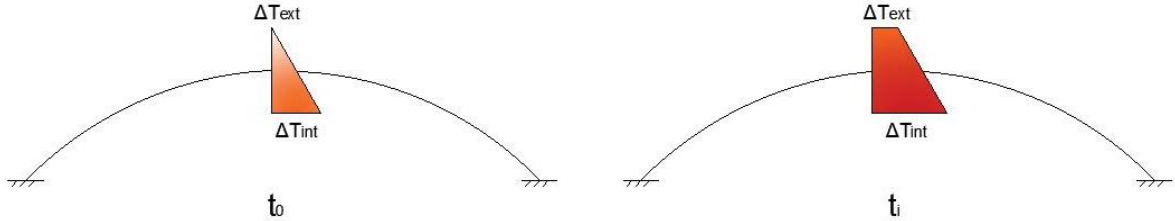


Figure 16 - Temperature distribution at the beginning of the fire and some instants later.

Both temperature distributions can be divided in constant and linear thermal changes, which are respectively linked to the growth of constant stresses on the whole transversal cross section and linear opposite stresses on intrados and extrados fibres (Figure 17). Constant stresses are responsible of axial normal force  $N_z(z)$  while opposite stresses are linked to bending moment around y axis,  $M_y(z)$ .

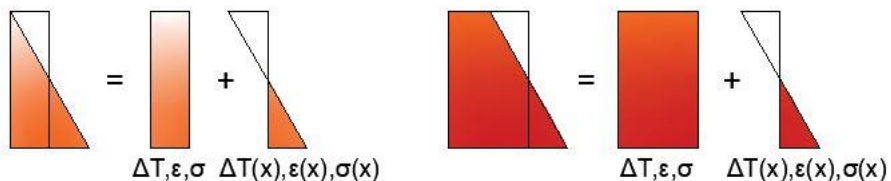


Figure 17 - Qualitative representation of temperature, strains and stresses.

When internal actions overcome the elastic limit  $N_{el}$ ,  $M_{el}$ , hinges formation leads to global collapse, as they reach the minimum sufficient number, in this case three. Therefore it is necessary to adopt non linear static analysis to study the behaviour of the structure beyond the elastic limit and to take into account material strength beyond the yield stress. However non linear procedure could be replaced by a linear analysis which allows a smarter computation of stress state avoiding the progressive adjustment of axial and bending

stiffnesses by imposing an initial value of normal strain and curvature. Procedure is described below, formulas valid in linear elastic field are used, therefore superposition principle is applied:

$$\Delta T = T_f - T_{RT} = T_f - 20^\circ C$$

$$\Delta T_{const} = \frac{\Delta T_{int} + \Delta T_{ext}}{2}; \Delta T_{lin}(x) = \frac{\Delta T_{int} - \Delta T_{ext}}{2}$$

where:

- $\Delta T_{int}$  is the change in temperature at the intrados
- $\Delta T_{ext}$  is the change in temperature at the extrados

According to the Eurocode 6, Figure 7:

$$\varepsilon_z(\Delta T_{const}) = \begin{cases} 0; & \Delta T_{const} \in (-20^\circ C, 0^\circ C) \\ \alpha_T \Delta T_{const}; & \Delta T_{const} \in (20^\circ C, 730^\circ C) \\ 5\%; & \Delta T_{const} > 730^\circ C \end{cases}$$

$$\varepsilon_z(\Delta T_{lin}, x) = \begin{cases} 0; & \Delta T_{lin} \in (-20^\circ C, 0^\circ C) \\ 2\alpha_T \Delta T_{lin} \cdot x/h; & \Delta T_{lin} \in (20^\circ C, 730^\circ C) \\ 5\%; & \Delta T_{lin} > 730^\circ C \end{cases}$$

where  $h$  is the thickness of the cross section. Although this relationship is the only suggested by the Code, in Chapter 5 new ones will be proposed in order to describe experimental results.

Considering temperature changing in a generic cross section:

$$\Delta T_{const} \rightarrow \varepsilon_z(\Delta T_{const}) \rightarrow \sigma_{z, const} \rightarrow N_z$$

$$\Delta T_{lin} \rightarrow \varepsilon_z(\Delta T_{lin}, x) \rightarrow \sigma_{z, lin} \rightarrow M_y$$

Total constant and linear strains on a generic cross section  $i$  are:

$$\varepsilon_{z, const} = \frac{N_i}{EA} + \varepsilon_z(\Delta T_{const})$$

$$\varepsilon_{z lin} = \frac{M_i}{EI} + \varepsilon_z(\Delta T_{lin}, x)/x$$

Where both mechanical and thermal loads are accounted and constant transversal sections are assumed. Therefore total strains, internal actions and bending moments in a generic cross section can be written as:

$$\varepsilon_z = \varepsilon_{z const} + \varepsilon_{z lin}x$$

$$N_z = \int_{A_i} \sigma_{z const} dA$$

$$M_y = \int_{A_i} \sigma_{z lin} x dA$$

Where constitutive law has been used.

Then model checks for each section  $i$ :

$$|N_i - N_z| > threshold \rightarrow real \varepsilon_z(\Delta T_u) = \varepsilon_z(\Delta T_{const}) + \Delta \varepsilon_z(\Delta T_{const}) = \varepsilon_z(\Delta T_{const}) + \frac{N_i - N_z}{EA}$$

$$|N_i - N_z| < threshold \rightarrow real \varepsilon_z(\Delta T_{const}) = \varepsilon_z(\Delta T_{const})$$

$$\begin{aligned} |M_i - M_y| > threshold \rightarrow real \frac{\varepsilon_z(\Delta T_{lin}, x)}{x} &= \frac{\varepsilon_z(\Delta T_{lin}, x)}{x} + \frac{\Delta \varepsilon_z(\Delta T_{lin}, x)}{x} \\ &= \frac{\varepsilon_z(\Delta T_{lin}, x)}{x} + \frac{M_i - M_y}{EI} \end{aligned}$$

$$|M_i - M_z| < threshold \rightarrow real \frac{\varepsilon_z(\Delta T_{lin}, x)}{x} = \frac{\varepsilon_z(\Delta T_{lin}, x)}{x}$$

Axial and bending stiffnesses are assumed constant on each section.

Before describing arch collapse mechanism, it can be useful to spend some words on its peculiar static behavior. In fact the working principle of this element is far different from beam's. Arch is a pure compression structural element able to resolve forces into compressive stresses, thereby eliminating tensile stresses. This is why materials commonly used, such as masonry, natural stones and concrete, are characterized by great compressive

strength while little importance is attached to the low tensile strength. However pure compressive stresses occur in voussoirs' cross sections when arch design is appropriate for loads applied during the life cycle of the element. This condition is strictly linked to thrust-line position: it has to be within cross sections' cores. By increasing loads magnitude thrust-line gradually gets away from the safe area, causing internal bending moments hence tensile stresses growth. Once they easily overcome the low tensile strength, material starts cracking and failure occurs. One of main collapse mechanisms of the arch is shown in Figure 19. It is a three hinges mechanism, linked to tensile failures at the intrados of the crown and at the extrados of springings. This mechanism is linked to an underestimation of mechanical loads applied over the extrados of the arch. However considering the study of this thesis, cracks opening is opposite. Tensile failure is reached at the extrados of the crown and at intrados of springing. Therefore resultants shown in Figure 20 will be applied on the opposite vertex of the core section: the lowest at the crown and the vertex on the left at the springing on the left. This is related to the heat increasing applied at arch intrados: it induces upward displacements at the crown while springings gradually fall downward.

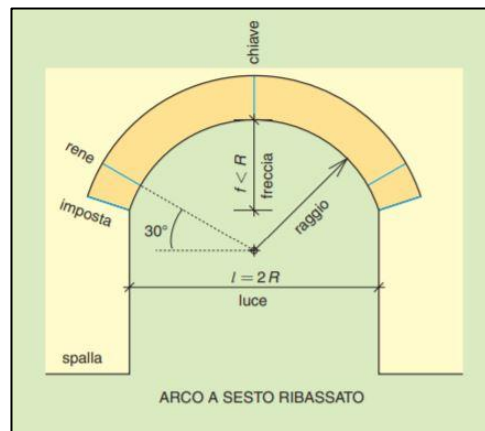


Figure 18 - Segmental arch geometry.

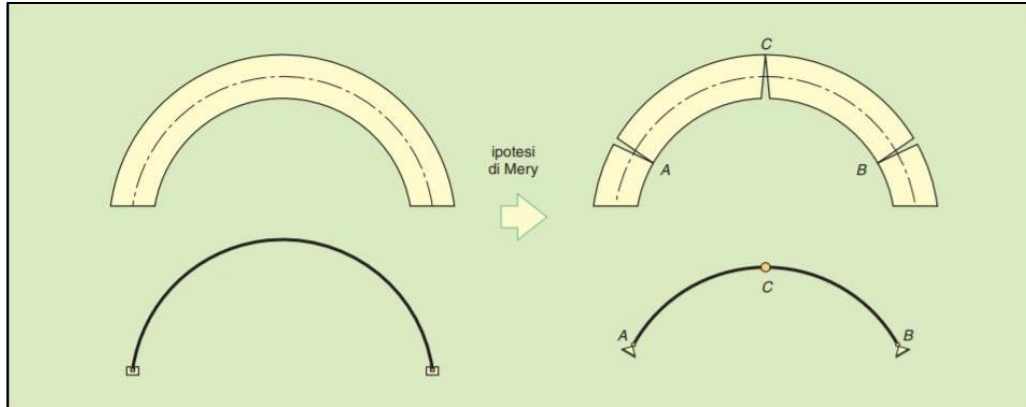


Figure 19 - Three hinges collapse mechanism due to dead loads.

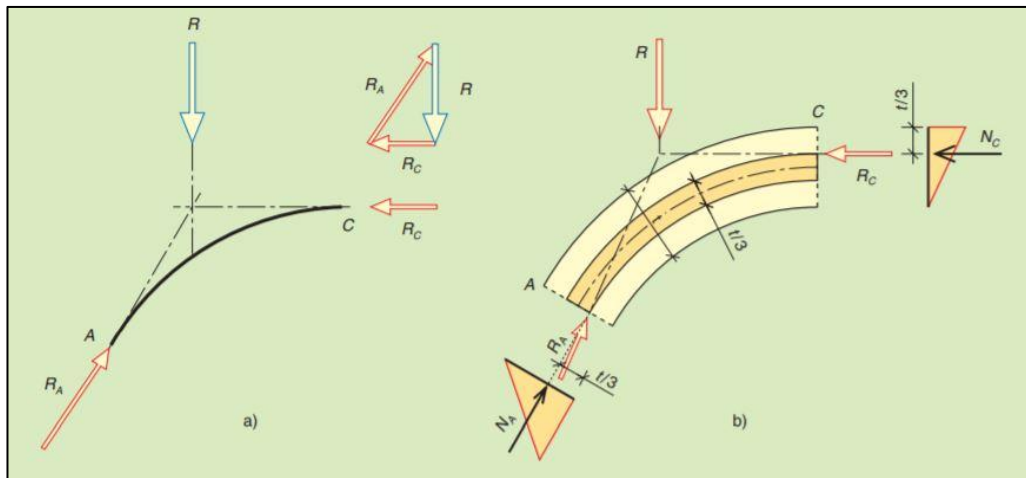


Figure 20 - Resultants on semi-arch.

It is important to underline that assumptions described in this chapter are linked to prescriptions of Codes currently in force (Figure 21). However when experimental results are available, they are used to replace hypothesis which are inconsistent with reality. It is the case of temperature curves and masonry mechanical and thermal properties. These aspects will be explained in chapter 5.

<b><i>Summary: main assumptions of the numerical model</i></b>	
<b>Static scheme</b>	fixed arch (three times statically indetermined), perfect restraints, one-dimensional element.
<b>Heat transfer</b>	radial direction; uniform along arch axis z and depth y; ISO 834 fire curve directly applied at intrados; heat transfer within the cross section according to Figure 12.
<b>Material mechanical behavior</b>	Homogeneous, isotropic, infinite shear stiffness; infinitesimal displacements; plane strain conditions.
<b>Arch geometry</b>	Segmental arch, constant cross sections.
<b>Loading conditions</b>	Distributed vertical dead loads.
<b>Collapse mechanism</b>	Three hinges arch: plastic sections at springings and crown.

Table 4 - Summary of hypothesis adopted in the numerical procedure.

# *Chapter 3*

## *Experimental project*

---

In this part some words are spent to describe the project: laboratory, arch geometry, materials characteristics, loading conditions and devices used. Moreover three compressive tests are presented to obtain masonry mechanical properties. Results are subsequently used as input data in the numerical model.

---

### *3.1 Project description*

The experimental part of this thesis is carried out on two arches cast on site one at a time at Vigili del Fuoco laboratory in Roma Capannelle. Structures are placed on the ceiling of the oven located at “Laboratorio di Resistenza al Fuoco dell’Area di Protezione Passiva della Direzione Centrale per la Prevenzione e la Sicurezza Tecnica (DCPST)”. Technicians are able to control and monitor pressures and temperatures applied through the oven in time. Arch spring line is located on the extrados of lower flanges of two HEB 220 steel beams, which are part of the oven ceiling. It is a one ring masonry arch. Clay solid bricks are laid rowlock with cement mortar, extrados and intrados are left uncovered. Hence arch thickness is equal to brick depth, 120 mm. 38 bricks are in the ring and 4 bricks are aligned

in depth, therefore an arch stripe 1 meter long is built. Arch and oven sections are shown in Figure 12. Geometric dimensions are listed below:

- Arch thickness: 120 mm
- Spring angle:  $43^\circ$
- Arch angle:  $95^\circ$
- Clear span: 2180 mm
- Rise: 500 mm
- Longitudinal depth (perpendicular direction to the paper): 1 m

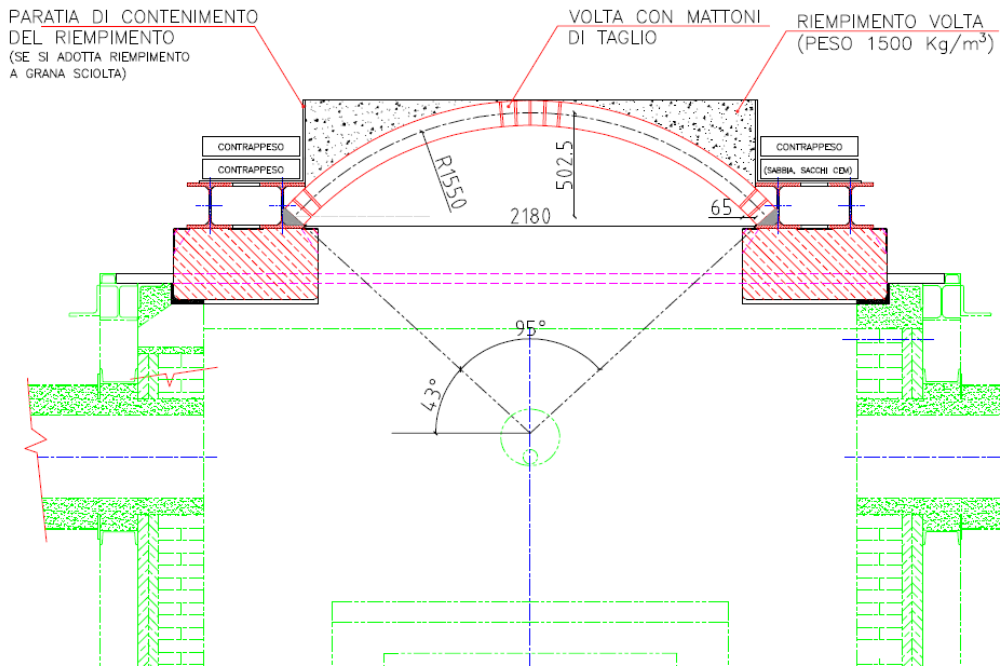


Figure 21 - Arch and oven section.

Materials used are solid clay units ( $25 \times 12 \times 5.5 \text{ cm} \times \text{cm} \times \text{cm}$ ) (Table 5) and cement mortar paste whose percentages in the mix are written in Table 6. Circular polystyrene template act as support during the construction phase as shown in Figure 22. After 28 days, according to minimum curing time, it is removed in order to leave the arch intrados directly exposed to oven.

## Chapter 3 – Experimental project

Prodotto marcato CE cat. I sistema 2+ CARATTERISTICHE (UNI 771-1)	
<b>DENOMINAZIONE</b>	Mattone pieno comune 5,5x12x25
<b>IMPIEGO E POSA IN OPERA</b>	Muratura portante in zona sismica
<b>DIMENTIONI</b>	25X12X5,5 cm (spessore muro 12 o 25 cm)
<b>PERCENTUALE DI FORATURA</b>	0%
<b>MASSA VOLUMICA A SECCO</b>	1705 Kg/m <sup>3</sup> (categoria D1)
<b>PESO DEL BLOCCO SECCO</b>	2,7 Kg al pezzo
<b>RESISTENZA CARATTERISTICA A COMPRESSIONE</b>	Base >10,0 N/mm <sup>2</sup> - Testa >2,5 N/mm <sup>2</sup>
<b>CONDUTTIVITÀ EQUIVALENTE</b>	$\lambda_{S12} = 0,332 \text{ W/mK}$ - $\lambda_{S25} = 0,332 \text{ W/mK}$ (valore asciutto)

Table 5 - Solid units clay technical data.

<b>Dati Tecnici</b>	
Peso specifico della polvere	ca. 1.500 kg/m <sup>3</sup>
Granulometria	< 3 mm
Spessore minimo	10 mm
Acqua di impasto	17,5-19,5%
Resa come intonaco	ca. 15 kg/m <sup>2</sup> con spessore 10 mm
Resa	ca. 17 q di malta secca per ottenere 1.000 l di malta bagnata (con 1 sacco da 25 kg si ottengono ca. 14,5 l di malta bagnata)
Densità malta indurita (UNI EN 1015-10)	ca. 1.850 kg/m <sup>3</sup>
Resistenza a compressione a 28 gg (UNI EN 1015-11)	> 5 N/mm <sup>2</sup>
Modulo di elasticità a 28 gg	ca. 8.000 N/mm <sup>2</sup>
Fattore di resistenza alla diffusione del vapore (UNI EN 1745)	$\mu = 15/35$ (valore tabulato)
Classe	M5 secondo UNI EN 998-2

Table 6 - High strength cement mortar technical data.



Figure 22 - Arch built for experimental test 1. Photo has been taken on the ceiling of the oven.

Once the arch has been built up, thermocouples and extensometers have been positioned in some points in order to detect temperatures and displacements. These special devices are able to send information to computers of technicians. In order to have a proper evaluation of heat transfer and mechanical behavior of the structural element, it is advisable to place devices both at inner and outer surfaces and at the arch median axis.

Two different thermal sensors types are used (Figure 23), hence their positioning is different (Figure 24, Figure 25). The one which measures temperature on the outer surface is installed on the arch through a thermal sensitive plate, glued at the extrados. Therefore the device is linked to the plate by means of a wire; the other sensor type is positioned in the masonry (two in cement mortar and two in bricks) till the tip of the bar reaches the point of interest (intrados or median axis). Both devices send information through the green cap.

In order to collect displacements two different one-direction extensometer are used: contact and non-contact. The former has two edges which are mechanically attached to the transversal section of the structure. As the arch deforms the distance between the two edges changes and the displacement is obtained; the latter uses a laser beam directed to the arch. Resultant reflections from the extrados are received by a device whose information are processed.

### Chapter 3 – Experimental project

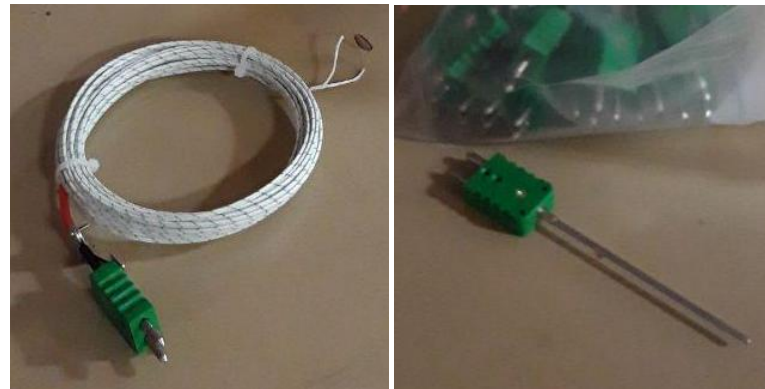


Figure 23 - Thermocouples devices. Device on the left collects data at the outer surface, on the right at the inner surfaces (median axis and intrados).



Figure 24 - Devices positioning (1).

Chapter 3 – Experimental project



Figure 25 - Devices positioning (2).

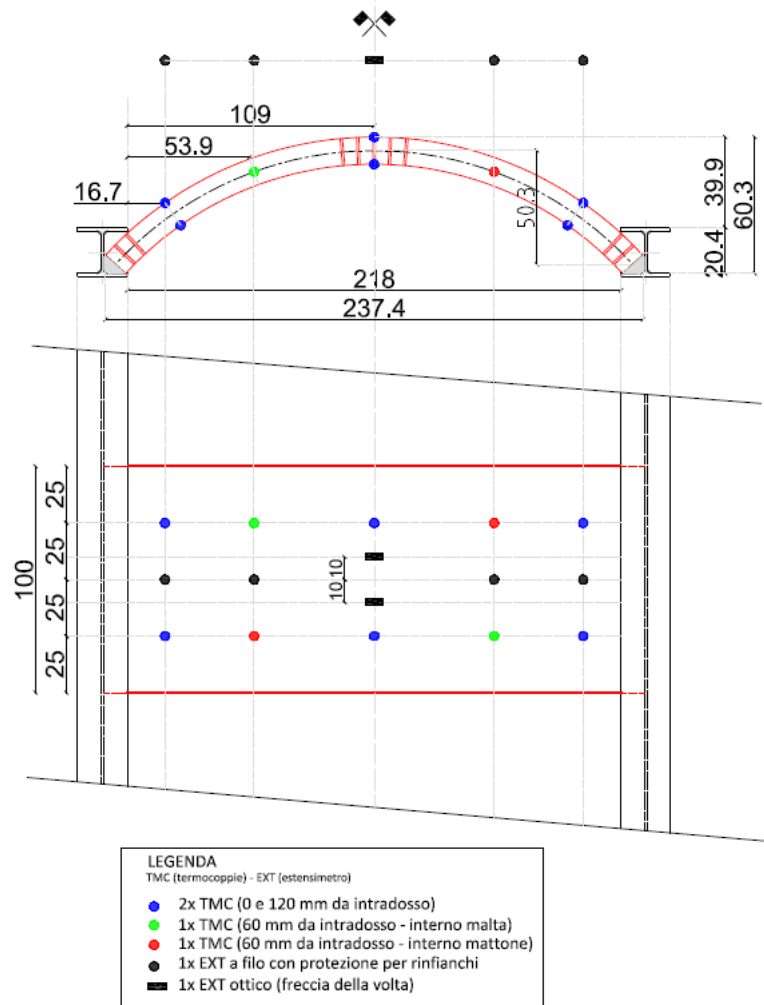


Figure 26 - Cross and plan views of thermocouples and extensometers positioning.

After devices positioning and 28 days curing, the arch can be loaded. Different loads are applied for each test considered.

- The first one is carried out to assess critical conditions hence the minimum mechanical load is applied on the arch. This is the most dangerous situation since mechanical loads tend to reduce upward displacements of the arch in fire conditions. The higher is the load on the arch the lower it will displace when subject to fire thanks to the higher stabilizing effect.

- In the second test an higher value of mechanical load is applied to the arch. This configuration is linked to usual usage of the structure. Smaller displacements and later collapse are expected.

In practice plasterboard formworks are used to contain the load on the arch.

In the first test 405 kg of sand are distributed on the arch as shown in Figure 27, therefore  $810 \text{ daN}/(2.18 \times 1 \times 0.2 \text{ m}^3) = 1858 \text{ daN/m}^3$ , considering 1 kg approximately equal to 10 N and the arch span 2.18 m. However the model considers the load spread on the arch as shown in the Figure 27, hence a coefficient is introduced in order to make two configurations equal. Thermal insulators layers are properly fixed on inner surfaces of formworks in order to confine the heat (Figure 28).

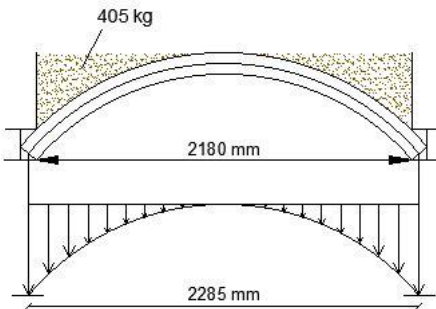


Figure 27 - Model of test 1.

### Chapter 3 – Experimental project



Figure 28 - Top, lateral, bottom views of arch and confinement for filler material and thermal insulation.

In test 2 the arch has been loaded by lean concrete and sand layers as shown in Figure 29. Lean concrete load is known by considering that cubic samples  $15 \times 15 \times 15 \text{ cm}^3$  weigh 7 kg, therefore density considered is approximately  $2080 \text{ kg/m}^3$ . Regarding sand layer it is  $1071 \text{ kg/m}^3$  dense, 20 bags 22,5 kg each are laid on lean concrete layer. Therefore load referred to filler material is  $3150 \text{ daN/m}^3$ ,  $1940 \text{ daN/m}^3$  is set in the model.

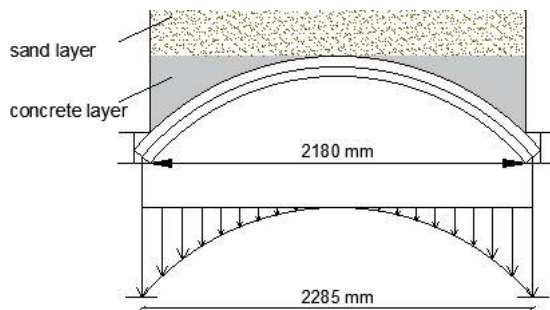


Figure 29 - Model of test 2.

The goal is to validate and improve the numerical model by comparison with experimental results. Tests are also useful to qualify arch resistance during fire events. Fire resistance rating (REI) is defined by following characteristics:

- “R” means load bearing capacity. It is the ability of the construction element to preserve its mechanical characteristics and the relevant load capacity during a normal fire.
- “E” means integrity. It is the structure ability to not allow the passage or production of gas or vapor to the area not exposed to the fire.
- “T” means thermal insulation. It is the ability to reduce within a temperature limit, usually 140 °C, the transfer of heat to the unexposed (cold) side.

Consequently:

- REI (followed by the number  $n$  which indicates the classification). The constructive element which must preserve for a determined amount of time  $n$  (expressed in minutes) its mechanical resistance, the integrity of flames and gases, and the thermal insulation. Both separating and loadbearing properties must be ensured.
- RE (followed by the number  $n$  which indicates the classification). The constructive element which must preserve for a determined amount of time  $n$  (expressed in minutes) its mechanical resistance, the integrity of flames and gases.
- R (followed by the number  $n$ , which indicates the classification). The constructive element which must preserve for a determined amount of time  $n$  (expressed in minutes) its mechanical resistance. Only loadbearing properties are ensured.

Load bearing capacity “R” is evaluated by measuring displacements and displacement speed of the arch; integrity “E” by the insertion of a cotton thermal insulating layer;

thermal insulation “I” by monitoring temperature on the extrados by means of thermocouples. Maximum limit threshold of displacement speed is fixed according to EN 1363-1:2012:

$$v_{lim} = \frac{L^2}{9000 \text{ min} \cdot d} = \frac{(2180 \text{ mm})^2}{9000 \text{ min} \cdot 120 \text{ mm}} = 4,4 \text{ mm/min}$$

where  $L$  is the arch clear span and  $d$  is the brick width.

### ***3.2 Compressive tests***

Some input data have to be set in order to run the numerical code and therefore compare experimental and code results in homogeneous terms. Procedures to obtain important mechanical parameters are listed and precisely described in the 11.10.3 section of the NTC 2018 both for existing and new masonry structures: characteristic compressive strength  $f_{ck}$ , characteristic shear strength without considering normal forces  $f_{vk0}$ , normal and shear elastic modules  $E, G$ . These values can be computed through tables or experimental tests.

In this case only compressive strength  $f_c$ , characteristic compressive strength  $f_{ck}$  and elastic modulus  $E$  are computed. Three samples are subjected to compressive test (Figure 30) by means of the apparatus shown in (Figure 31), (EN 12390 – 3).



Figure 30 - Samples tested.



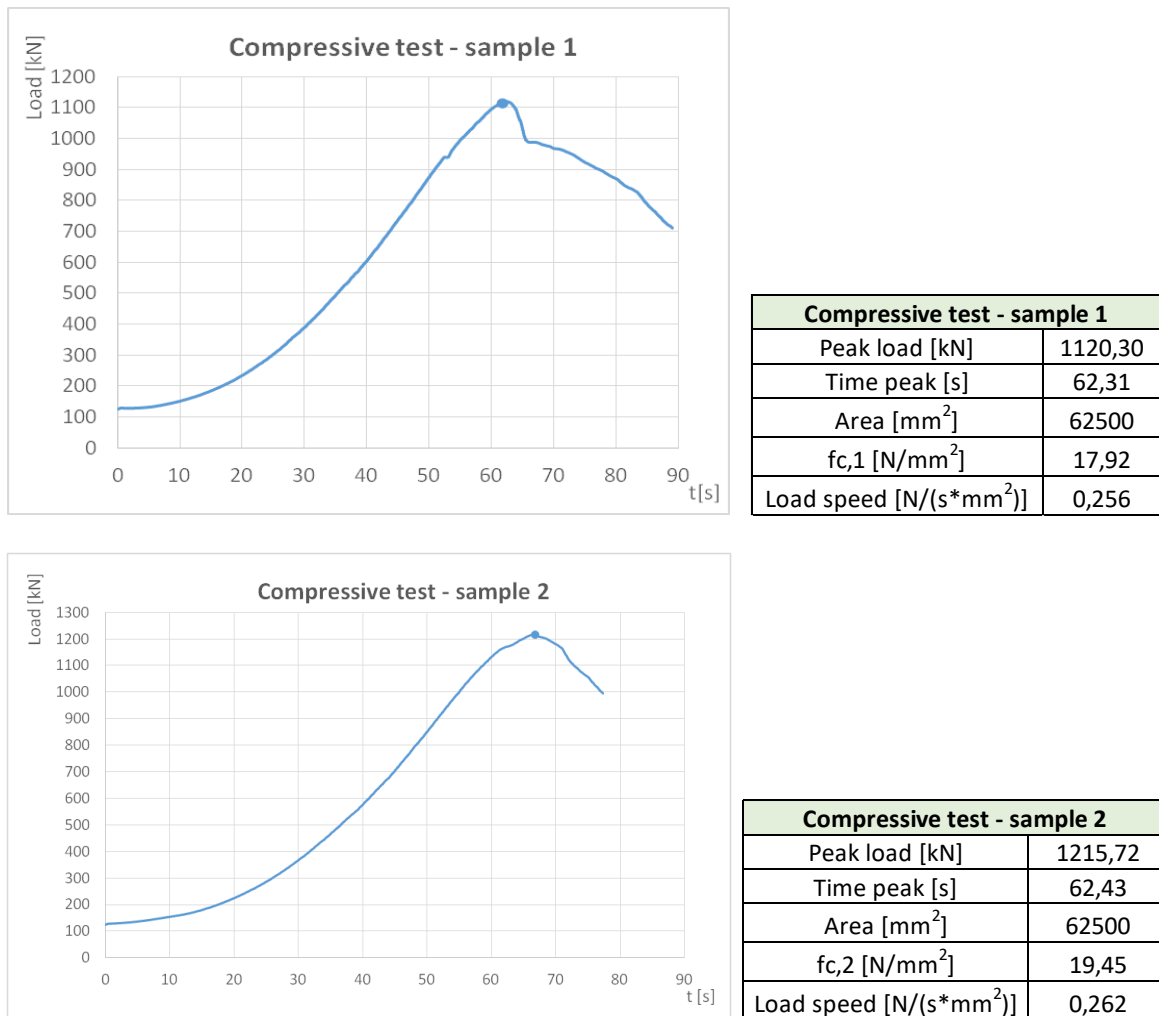
Figure 31 - Compressive test apparatus (DCPST laboratory).

Tests are performed at room temperature. Procedures to obtain compressive strength and Young modulus are described:

- In order to compute masonry compressive strength  $f_c$  only experimental interpretation is performed. Value set in the numerical code is the mean value obtained during three compressive tests. Following formula is used:

$$f_c = \frac{f_{c,1} + f_{c,2} + f_{c,3}}{3} = 19,08 \text{ MPa}$$

Where  $f_{c,1}$ ;  $f_{c,2}$ ;  $f_{c,3}$  are maxima stresses computed as maxima loads reached during compressive tests divided by the transversal area of the sample, constant and equal to  $25 \times 25 \text{ cm}^2$ . Results of three experimental test considered are presented in graphs load-time (Figure 32). Tables explain main characteristics and test outputs of each masonry sample.



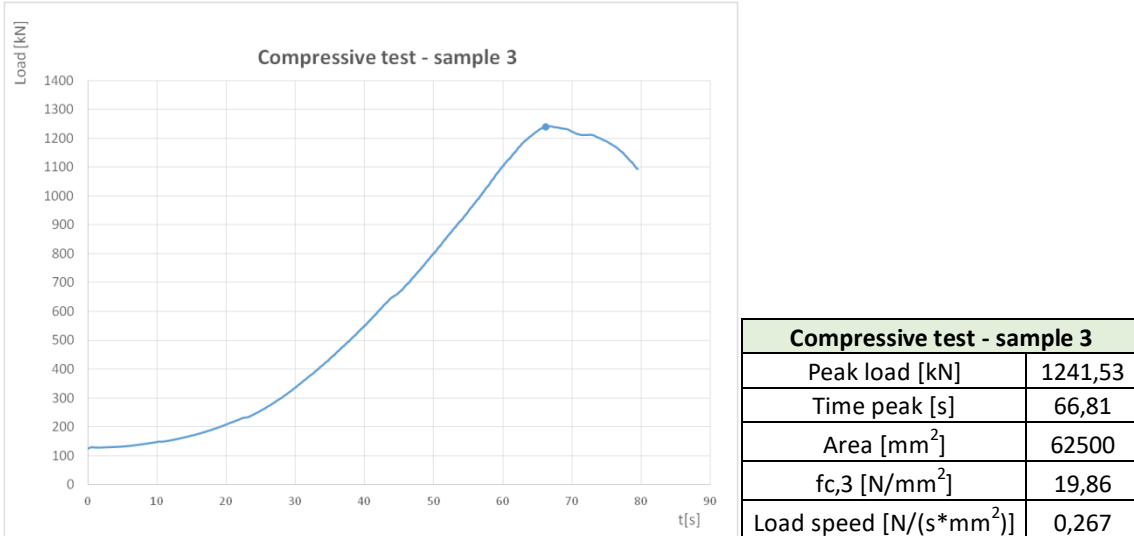


Table 7 - Compressive tests results.

<b>f<sub>c</sub> computation</b>	<b>f<sub>c,n</sub> [N/mm<sup>2</sup>]</b>
sample 1	17,92
sample 2	19,45
sample 3	19,86
Average value	<b>19,08</b>

Table 8 - Masonry compressive strength.

- Whereas Young modulus computation involves characteristic compressive strength.

In order to obtain characteristic value, Codes prescriptions are considered. In design stage, tables suggested by the Rule can be used to estimate masonry compressive strength starting from mechanical strength of bricks and lime plaster mix. Table 11.10.VI is considered according to section 11.10.3.1.2 of the NTC 2018, elastic module can be computed using following formula:

$$E = 1000f_{c,k}$$

Resistenza caratteristica a compressione $f_{ck}$ dell'elemento N/mm <sup>2</sup>	Tipo di malta			
	M15	M10	M5	M2,5
2,0	1,2	1,2	1,2	1,2
3,0	2,2	2,2	2,2	2,0
5,0	3,5	3,4	3,3	3,0
7,5	5,0	4,5	4,1	3,5
10,0	6,2	5,3	4,7	4,1
15,0	8,2	6,7	6,0	5,1
20,0	9,7	8,0	7,0	6,1
30,0	12,0	10,0	8,6	7,2
40,0	14,3	12,0	10,4	–

Table 9 - Compressive strength values for masonry of solid units and 5-15 mm lime plaster joints thickness.

However the characteristic compressive strength obtained should be adjusted in function of the class and the category which brick and lime plaster belong to. Table 4.5.II of the NTC 2018 is considered. In this case class and category of both elements are 1 and the lime plaster is performance guaranteed (M5), therefore the design compressive strength value is computed, the latter value has been considered:

- at room temperature

$$f_{c,d} = \frac{f_{c,k}}{\gamma_M} = \frac{10,4 \text{ N/mm}^2}{2,0} = 5,2 \text{ N/mm}^2$$

- in fire conditions

$$f_{c,d} = \frac{f_{c,k}}{\gamma_M} = \frac{10,4 \text{ N/mm}^2}{1,0} = 10,4 \text{ N/mm}^2$$

Materiale	Classe di esecuzione	
	1	2
Muratura con elementi resistenti di categoria I, malta a prestazione garantita	2,0	2,5
Muratura con elementi resistenti di categoria I, malta a composizione prescritta	2,2	2,7
Muratura con elementi resistenti di categoria II, ogni tipo di malta	2,5	3,0

Table 10 - Partial coefficient for masonry.

Starting from the compressive strength  $f_c$  previously computed, an adjustment is applied to obtain the characteristic compressive strength, which is defined as the value which has the 95% possibility to be overcome.

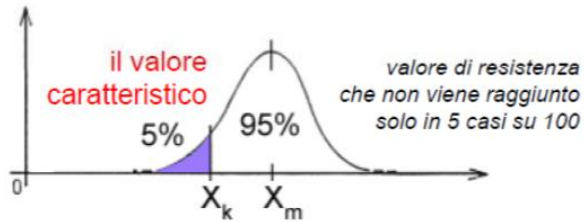


Figure 32 - Characteristic value according to Gaussian distribution.

The following formula has been considered:

$$f_{c,k} = f_c - k \cdot s$$

Where  $f_c$  is the mean value of experimental compressive strengths,  $s$  is standard deviation of values,  $k$  is function of number of samples  $n$  considered. Statistical coefficients are obtained:

$$s = \sqrt{\frac{\sum_n (x_n - \bar{x})^2}{n-1}} = \sqrt{\frac{(f_{c,1} - f_c)^2 + (f_{c,2} - f_c)^2 + (f_{c,3} - f_c)^2}{2}}$$

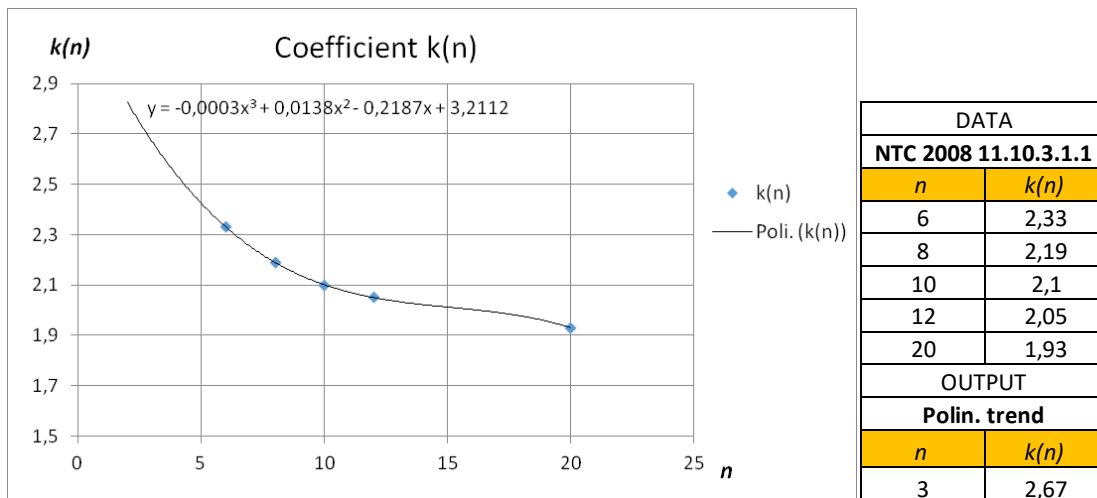


Table 11 - Graphic computation of  $k(3)$  by means of third order polynomial regression.

Once characteristic compressive strength  $f_{c,k}$  has been computed, Young modulus is obtained by multiplying by 1000. However considering the large variability of masonry Young Modulus related to the heterogeneity of the material, this value should be considered carefully.

According to results obtained in “Archi in muratura soggetti ad elevati gradienti termici” master thesis by Nicholas Sergio Burello, tensile strength is assumed equal to  $2\%f_c$ .

In conclusion compressive strength is related only to compressive tests results, Young modulus is computed in function of the characteristic compressive strength based on experimental results and verified by the Rule, tensile strength is assumed considering conclusions of previous paper.

Compressive strength $f_c$	
$f_c$ [N/mm <sup>2</sup> ]	$f_{c,n}$ [N/mm <sup>2</sup> ]
sample 1	17,92
sample 2	19,45
sample 3	19,86
<b>mean value</b>	<b>19,08</b>
Young modulus E	
s [N/mm <sup>2</sup> ]	1,02
k [ ]	2,7
$f_{c,k}$ [N/mm <sup>2</sup> ]	16,32
$f_{b,k}$ [N/mm <sup>2</sup> ]	10,4
Code prescription	16,32 > 10,4
<b>E [MPa]</b>	<b>16322</b>
Tensile strength $f_{ct}$	
$f_{ct}$ [N/mm <sup>2</sup> ]	<b>0,4</b>

Table 12 - Summary of masonry mechanical parameters.

# *Chapter 4*

## *Tests procedure and results*

---

This section is spent in the description and analysis of experimental results. First some observations on temperatures are presented, therefore displacements are examined. The aim is to obtain values to compare with numerical model outputs.

---

### ***4.1 Experimental and design temperature curves***

Once the oven has been closed and switched on, an almost uniform heat starts to transfer as consequence of naphtha combustion, therefore the bottom part of the arch starts to warm up. The oven is calibrated to apply temperatures in time described by the ISO 834, which is the curve the Code refers to. Obviously temperatures obtained in the oven chamber will not be exactly ones given by the ISO 834 equation. However we prefer them as close as possible to design values, hence acceptable for a proper validation of the model. Comparison and deviation in time between experimental and design temperature curves are shown. In the meanwhile pressures changes stays almost within limit thresholds fixed at 5-15 Pa, unless some short and small inaccuracies. Room temperature recorded in laboratory was 13°C. Data used are referred to experimental test 1A performed on January 22<sup>nd</sup>, 2020, however same consideration apply for oven temperatures during tests 1B and 2.

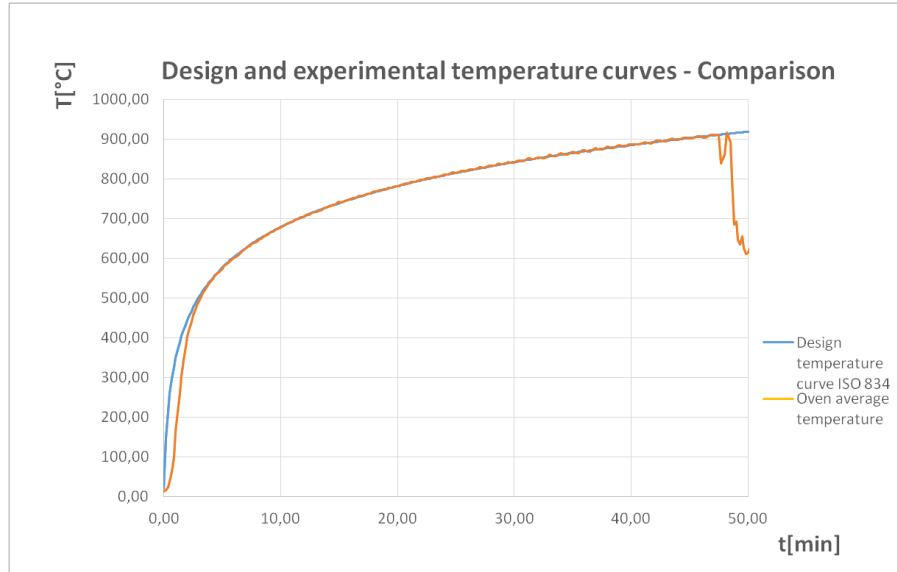


Figure 33 - Comparison between design and experimental temperature curves in time.

Experimental temperatures are values recorded by the monitoring system of the oven. Data are collected each 10 seconds, while the design curve is continuously known in time. Looking at Figure 33 is clear that until minute 3, when temperature is almost 500 °C, difference between curves is great. However this fact can be neglected since do not influence subsequent temperature trends. In fact after the first part temperatures are well described, the average percentage difference between the two curves is less than 1%. Lastly at minute 47.50 the oven has been switched off, hence the temperature gradually decrease, unless some instants, probably due to turbulences.

For the purpose of quantifying the discrepancy between design and experimental values, absolute difference  $|\Delta T(t)|$  and percentage difference have been considered. The following equation has been used:

$$\frac{\Delta T}{T}(t) [\%] = \frac{T_{exp}(t) - T_{ISO\ 834}(t)}{T_{ISO\ 834}(t)} \cdot 100$$

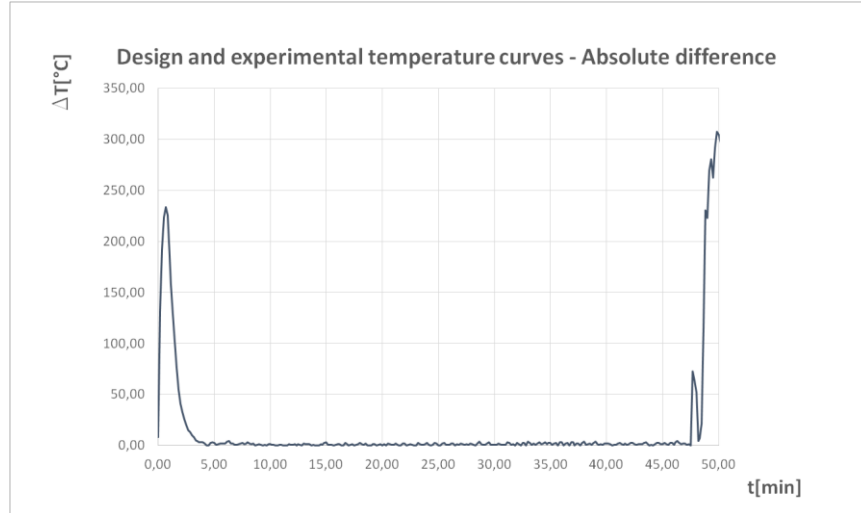


Figure 34 - Absolute difference between design and experimental temperature curves in time.

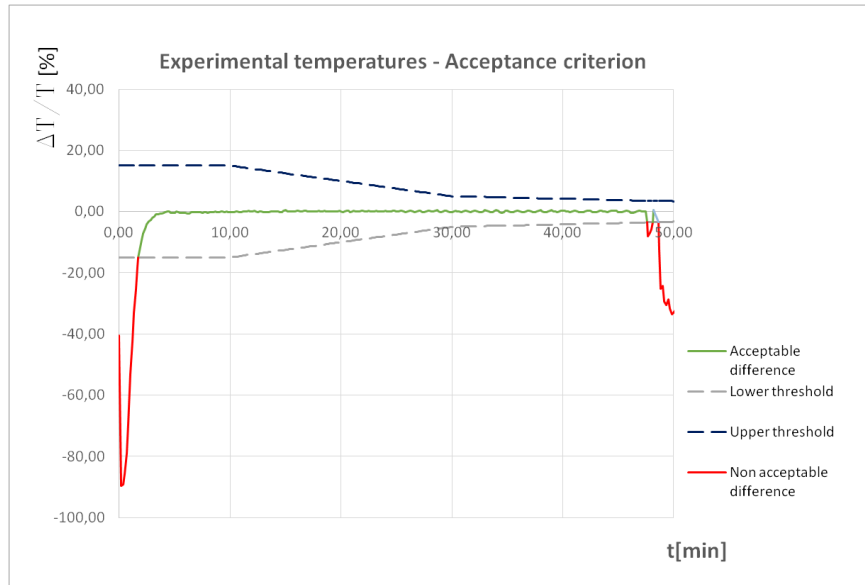


Figure 35 - Acceptance criterion of temperatures applied during test 1A.

In order to assess the reliability of the oven, some limit values are fixed in time. Upper and lower thresholds gradually become more restrictive as time passes since more accurate values are expected. Although some instants do not fulfill requirements, the most important part of the fire simulation is very close to design temperatures. Anyway the initial lack of accuracy due to the thermal inertia of the oven, does not affect final results considering the

narrow time window involved. It is worth remembering that experimental temperatures studied so far are related to the oven chamber and not applied at the arch intrados.

## 4.2 Tests 1

Results and comments related to test 1 are now described (Figure 27). The minimum mechanical load is applied on the arch. This configuration is of paramount importance since it is the most dangerous in terms of stability. Test 1 has been performed in two different moments, test 1A and test 1B, while the first is carried out for few instants, the second leads the arch to collapse.

### 4.2.1 Test 1A: temperatures

Thermometers outputs are presented. As expected, the increment of temperature has been recorded at intrados first, then at the middle line and lastly at the extrados. Delays of 10 minutes on the middle line and of 20 minutes on the extrados are compliant with thermal conductivity of bricks and cement mortar. In fact cement mortar thermal conductivity is higher, as shown in Figure 40, hence the material is heated up more rapidly.

Considering graph related to intrados, all devices follow the same trend unless some fluctuations due to turbulences. Moreover some curves grow faster (T46) probably because the device tip is completely exposed, while others grow slower (T41-T42-T43-T44-T45) because tips may be partially covered by cement mortar. Dotted lines related to devices on keystone do not show significant difference compared to devices located at 55° and 70°. The hypothesis assumed in the numerical model, which consider constant temperature variations along z axis, is not completely satisfied by experimental results since important differences are recorded. However it can be acceptable considering constant average values.

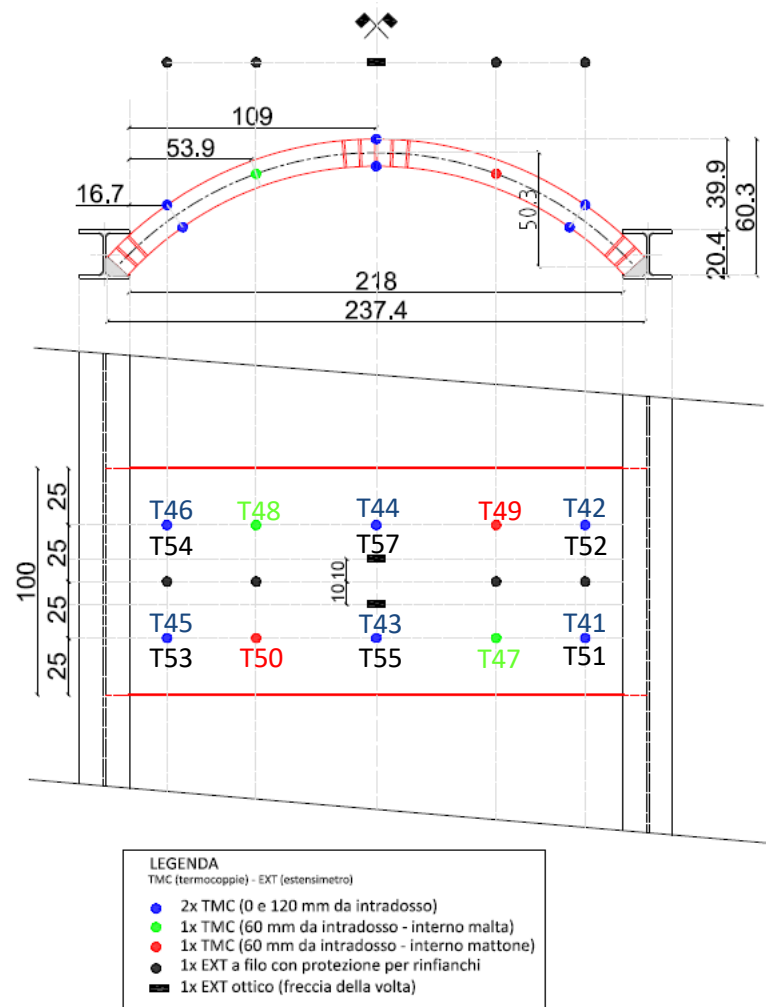


Figure 36 - Thermal devices positioning and definition. Blue devices are at intrados, black ones at extrados.

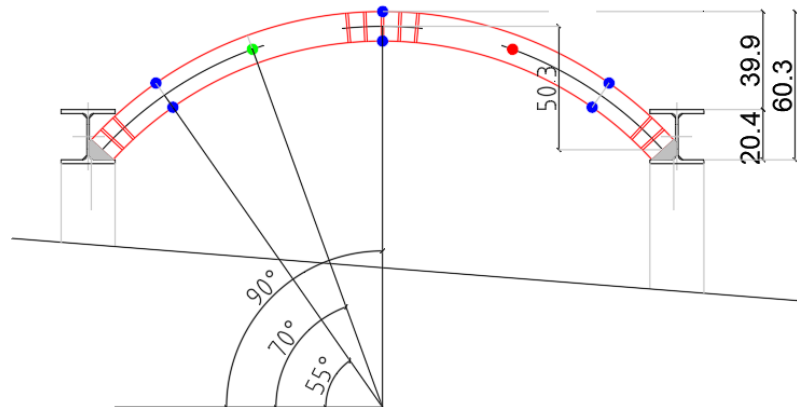


Figure 37 - Thermocouples positioning at 55°, 70°, 90°. (Relazione Poc 2019, Fantilli).

## Chapter 4 – Tests procedures and results

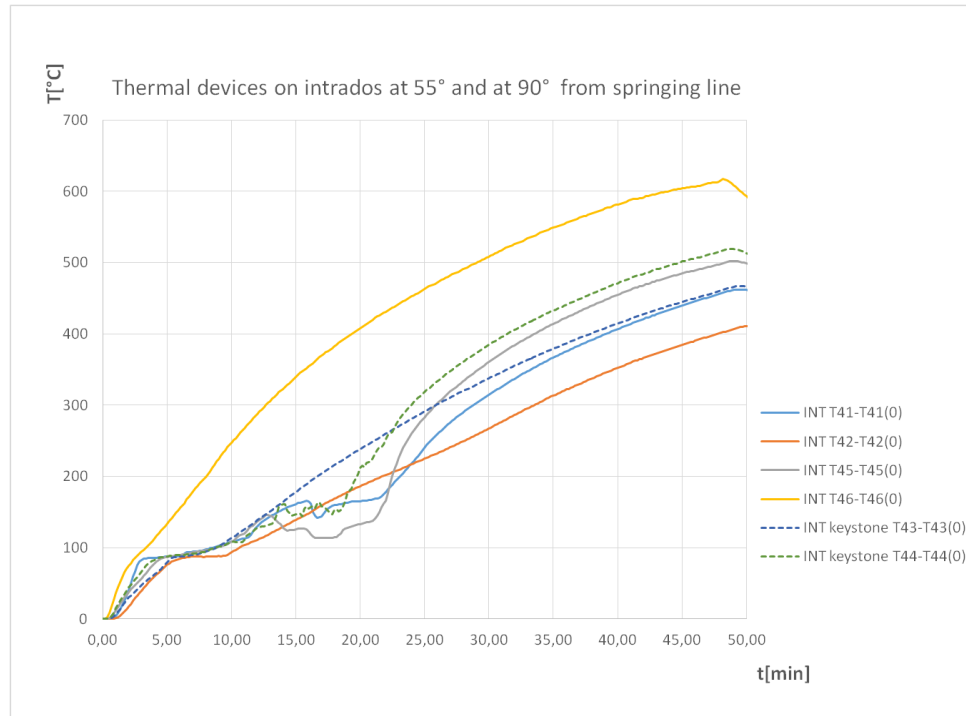


Figure 38 - Experimental temperatures at intrados.

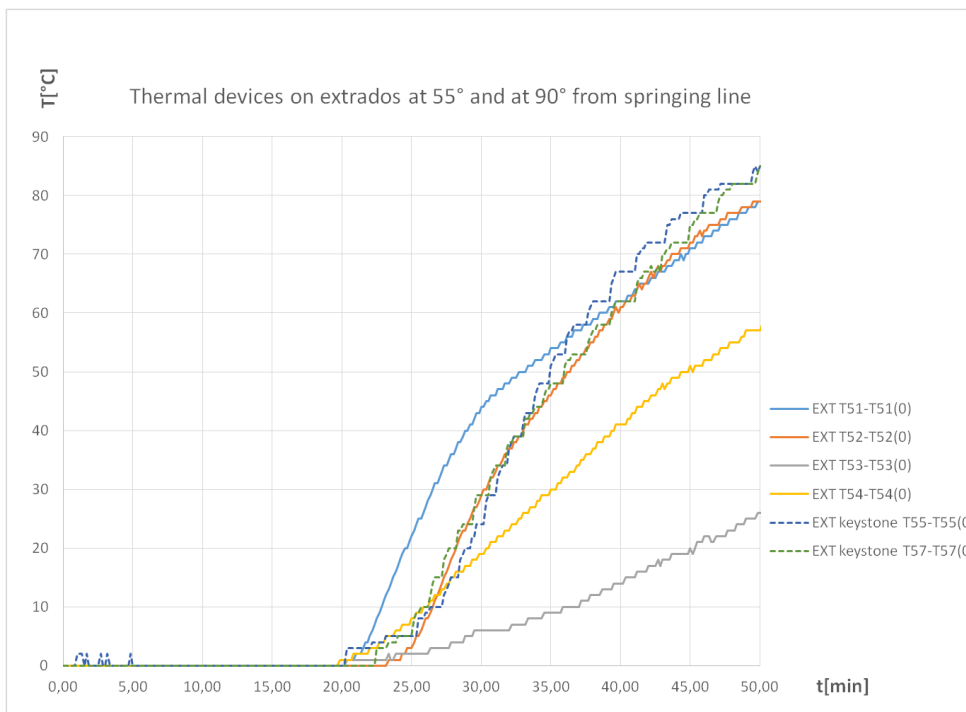


Figure 39 - Experimental temperatures at extrados.

Considering graph related to extrados, same considerations apply. It can be observed that devices at keystone show peculiar behavior: curves have sudden vertical increment and null increment repeated in time. This effect can be related to the growth of some holes in cement mortar which give the possibility to maintain constant temperature although oven keeps warming up.

Regarding Figure 40, constant temperatures in cement mortar after minute 20 can be due to its thermal capacity: binder needs a greater heat increasing to keep the same slope in temperature-time graph. Looking at different slopes related to two materials, it can be stated that clay units have an higher thermal inertia due to the lower thermal conductivity, which produces a slower temperature increase.

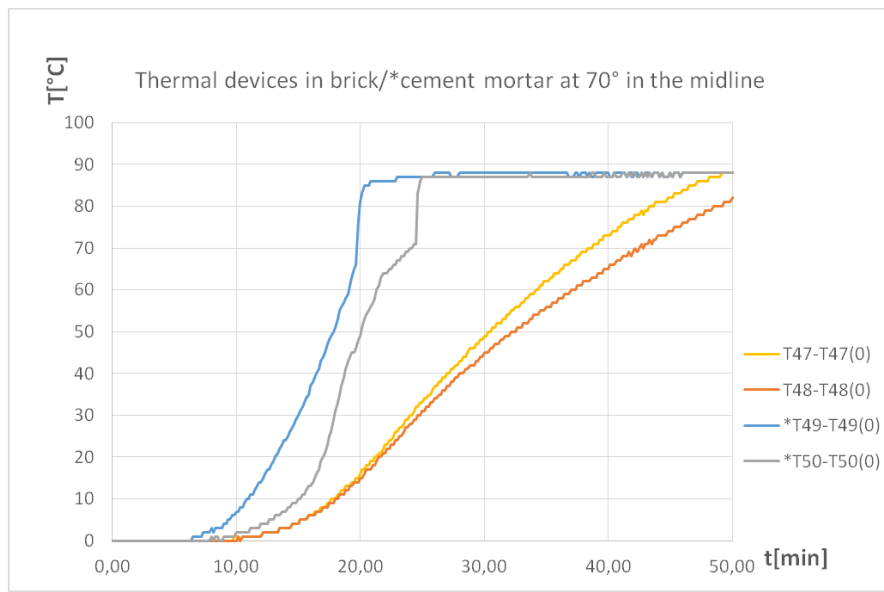


Figure 40 - Experimental temperatures at cross sections midline.

Although several values have been collected by thermal devices, most interesting results for model validation purposes are extrados and intrados trends. In order to obtain these curves, temperature-time values at extrados and intrados of the keystone are considered. Only keystone curves are used since are the closest to each other therefore assumed more

## Chapter 4 – Tests procedures and results

reliable. These values are used to build temperature curve applied by the model at arch surfaces. Trends will be useful in model inputs and following analysis. Average values are computed and plotted, graphs below are considered.

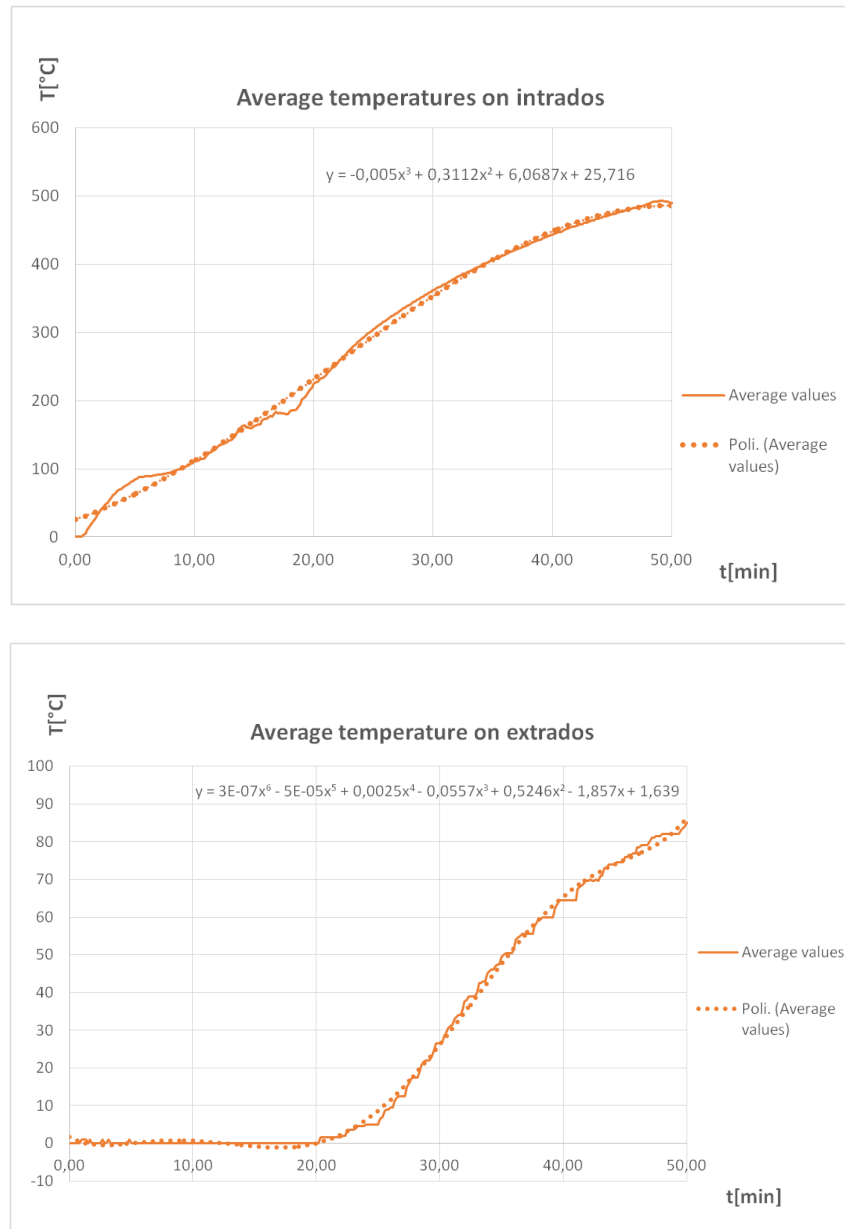


Figure 41 - Average temperatures recorded at intrados and extrados.

### 4.2.2 Test 1A: displacements

Extensometer outputs are presented in graphs displacements-time. All results are compliant with displacements expected, according to the collapse mechanism of the arch: points at the crown go upward while springings go downward. In graph below downward displacements are assumed positive, upward ones negative. Results almost respect the symmetry of the problem.

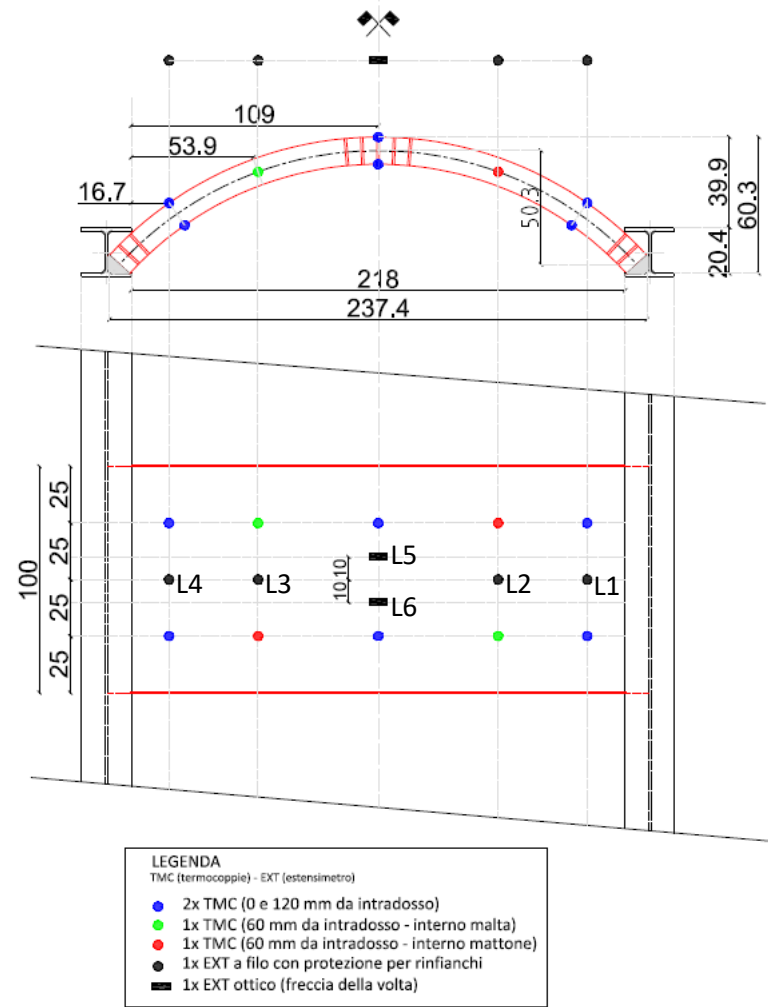


Figure 42 - Extensometers positioning and definition.

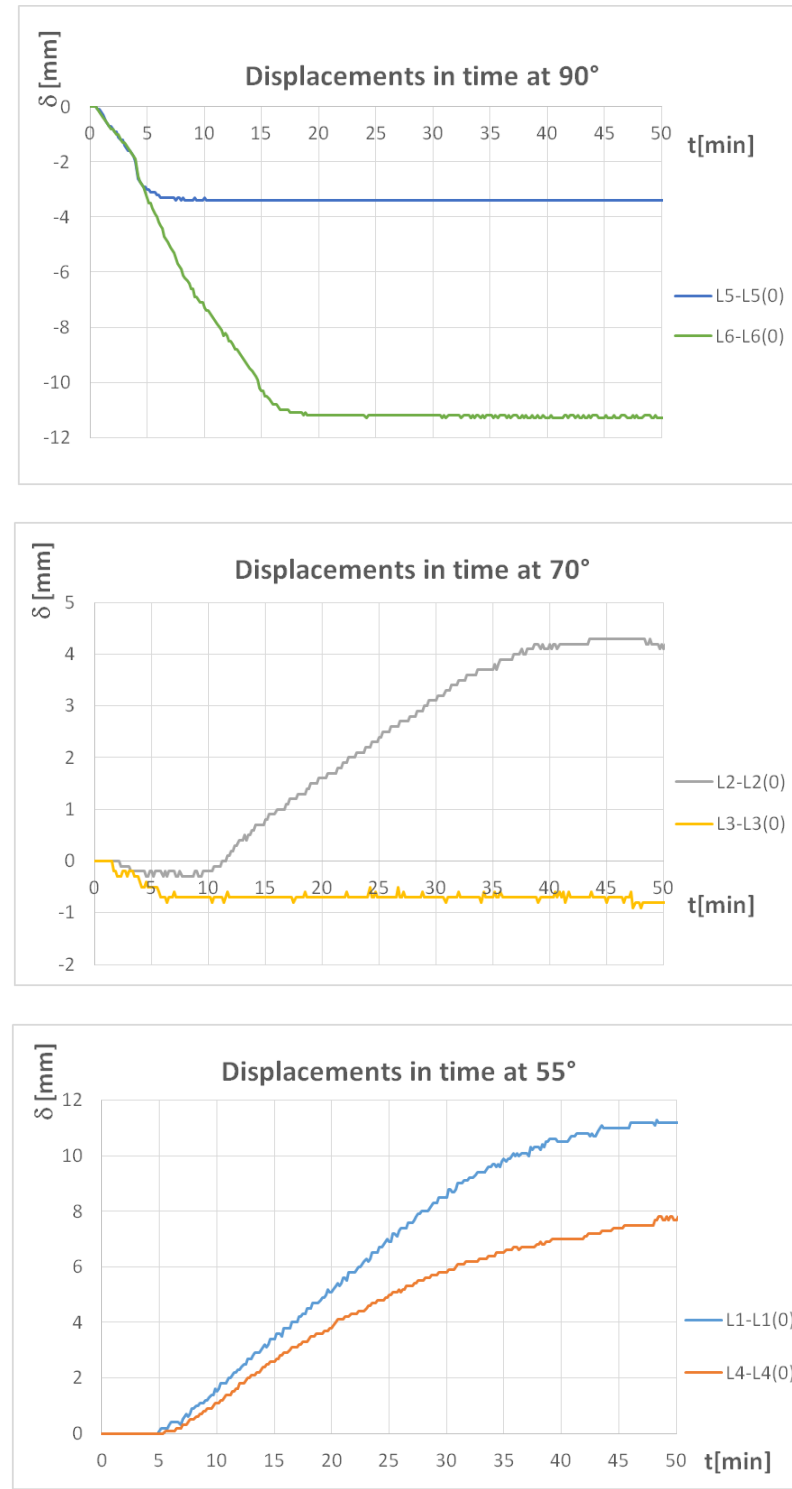


Figure 43 - Extensometers records.

It can be observed that records at springings ( $55^\circ$ ) quite match according to the symmetry of the problem, therefore outputs of both devices L1, L4 are considered reliable. On the other hand displacements recorded at crown and at  $70^\circ$  exhibit great differences. However deformed shape expected can give a good interpretation of experimental results. Considering displacements at keystone, L6 records are probably the best since the order of magnitude is consistent with records at springing. After a while both extensometers keep on reading constant displacements because of the wire has been too short. Displacements expected at  $70^\circ$  are downward, therefore L2 device is considered.

Rapid displacements are observed at crown, while displacements at springings are slower and keep on increasing in time.

In general it can be stated that displacements occur first at the keystone ( $90^\circ$ ), then at  $70^\circ$  and lastly at springings. However maxima are recorded at keystone and springings, while graph at  $70^\circ$  shows smaller displacements.

All records can be well represented by bilinear graphs which show a first elastic branch where displacements increase linearly in time and a second branch where displacements remain constant.

It is important to observe that displacements recorded in laboratory are perpendicular to the devices horizontal support, while displacements computed numerically are radial, perpendicular to the arch axis, in each point. Hence outputs will match only at the crown, while at  $70^\circ$  and  $55^\circ$  vertical component should be computed in order to make a consistent comparison with experimental results. Angles shown in Figure 44 are used.

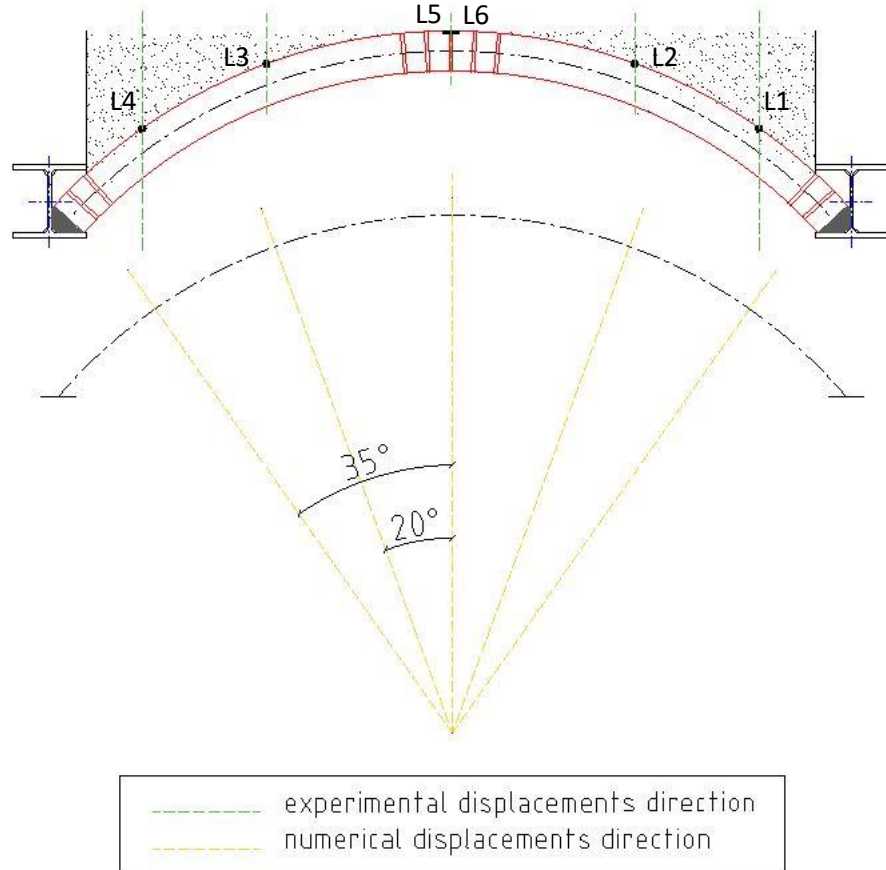


Figure 44 - Experimental and numerical displacements directions.

Figure 44 shows numerical displacements direction in same points considered during experimental tests. Although former values are known along the whole arch axis, only sections shown are considered, since comparable with experimental results available. Figure 44 highlights different directions of numerical and experimental displacements due to the working principle of extensometers and numerical model respectively. Numerical displacements directions is converted into experimental displacements directions by using followings equations:

$$v_{num,vert} = v_{num,radial} \cdot \cos 35^\circ$$

$$v_{num,vert} = v_{num,radial} \cdot \cos 20^\circ$$

$$v_{num,vert} = v_{num,radial} \cdot \cos 0^\circ$$

respectively applied for sections in positions: L1, L4; L2, L3; L5, L6.

Failure at the crown and supporting structure ignition during test 1A are shown below.

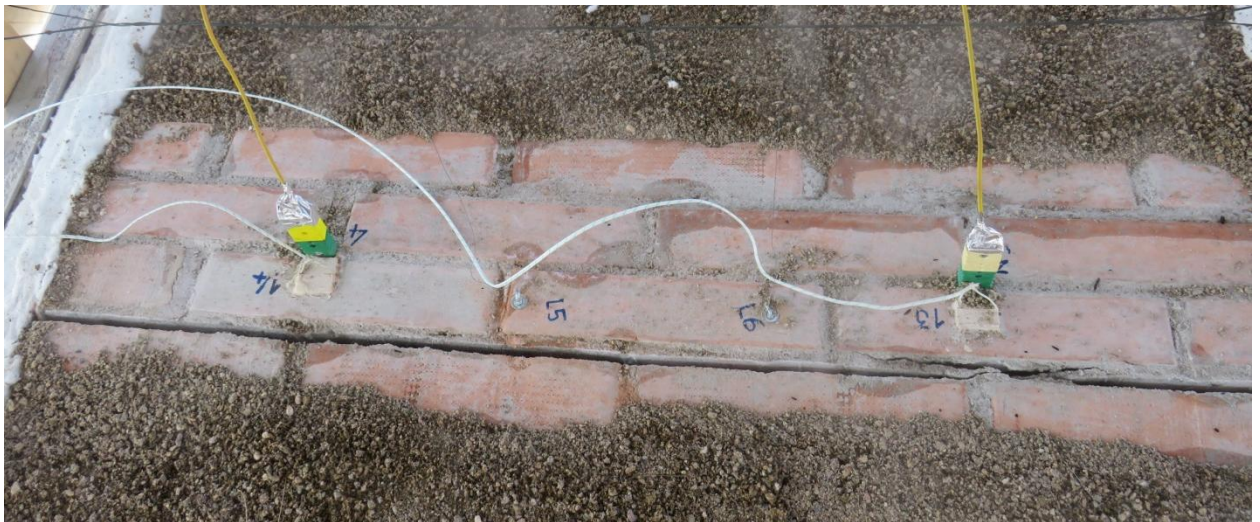


Figure 45 - Crack at crown.



Figure 46 - Ignition of supporting structure.

### 4.2.3 Test 1B: temperatures

Thermocouples positioning and definitions shown in Figure 36 are maintained. The same arch, already cracked during test 1A, has been employed. Test 1B has been performed till the collapse of arch, reached at one hour and half. Thermocouples outputs are now presented in graphs temperature-time and described. Initial results are overlapped with records of test 1A, however since more data are available in test 1B, a great overview of the general behaviour both in terms of temperatures and displacements is provided.

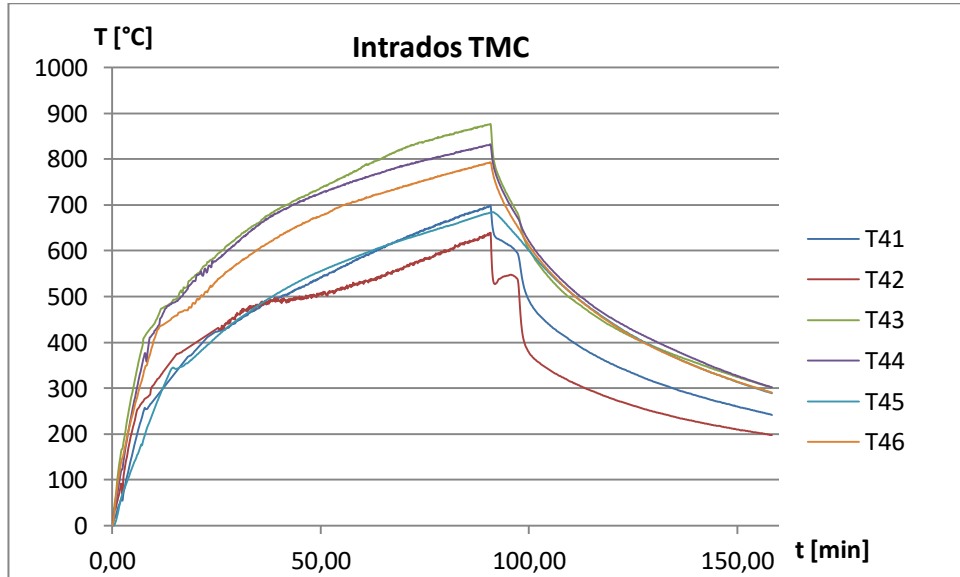


Figure 47 - Temperatures recorded at intrados during test 1B.

Oven has been switched off at one hour and half, however temperatures have been recorded till two hours and half, as shown in Figure 47.

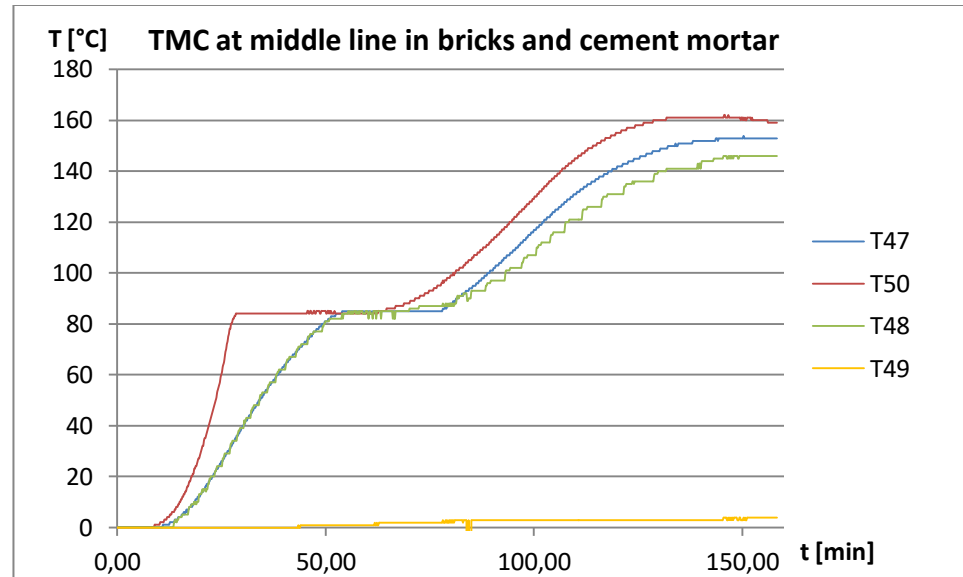


Figure 48 - Temperatures recorded at middle line during test 1B.

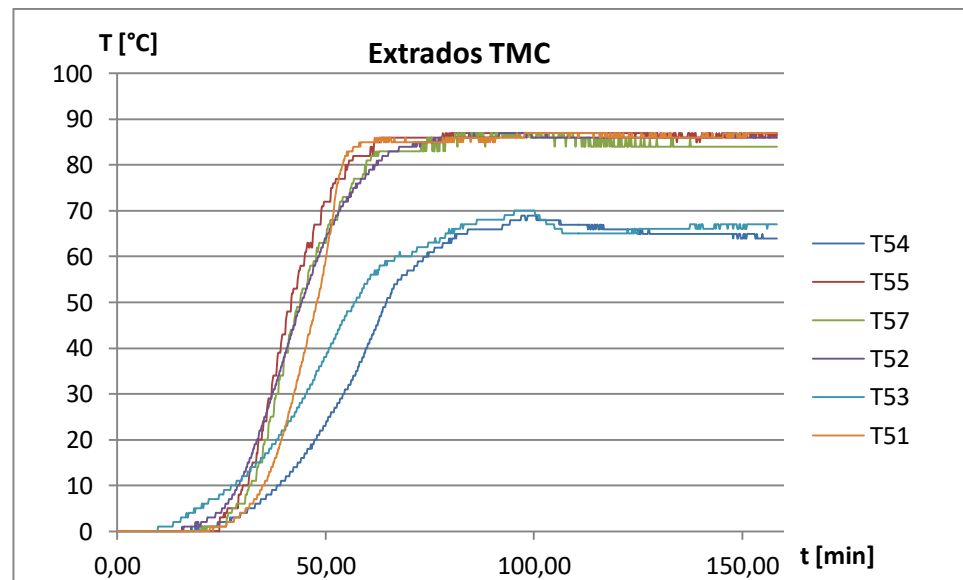


Figure 49 - Temperatures recorded at extrados during test 1B.

#### 4.2.4 Test 1B: displacements

Initial records are overlapped to values obtained during test 1A. Here bilinear behaviour can be easily observed. As expected displacements at crown and springing have same order of magnitude but opposite sign. Following figures are considered.

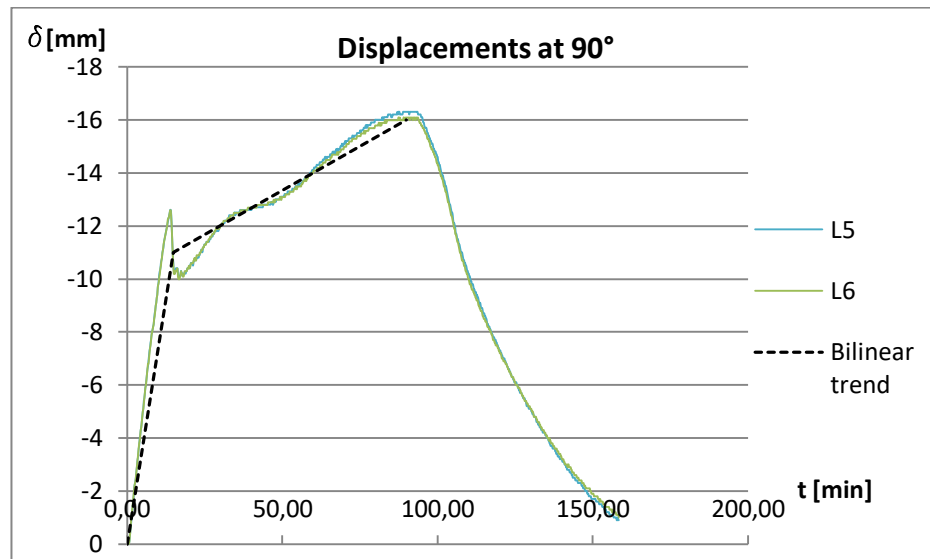


Figure 50 - Experimental displacements at  $90^\circ$ , test 1B.

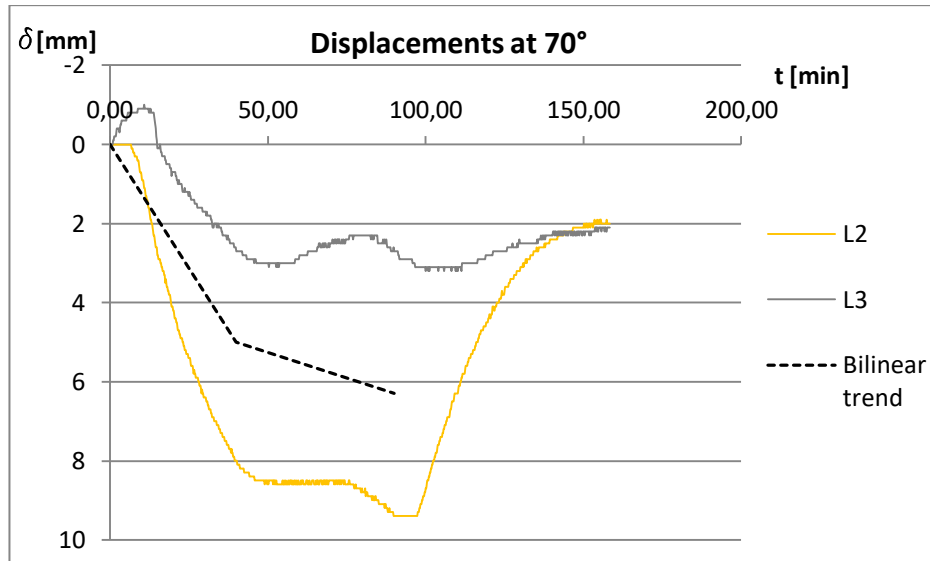


Figure 51 - Experimental displacements at  $70^\circ$ , test 1B.

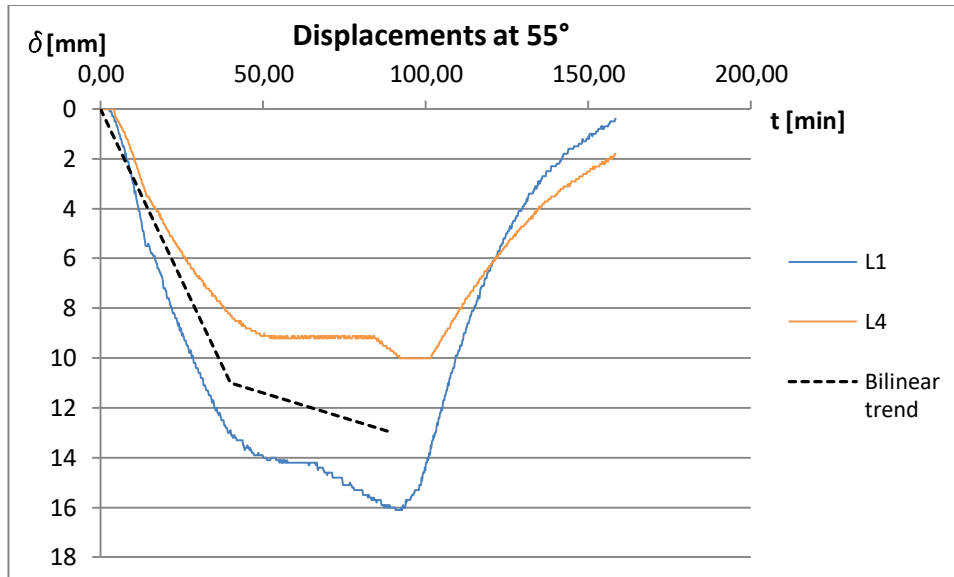


Figure 52 - Experimental displacements at 55°, test 1B.

According to paragraph 3.1, code EN 1363-1:2012 states that experimental records can be used to assess the element in REI terms only if the displacement speed does not exceed the value previously computed. Table 13 shows results obtained. Minutes considered are chosen taking into account slopes in Figure 50, displacements at crown. Average values of extensometers L5 and L6 are considered.

Displacement speed at crown				
$t$ [min]	$\delta$ [mm]	$\Delta t$ [min]	$V$ [mm/min]	$< 4,4$ mm/min
0,00	0,00			
14,00	-12,60	14,00	0,90	verified
17,00	-10,10	3,00	-0,83	verified
35,00	-12,5	18,00	0,13	verified
48,00	-13,00	13,00	0,04	verified
60,00	-14,10	12,00	0,09	verified
90,00	-16,20	30,00	0,07	verified

Table 13 - Displacement speed in test 1B.

## 4.3 Test 2

Temperatures and displacements recorded during test 2 carried out on July 6<sup>th</sup>, 2020 are presented. One thermocouple at intrados, T41, is not working therefore its records are discarded in the analysis. Test is performed for two hours than devices keep on recording data, in order to collect information during the cooling phase simulated by switching the oven off.

### 4.3.1 Test 2: temperatures

Temperatures are plotted in graphs time-temperature. Hence some observations follow.

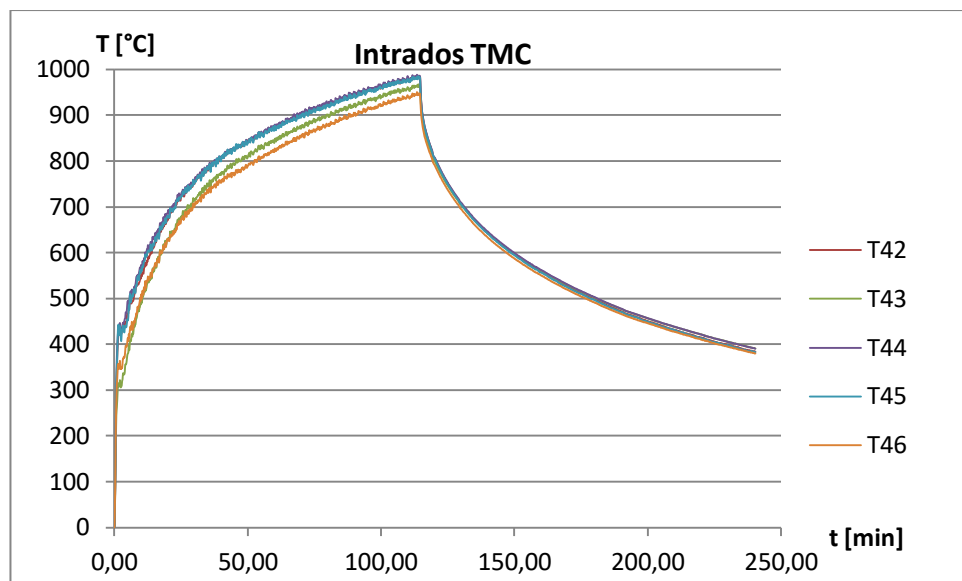


Figure 53 - Temperatures at intrados, test 2.

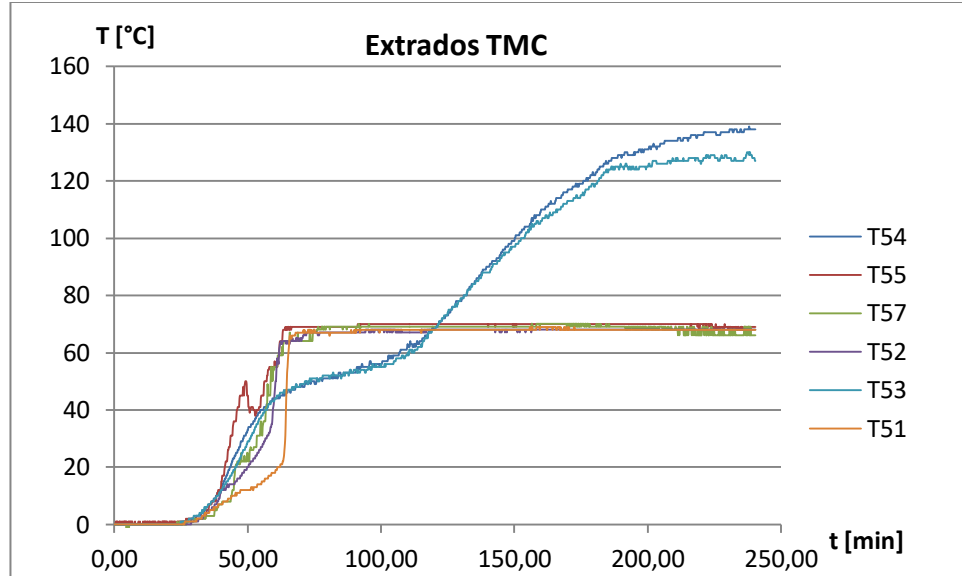


Figure 54 - Temperatures at extrados, test 2.

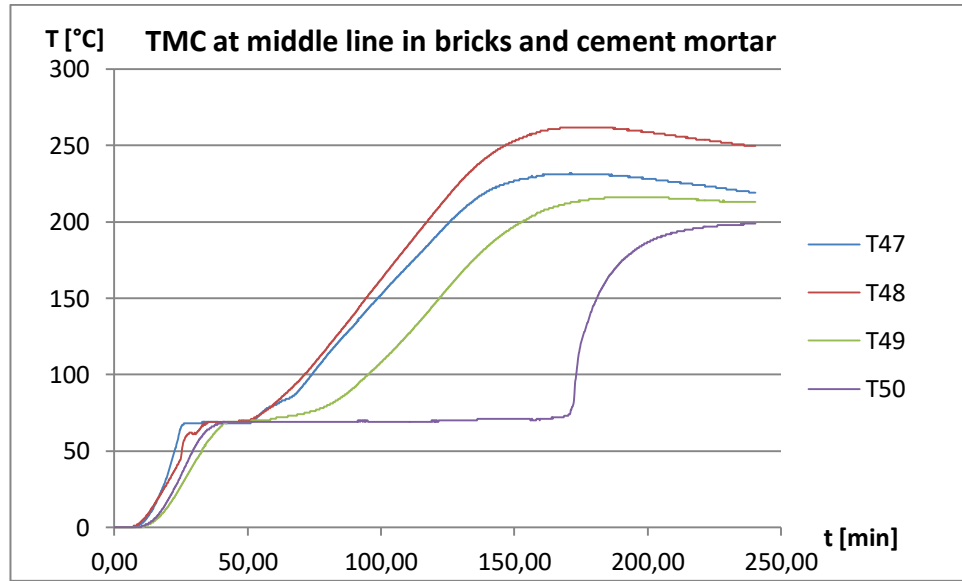


Figure 55 – Temperatures at middle line, test 2.

In graph related to temperatures recorded at intrados can be easily detected the instant when the oven has been switched off since temperatures start decreasing clearly. However the same behavior is not shown by thermocouples at middle line and extrados. In fact a greater role is played by the heat transfer within clay units and cement mortar. Horizontal trends are related to water phase change, temperature is constant while water vapor is

clearly visible on the top of the arch. Once the phenomenon is finished up, temperature starts increasing again because of the heat transfer. It can be observed that a greater presence of moisture has been recorded near T50 than near the other devices since temperature has been maintained constant for longer. Same observations apply for devices at extrados.

#### 4.3.2 Test 2: displacements

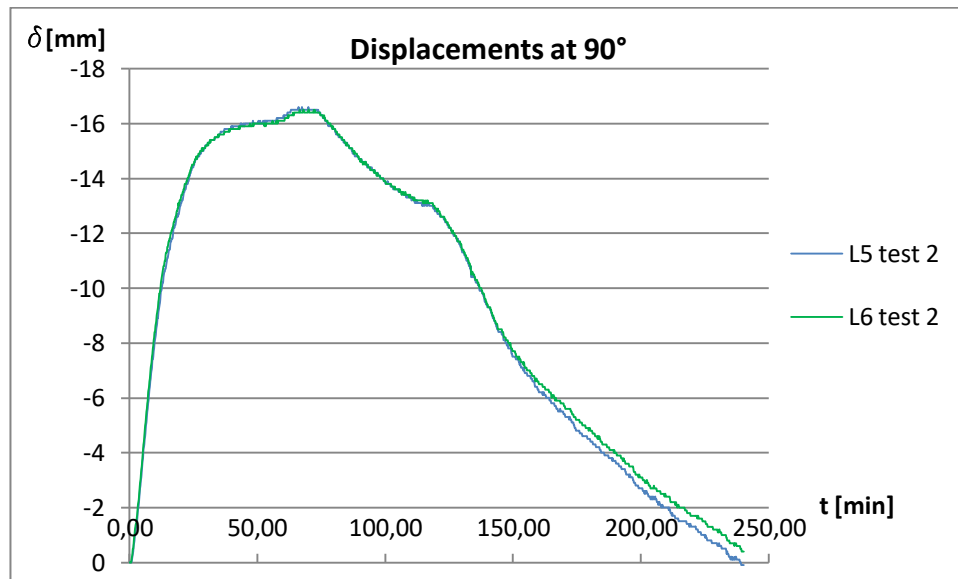


Figure 56 - Experimental displacements at  $90^\circ$ , test 2.

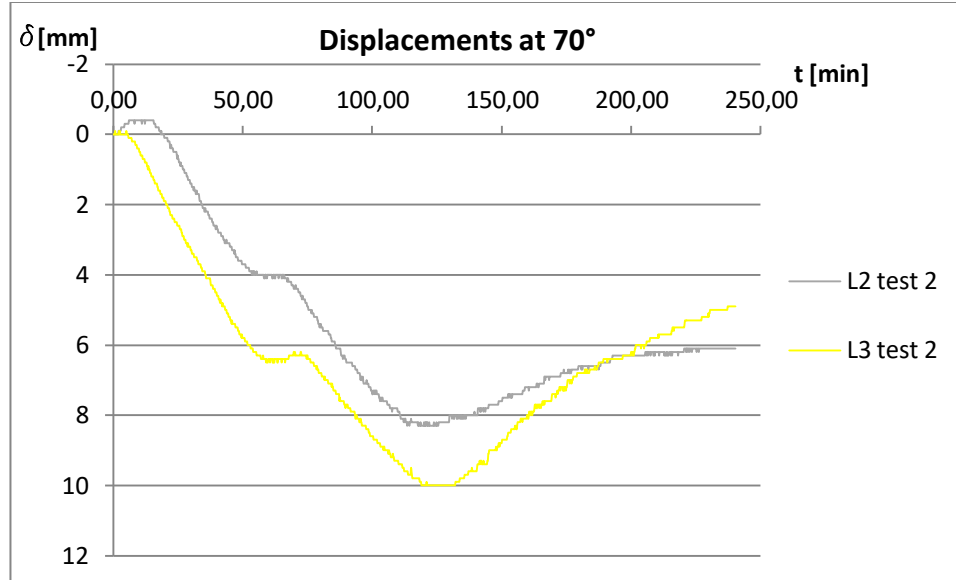


Figure 57 - Experimental displacements at  $70^\circ$ , test 2.

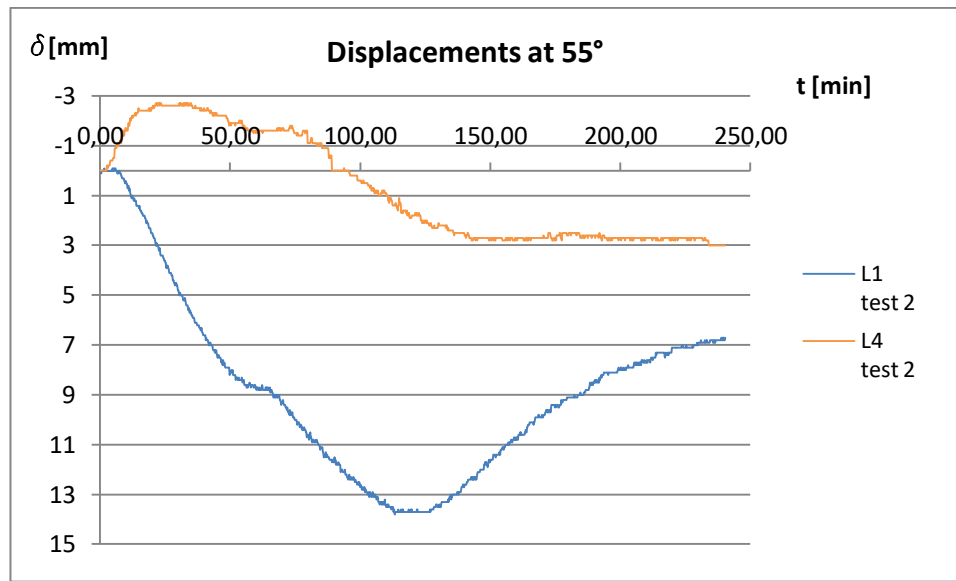


Figure 58 – Experimental displacements, test 2.

Considering that the instant at which the oven has been switched off is subsequent to the displacements decreasing recorded at crown, the latter phenomenon is related to the progressive degradation of the material due to high temperatures applied for long time on the arch. Only a linear behavior is shown. Displacements are kept constant during the same instants.

## Chapter 4 – Tests procedures and results

Displacement speed at crown				
t [min]	$\delta$ [mm]	$\Delta t$ [min]	V [mm/min]	< 4,4 mm/min
0,00	0,00			
28,67	-15,00	28,67	0,52	verified
70,00	-16,55	41,33	0,04	verified
120,00	-12,85	50,00	-0,07	verified

Table 14 - Displacement speed in test 2.

## 4.4 Results comparison

In this section displacements related to tests 1B and 2 are compared graphically.

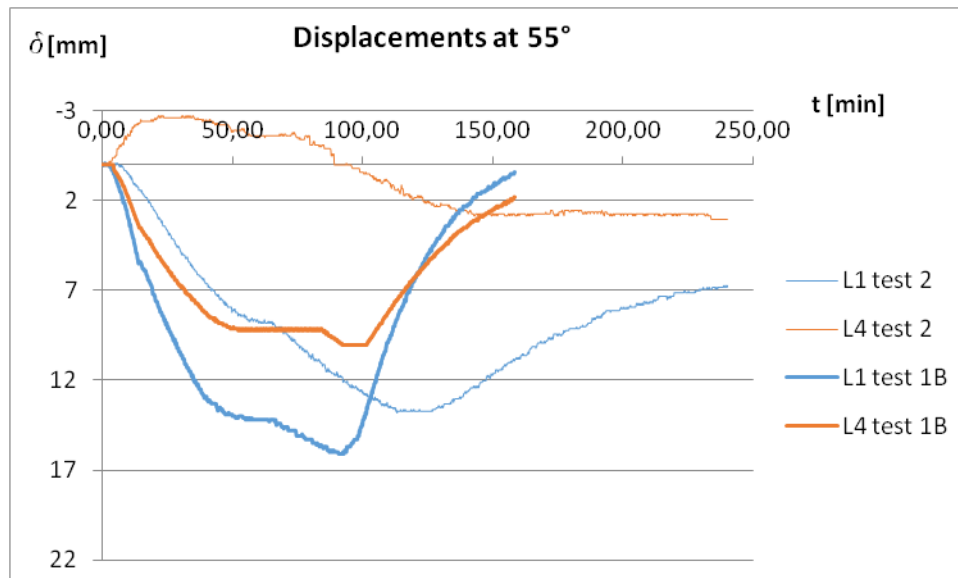


Figure 59 - Displacements comparison at 55°.

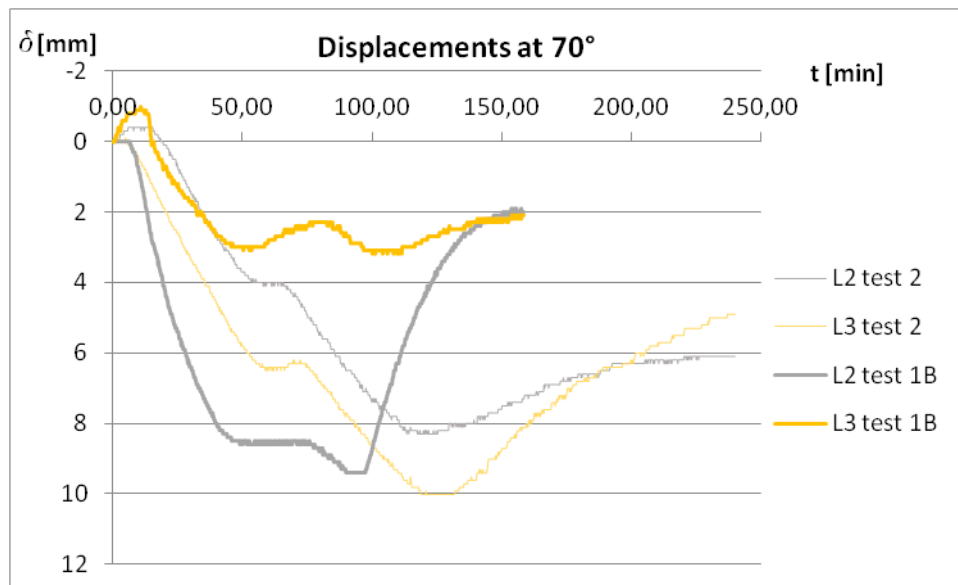


Figure 60 - Displacements comparison at 70°.

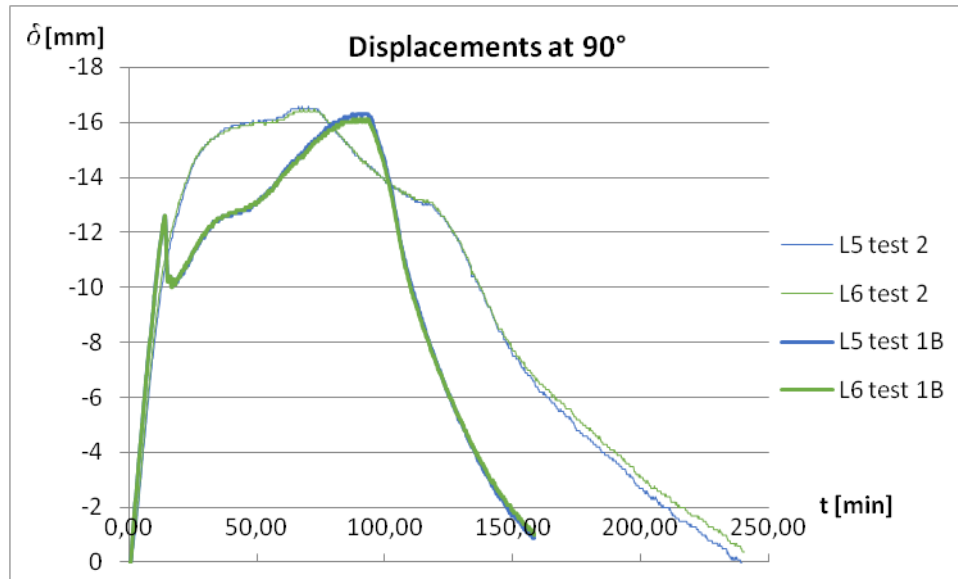


Figure 61 - Displacements comparison at 90°.

# *Chapter 5*

## *Model validation*

---

FireArM numerical model is described and validated. In the first part all steps of the numerical procedure are presented. Later comparison with experimental results in terms of temperature distribution, displacements and deformed shape is shown graphically. Validation is performed by observing how results change as different parameters are set.

---

### **5.1 How the model works**

It is an Excel Macro based on Visual Basic for Applications (VBA) programming language. It is specially designed to study curvilinear structures in fire conditions. It is organized in many spreadsheets, each of them collects or compute different quantities, useful to characterize and solve the problem. Each excel box is linked to a function defined in the macro: temperature-time relation, thermal strain associated to temperature, hence total strains, stresses, internal actions, displacements and eccentricity computation. Since the non linear analysis is based on “forecast error - correction” method, a number of steps should be initially defined. Values just listed are computed per each time step called “step\_th”, for a number of load increment “NN”, both numbers can be chosen by the user. Allowable number of load increment leads a final output, while when overflow occurs for a

given “NN” macro is not able to compute output values, therefore a new analysis should be run setting a lower “NN” which leads to convergence, shown in the warning. Considering that tests studied in this thesis always deal with fire, “load increment” stands for “thermal variation” which is computed using temperatures associated at each time stated in “step\_th” in the temperature distribution within the arch cross section. It is built by imposing average temperatures recorded at crown at extrados and intrados as time goes by (Figure 41). Temperatures in time within the cross section are obtained by finite difference method shown graphically in Figure 12. This procedure is allowable since a great overlap among oven temperatures and ISO 834 curve proposed by the Code is found (Figure 33). In this case a more accurate result is obtained by applying real temperatures recorded through thermocouples directly at arch surfaces, rather than imposing temperatures related to the oven “or room involved in fire”, as Code suggests instead. Regarding the computation of stresses starting from strains, many constitutive laws are available in the model: first five laws do not account temperature variations, hence are discarded in this paper, laws “6” and “7” are related to thermal gradient and used for the validation of the model. Input parameters are shown in Table 14. The final goal is to compare numerical results, obtained by means of different input parameters, to experimental ones in order to validate the model.

Following spreadsheets are present:

- INPUT: in this part user can set general data of the problem. It is organized in several sections: arch general data, constitutive laws  $\sigma - \varepsilon$  available, material mechanical characteristics such as compressive strength  $f_y$ , Young Modulus  $E$ , tensile strength  $f_{ct}$ ,

instant of fire evaluation, fire curve, thermal characteristics of the material and arch geometry. It is important to make clear that parameter “ $G_{2,riemp}$ ” refers to filler material load which is considered spread on the whole surface, while in laboratory part of the surface at springing is not actually loaded since it acts as support (Figure 21). In order to consider this discrepancy between numerical modeling and real configuration in laboratory, density of the filler material is adjusted, it is decreased in the macro since larger volume is occupied. Voussoirs number “N” is linked to the level of accuracy of the final result, higher discretization leads to preciser values and longer computational times. Hence “N” is the number of rows in Table 15. Perfect constraints are assumed since imposed displacements are null, arch fixed at both ends is the static scheme used. Seven possible constitutive laws  $\sigma - \varepsilon$  are available, however only “EC 1-2 – decadimento legame costitutivo” and “Sassu et al.” are assumed as they consider temperature changes. Regarding laws which relates thermal strains to temperature  $\varepsilon_T - T$ , three possible functions are defined in the VBA code: EC6 which fixes maximum thermal strain at 5%, two relations which maintain trend proposed by the Rule but changing maxima values by applying 0.5 and 1.5 coefficients. Looking at fire curve listed, only the last one which is built on experimental data recorded during test 1A is used, since it is the most accurate. Generally other curves are applied during the design stage of buildings and the “6” was considered in the previous paper.

## Chapter 5 – Model validation

Dati generali dell'arco			
L=	2.285	Luce arco (mm)	
B=	1.000	Base dell'arco (mm)	
G <sub>2,riemp</sub> =	1.145	Peso specifico riempimento (daN/m <sup>3</sup> )	
G <sub>1,arco</sub> =	1.800	Peso specifico arco (daN/m <sup>3</sup> )	
G <sub>2,v+Qk</sub> =	0	Carico verticale agente (daN/m)	
N=	120	Numero di conci dell'arco	
interarch=	1.000	Interasse degli archi (mm)	
tuttocarico=	1	1=tuttocarico; 0=metà carico	
yg=	0	Posizione del baricentro delle sezioni rispetto ad H/2	
NN=	16	Numero di incrementi del carico esterno (NN=1 coincide con carico iniziale senza incremento)	
factor=	0,00	Incremento di carico variabile per ogni step (daN/m)	
factor2=	0,00	Incremento di carico concentrato per ogni step (%) laddove già presenti	
coefforizz=	0,00	Rappporto tra carichi verticali e orizzontali	
Dati delle leggi costitutive			
Tipo=	6	1 Lineare elastico traz e comp 2 Lineare fino a rottura traz. e comp. 3 Lineare fino rottura solo compressione 4 Lineare e plastica solo compressione 5 Lineare e plastica trazione e compressione 6 EC6 1-2 - Decadimento legame costitutivo 7 Sassu et al.	
fy=	20,00	Tensione di rottura a compressione [MPa]	
E=	5.000	Modulo elastico [MPa]	
fct=	1,80	Resistenza a trazione [MPa]	
Istante di valutazione dell'incendio			
t=	0	Tempo di stima delle sollecitazioni (30-60-90-120-150-180) Inserire tempo / istante di inizio valutazione "0" = condizioni ordinarie	
Tipologia di incendio			
Tipo=	7	1 Iso 834 - prevalenza cellulosa 2 Fuoco esterno 3 Idrocarburi 4 Riscaldamento lento 5 RSW 6 Prova sperimentale VVF 2015 7 Prova sperimentale VVF 22/01/2020	
step_th	1	Incremento della variabile "tempo" ad ogni incremento di carico per raggiungere il tempo di valutazione dell'incendio (non alterare formula)	
Caratteristiche termiche materiale (mattone+malta)			
λ	0,84	Conducibilità termica [W/mK] - valori a T=20°C	
ρ	1.800	Densità volumica [kg/mm <sup>3</sup> ] - valori a T=20°C	
c	1.000	Calore specifico [J/kgK] - valori a T=20°C	
Geometria arco muratura (valido solo se arco di circonferenza)			
R	1.550,00	Raggio filo medio della sezione	
α	94,99	Angolo complessivo arco	
α0	42,51	Angolo di inizio arco	
H	120,00	Spessore sezione (costante)	

Table 15 - Input data.

Geometria arco	Geometria dei conci			Carichi impliciti		Carichi espliciti
	ascisse dei punti	ordinate dei punti	altezza della sezione	lambda imp	mu imp	concentrati verticali
Num. conci	Z (mm)	Y(mm)	H(mm)	(1/mm)	(1/mm)	(N)
0	0,00	0,00	120,00	0,00	0,00	0,00
1	14,58	15,69	120,00	0,00	0,00	0,00
2	29,37	31,17	120,00	0,00	0,00	0,00
3	44,38	46,44	120,00	0,00	0,00	0,00
4	59,60	61,51	120,00	0,00	0,00	0,00
5	75,02	76,37	120,00	0,00	0,00	0,00

Table 16 - Part of attachment 1, test 1A, function of input data.

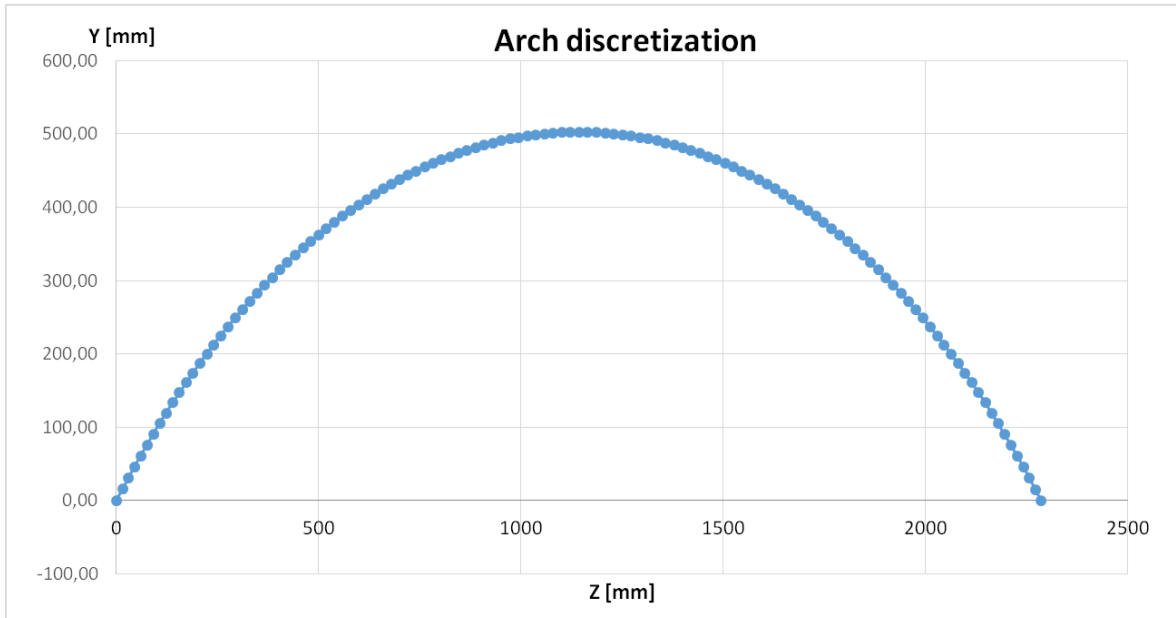


Figure 62 - "N" points discretization, function of input data.

cedimenti vincolari	
eta 1 (rad)=	0,00
eta 2 (mm)=	0,00
eta 3 (mm)=	0,00
eta 4 (rad)=	0,00
eta 5 (mm)=	0,00
eta 6 (mm)=	0,00

Figure 63 - Imposed displacements at constraints.

- **THERMAL MAP COMPUTATION:** temperature changing within the arch thickness is described in 120 fibers, including arch intrados (0) and extrados (120). These data depend on curve set in the previous spreadsheet in the section “fire type” and “thermal

characteristics of the material”. In this part the procedure described in chapter 2.2 is adopted to represent the heat transfer within the arch. Since the model considers an uniform thickness along the curvilinear axis z, thermal map is valid for each section. On the bottom right of the graph it can be observed that fibers closer to extrados record later warming since room temperature is maintained for longer. On the contrary on the top left intrados is heated more quickly, as expected. Red curve describing temperatures at 60' shows a failure which can be easily detect on fibers closer to intrados: here temperatures are lower with respect to previous instants. This is due to the fact that fire curve used “Prova sperimentale VVF 22/01/2020” provides temperatures till 50', then no info are available and the model cannot work properly. In this example the last instant of interest is at 48', last reliable curve is at 50'.

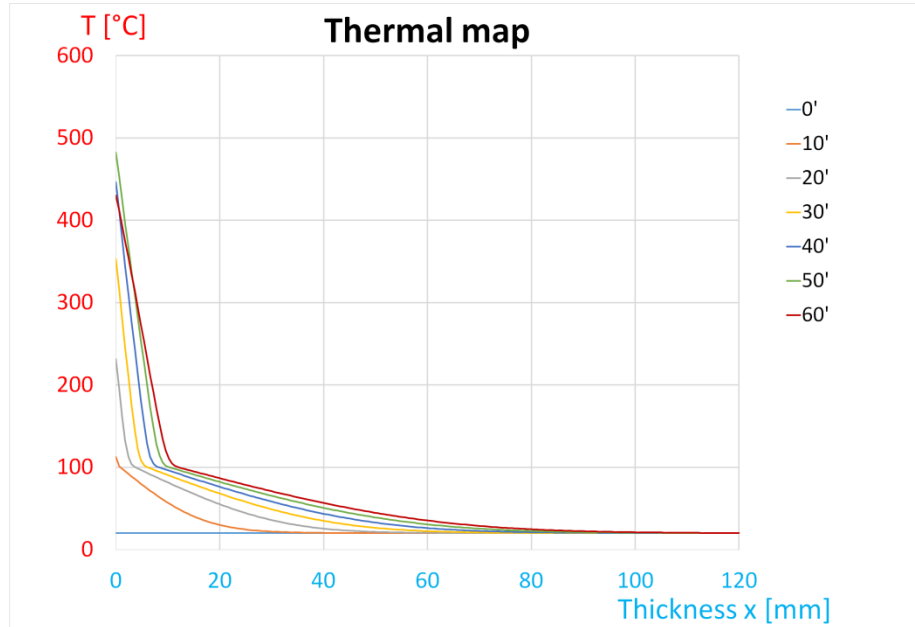


Figure 64 - Thermal map example till minute 50, test 1A (attachment 2).

- **COMPUTATION OF DEFORMABILITY AND STIFFNESS MATRICES:** are two matrices  $[d]$  3x3 and  $[K]$  6x6 respectively which are assumed constant thanks to

hypothesis described in paragraph 2.3, values do not depend on temperature changing in time. Deformability matrix is symmetric. Elements are displacements due to unitary force or moment applied to restore restrain degrees removed in the equivalent isostatic arch. Principle of virtual works is used, shear effects are neglected. Stiffness matrix defined as  $[K] = [d]^{-1}$  relates unitary nodal displacements to internal actions in the equivalent isostatic structure.

- **COMPUTATION OF INTERNAL ACTIONS, DEFORMED SHAPE AND ECCENTRICITY:** for each section, set in step 1 (in this example 120), bending moments, normal forces and displacements are computed. Two graphs show internal actions and the deformed shape in time along the arch axis. The eccentricity which is compute as the ratio between bending moment and normal force, allows to understand stability conditions of the arch. In fact when eccentricity exceeds a threshold value thrust-line falls outside the cross section core, leading the arch to a wrong working mechanism.

$$e = \frac{M_y}{N_z}$$

- **COMPUTATION OF NORMAL STRAINS AND STRESSES:** for each fiber and at each instant strains and stresses are obtained. Model computes total strains as the sum of strains due to mechanical loads, arch own weight and distributed loads on the arch, and thermal strains due to temperature variations. Both lead to an increase of internal stresses because of the restrain degree of the arch.

## 5.2 Validation procedure

By setting experimental parameters related to Test 1A numerical model does not succeeds in convergence. Therefore the validation goes on by means of two procedures:

- Choice of the representative constitutive law of the material, both in terms of thermal strains – temperatures ( $\varepsilon_T - T$ ) and stresses – strains ( $\sigma - \varepsilon$ ).
- Change input data in order to reach displacements obtained during experimental results.

First the goodness of constitutive law used is tested, then numerical code inputs are modified in order to obtain results which fits best experimental ones. In the first part results of Test 1A related to displacements at the crown are considered, L6 records are used.

More than one constitutive law is available, first Eurocode prescriptions are tested, than laws proposed by academic articles. Although it is already known in the previous paper that Eurocode constitutive law does not describe properly the real behavior, it is the compulsory starting point since it is law.

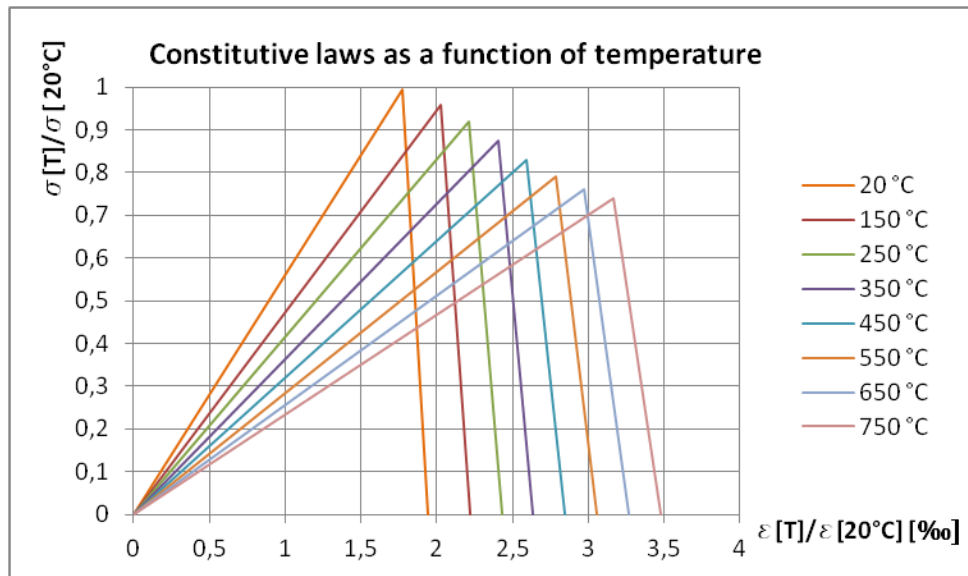


Figure 65 - Eurocode 6 constitutive laws.

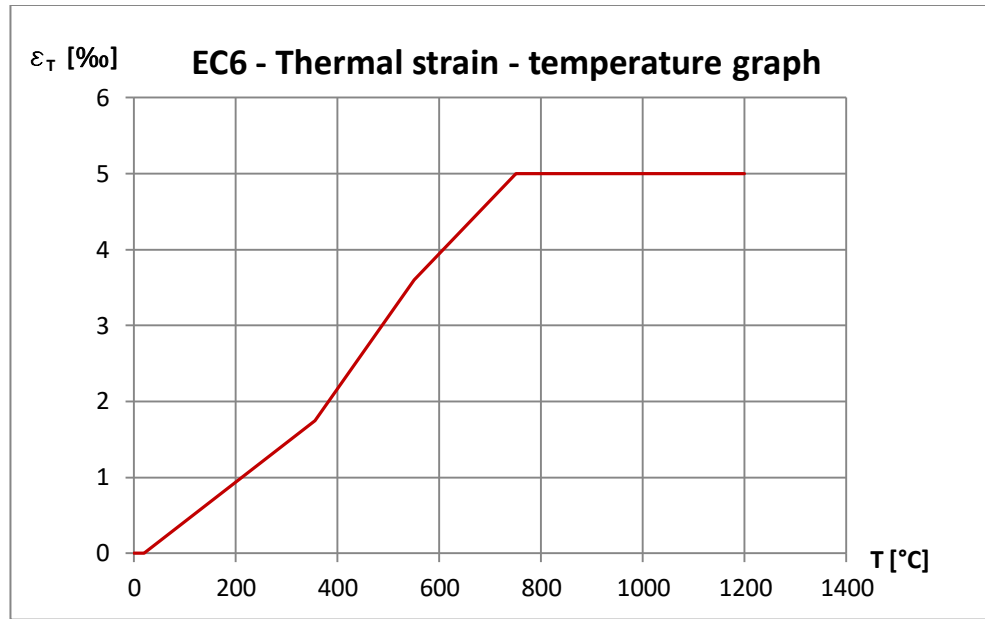


Figure 66 - Eurocode 6 thermal strain-temperature graph.

Relationships proposed by the Rule for thermal strain - temperature and stress - strain are implemented in the model and used to achieve following results. Are considered two values of tensile strength: null and 2% of the compressive strength. Also in this case it is already known that tensile strength exists and the second value best reproduces experimental results, however considering different tensile strength is useful to understand how the model works, therefore how to modify it properly. Looking at results, it is clear that thermal strains - temperatures law proposed by the Code is not representative of the thermal behavior of clay units used in the arch.

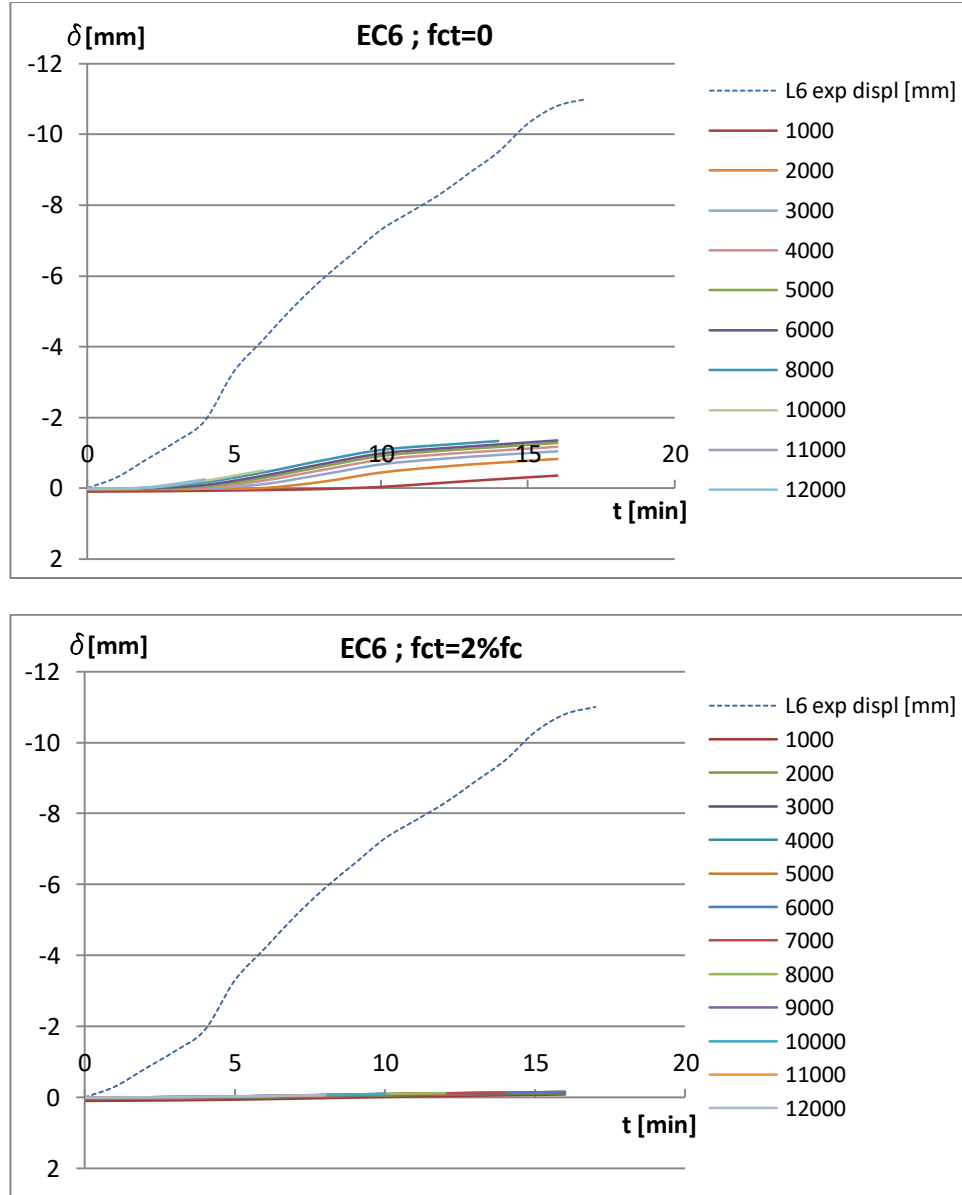


Figure 67 - Numerical results assuming relationships suggested by Eurocode 6.

In order to accomplish a better matching between numerical and experimental results, strains - temperatures law is modified maintaining same trend. Table 17 and Figure 68 show two different strains - temperature laws applying 0,5 and 1,5 factors to the European law. Stress-strain relationship is maintained equal to the previous one.

T [°C]	epsT EC6	epsT 0,5*EC6	epsT 1,5*EC6
0	0	0	0
20	0	0	0
355	1,75	0,875	2,625
550	3,6	1,8	5,4
750	5	2,5	7,5
1200	5	2,5	7,5

Table 17 - Thermal strains - temperatures laws according to Eurocode 6 and two possible alternatives.

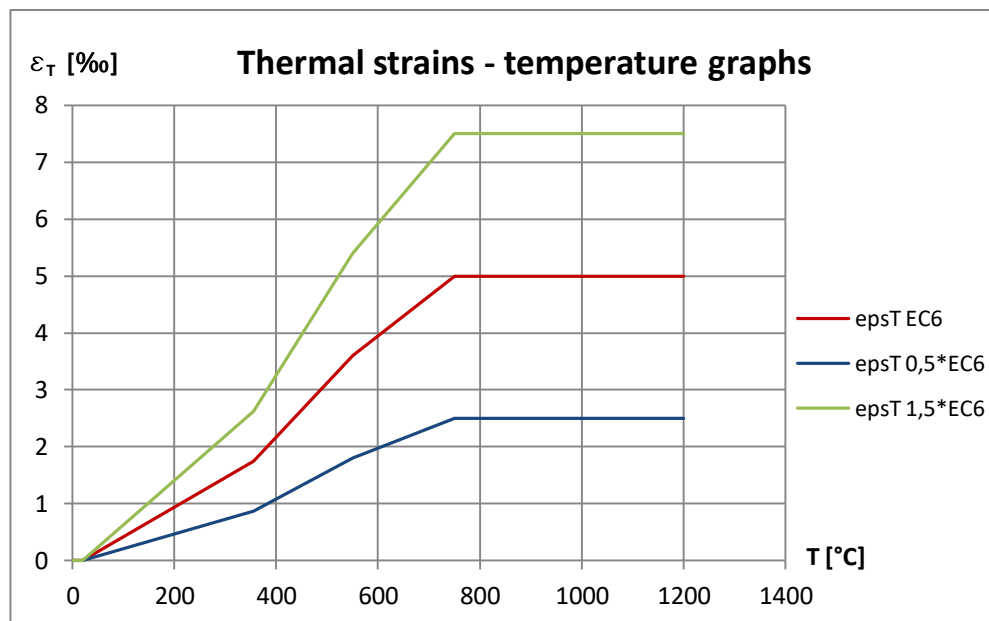


Figure 68 - Thermal strains - temperatures graphs related to data in table 16.

By increasing the masonry Young Modulus  $E$ , results obtained seems unrealistic since the stiffer is the material the higher are displacements computed by the numerical model (Figure 69). This is linked to the growth of a discontinuity at the crown, which prevent the convergence when higher loads increments are set.

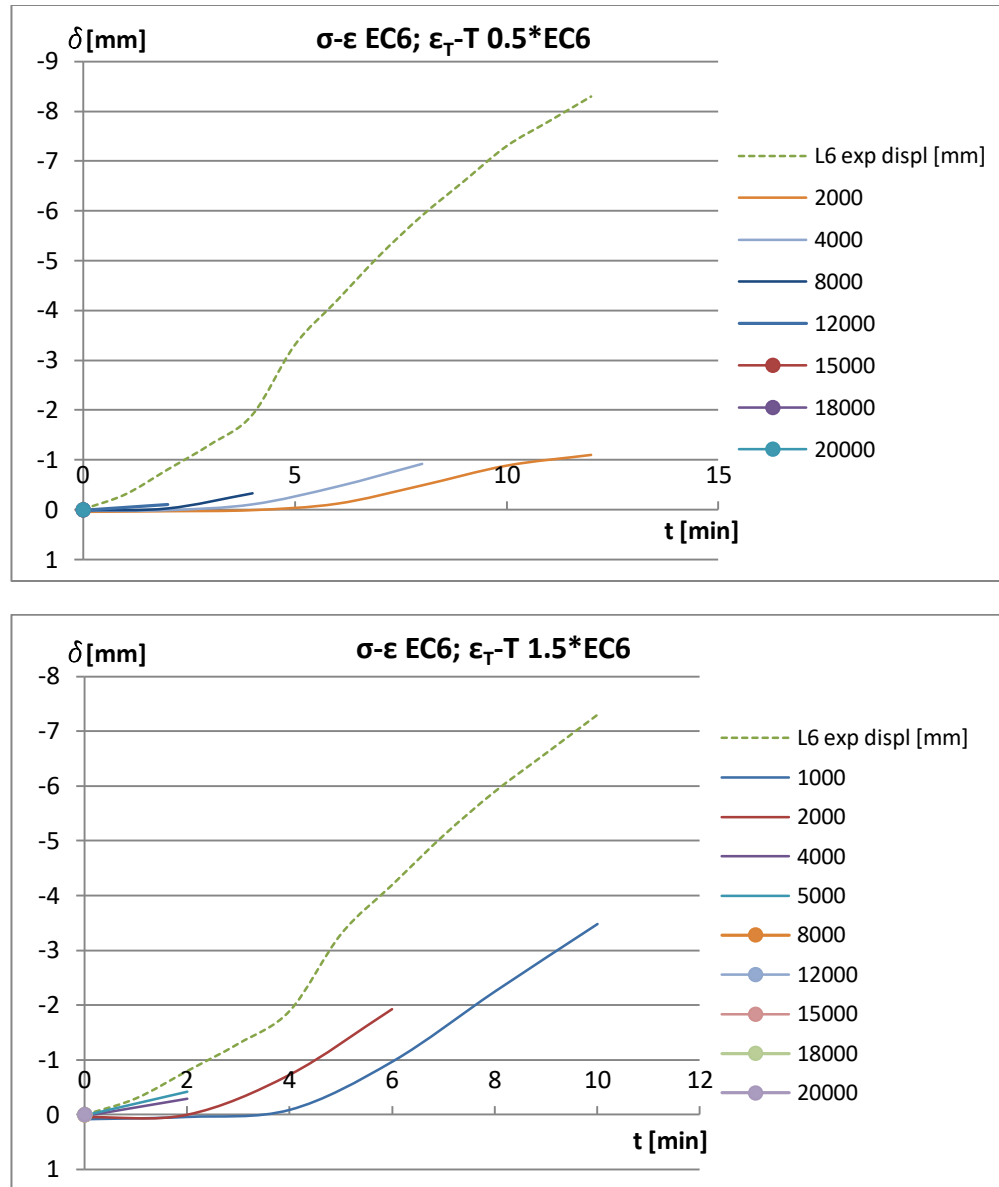


Figure 69 – Numerical results assuming alternative thermal strains – temperature graphs.

Regarding stresses – strains constitutive law, a possible alternative to EC 6 is Sassu et al. These laws are very different since the Rule describes clay units behavior using two branches, the linear elastic and the linear brittle while Sassu et al. paper shows only the first part till the yield stress (Figure 70). This difference is appreciable in numerical outputs (Figure 71, Figure 72). Thermal strains – temperatures proposed by the Code is used.

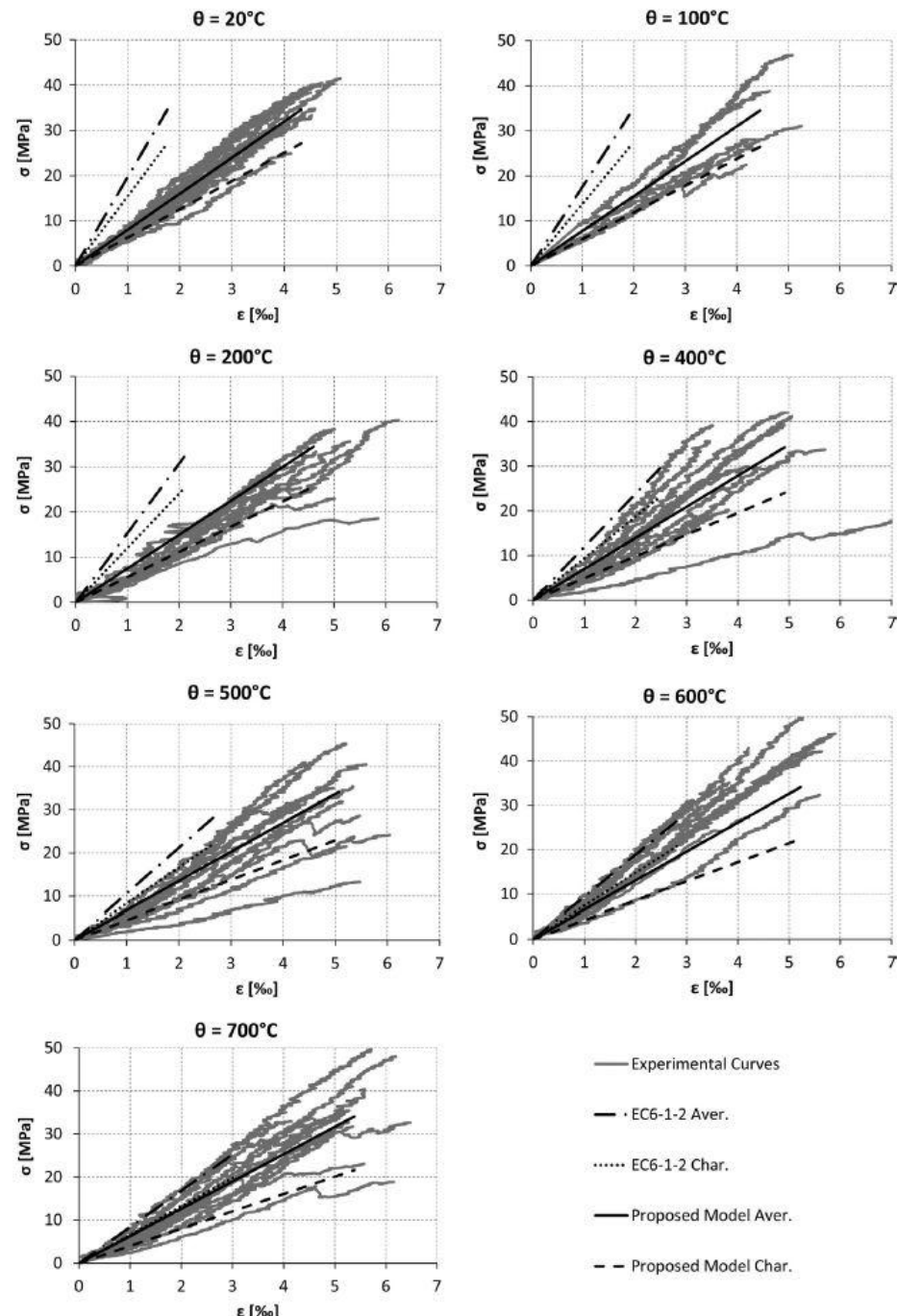


Fig. 5. CLAY: Comparison between EN 1996-1-2 [18] and proposed model with experimental curves.

Figure 70 - Sassu et al. constitutive laws.

## Chapter 5 – Model validation

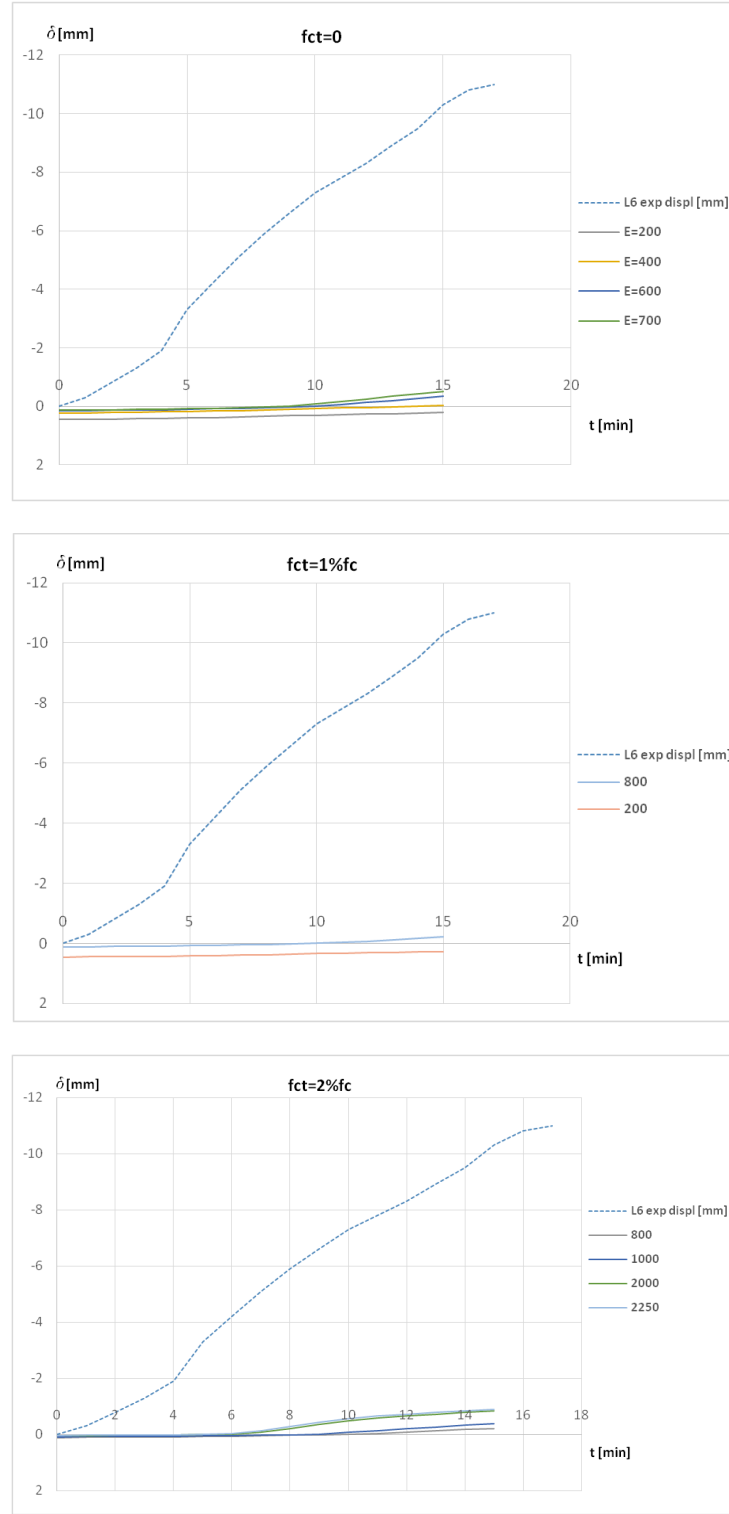


Figure 71 - Numerical results assuming Sassu et al. constitutive law, by changing tensile strength.

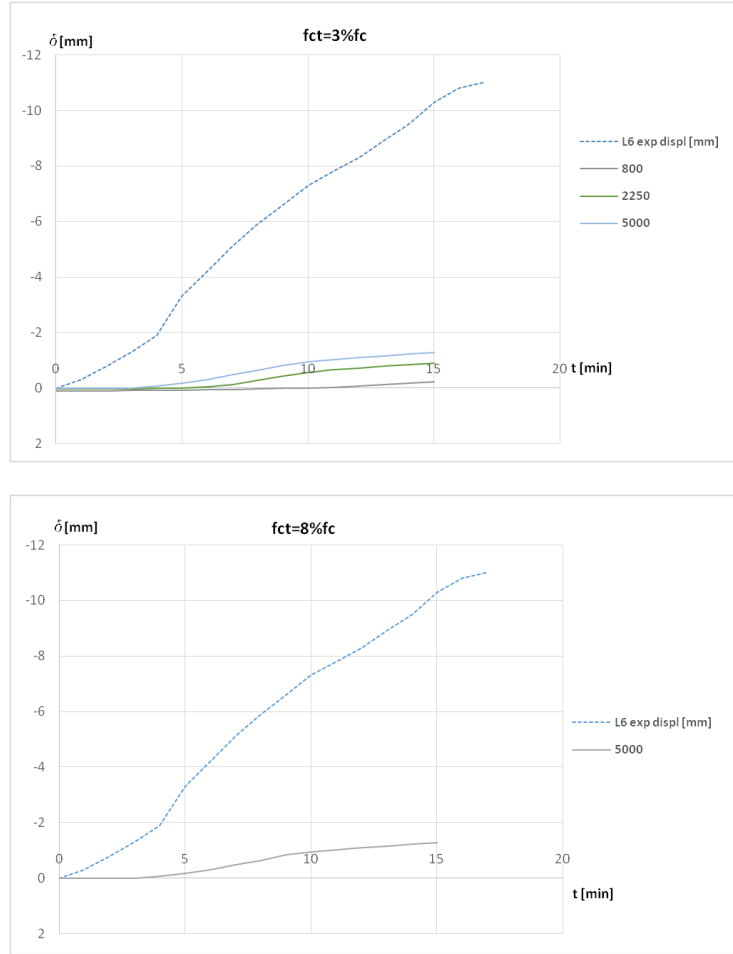


Figure 72 - Numerical results assuming Sassu et al. constitutive law, by changing tensile strength  
 (2).

The overall loss of matching between numerical and experimental results, can be probably due to a different configuration, grown as a consequence of local failure which leads to a new static scheme. In fact during test 1A section at the crown cracks completely, therefore the arch starts to behave as two separate cantilever semi-arches, statically determined. The section at the keystone is unloaded, it does not carry any normal, shear force or bending moment. Hence thermal variations will provide only strains and displacements in both semi-arches, while internal forces remain null considering structure own weight and filling material weight negligible. Whereas compatibility at the crown is changed, numerical

model cannot reach anymore the convergence at the cracked section, hence it cannot provide outputs for this configuration. These observations explain why numerical results are so far from experimental records.

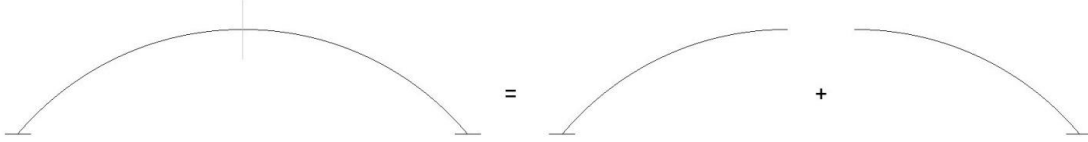


Figure 73 - New static scheme after the failure at the crown.

In order to set input parameters as closer as possible to real values and describe this behavior, coefficient of thermal expansion  $\alpha$  is computed by using Principle of virtual works (PVW), imposing the vertical displacement at the crown recorded during Test 1A. As the symmetry of the problem allows, only half arch is studied by assuming null rotations and horizontal displacements of the upper free edge. Regarding loading conditions the arch is supposed mass less, free from any mechanical loads, the thermal variation along the arch transversal cross section is assumed constant and linear applying the superposition principle (Table 19). Average values of thermocouples at crown T43-T44 and T55-T57 are considered. Instants  $t = 5; 10; 15 \text{ min}$  are used.

<b>t [min]</b>	<b>0</b>	<b>5</b>	<b>10</b>	<b>15</b>
<b><math>\Delta T_{ext} [\text{°C}]</math></b>	0	0	0	0
<b><math>\Delta T_{int} [\text{°C}]</math></b>	0	84	111	163

Table 18 - Average records of thermocouples at crown.

$$\Delta T_{const} = \frac{\Delta T_{intr} + \Delta T_{extr}}{2}$$

$$\Delta T_{lin} = \frac{\Delta T_{intr} - \Delta T_{extr}}{2}$$

$\Delta T [^{\circ}C] / t [min]$	0	5	10	15
<b>constant</b>	0	42	55,5	81,25
<b>linear</b>	0	42	55,5	81,25

Table 19 - Constant and linear temperature variations.

Considering that thermal strains - temperatures graphs links null thermal strains to a temperature change of  $20^{\circ}C$ , values used in the analysis are:

$\Delta T [^{\circ}C] / t [min]$	5	10	15
<b>constant</b>	22	35,5	61,25
<b>linear</b>	22	35,5	61,25

Table 20 - Adjusted thermal variations.

Now that thermal loading is defined, the parameter can be computed. The principle of virtual work states that the external virtual work is equal to the virtual external force multiplied by the real external displacement and the internal virtual work is equal to the virtual internal force multiplied by the real internal strain. External and internal virtual works are equal to each other. This is a method based on energetic principle, one of the energy methods in structural analysis, which generally allows to calculate deflections in statically determinate and indeterminate structures. However this section is introduced to compute thermal characteristics of the material, such as coefficient of thermal expansion, assuming displacements known by the experimentation. The length of the semi-arch is described in infinitesimal parts as:

$$ds = R d\varphi$$

Unitary forces are applied where displacement is known.

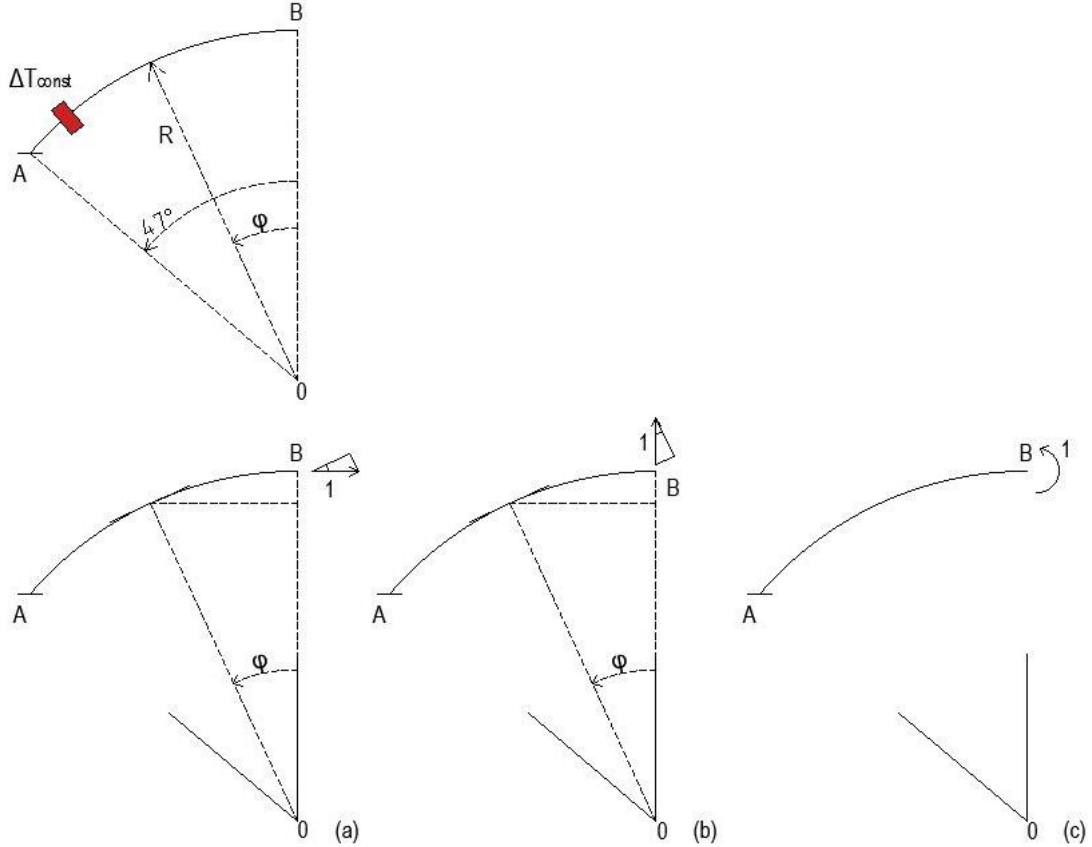


Figure 74 - Principle of virtual works applied to cantilever semi arch subject to constant thermal variation along transversal cross section and longitudinal axis.

Principle of Virtual Works can be written as:

$$L_{ext} = L_{int}$$

$$1 \cdot u_B = \int_S N' \cdot \varepsilon_T ds \rightarrow u_B = \int_0^{\frac{47\pi}{180}} R \cos \varphi \cdot \alpha \Delta T_{const} d\varphi$$

$$1 \cdot v_B = \int_S N'' \cdot \varepsilon_T ds \rightarrow v_B = \int_0^{\frac{47\pi}{180}} R \sin \varphi \cdot \alpha \Delta T_{const} d\varphi$$

$$1 \cdot \varphi_B = \int_S N''' \cdot \varepsilon_T ds \rightarrow \varphi_B = 0$$

Only equation related to vertical displacement is considered since it is the only experimental value available. The same procedure is followed considering the curvature

related to linear thermal variation. Considering temperatures for each instant, values of coefficient of thermal expansion can be obtained.

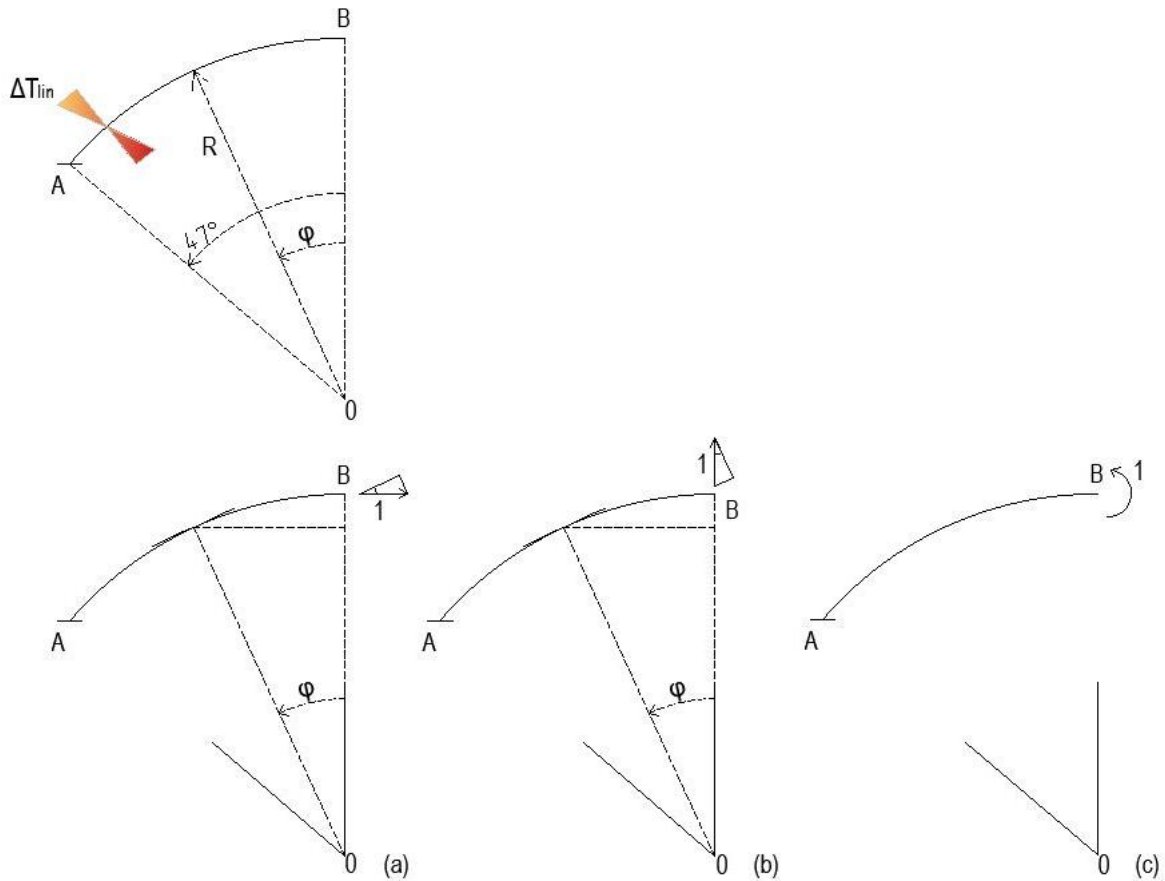


Figure 75 - Principle of virtual works applied to cantilever semi-arch subject to linear thermal variation along transversal cross section and longitudinal axis.

$$L_{ext} = L_{int}$$

$$1 \cdot u_B = \int_S M' \cdot \chi_T ds \rightarrow u_B = \int_0^{\frac{47\pi}{180}} R^2 (\cos \varphi - 1) \cdot \frac{2\alpha \Delta T_{lin}}{H} d\varphi$$

$$1 \cdot v_B = \int_S M'' \cdot \chi_T ds \rightarrow v_B = \int_0^{\frac{47\pi}{180}} R^2 \sin \varphi \cdot \frac{2\alpha \Delta T_{lin}}{H} d\varphi$$

$$1 \cdot \varphi_B = \int_S M''' \cdot \chi_T ds \rightarrow \varphi_B = \int_0^{\frac{47\pi}{180}} R \cdot \frac{2\alpha \Delta T_{lin}}{H} d\varphi$$

Since constant and linear thermal variations are applied at the same time on the semi-arch, according to Superposition Principle, experimental displacement can be written as:

$$\delta_B(t) = R\alpha\Delta T_{const}(t) \int_0^{47\pi/180} \sin\varphi d\varphi + R^2 \frac{2\alpha\Delta T_{lin}(t)}{H} \int_0^{47\pi/180} \sin\varphi d\varphi$$

<b>H [mm]</b>	120		
<b>R [mm]</b>	1550		
<b>integrale</b>	0,318		
<b>t [min]</b>	<b>5</b>	<b>10</b>	<b>15</b>
<b>v<sub>b</sub> [mm]</b>	-3,3	-7,3	-10,3
<b>α[°C<sup>-1</sup>]</b>	1,134E-05	1,55E-05	1,27E-05
<b>Average α[°C<sup>-1</sup>]</b>	1,3201E-05		

Table 21 - Coefficient of thermal expansion computation.

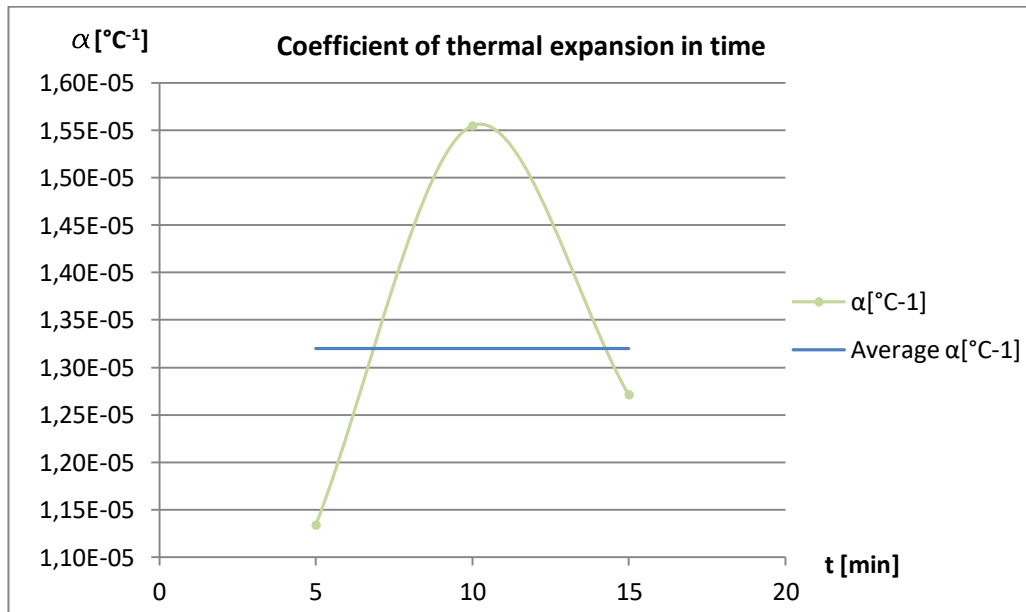


Figure 76 - Coefficient of thermal expansion in time.

T [°C]	$\alpha$ EC6	$\alpha$ 0,5*EC6	$\alpha$ 1,5*EC6
0	0	0	0
20	0	0	0
65	0,005224	0,00261194	0,00783582
355	0,005224	0,00261194	0,00783582
550	0,009487	0,00474359	0,01423077
750	0,007	0,0035	0,0105
1200	0	0	0

Table 22 - Coefficient of thermal expansion in thermal strains-temperatures graphs.

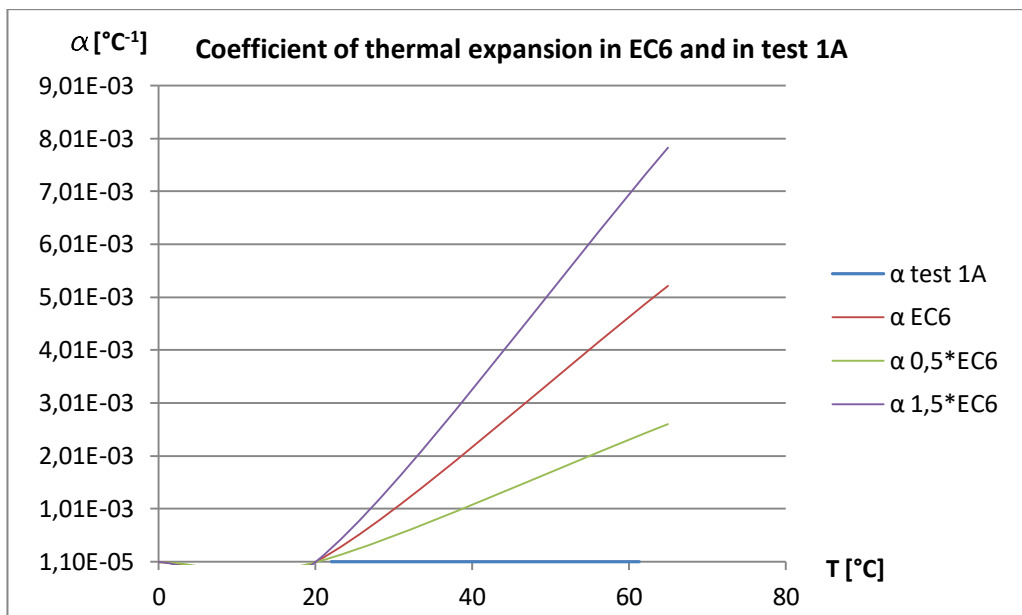


Figure 77 - Coefficient of thermal expansion comparison.

As shown in Figure 77 a great difference between coefficients of thermal expansion exists.

Validation is carried out by considering displacements at the crown obtained during the second test. Constitutive law suggested by the European Rule are assumed, while thermal strains-temperature relationship is modified. For each graph different Young Modula [MPa] are tested.

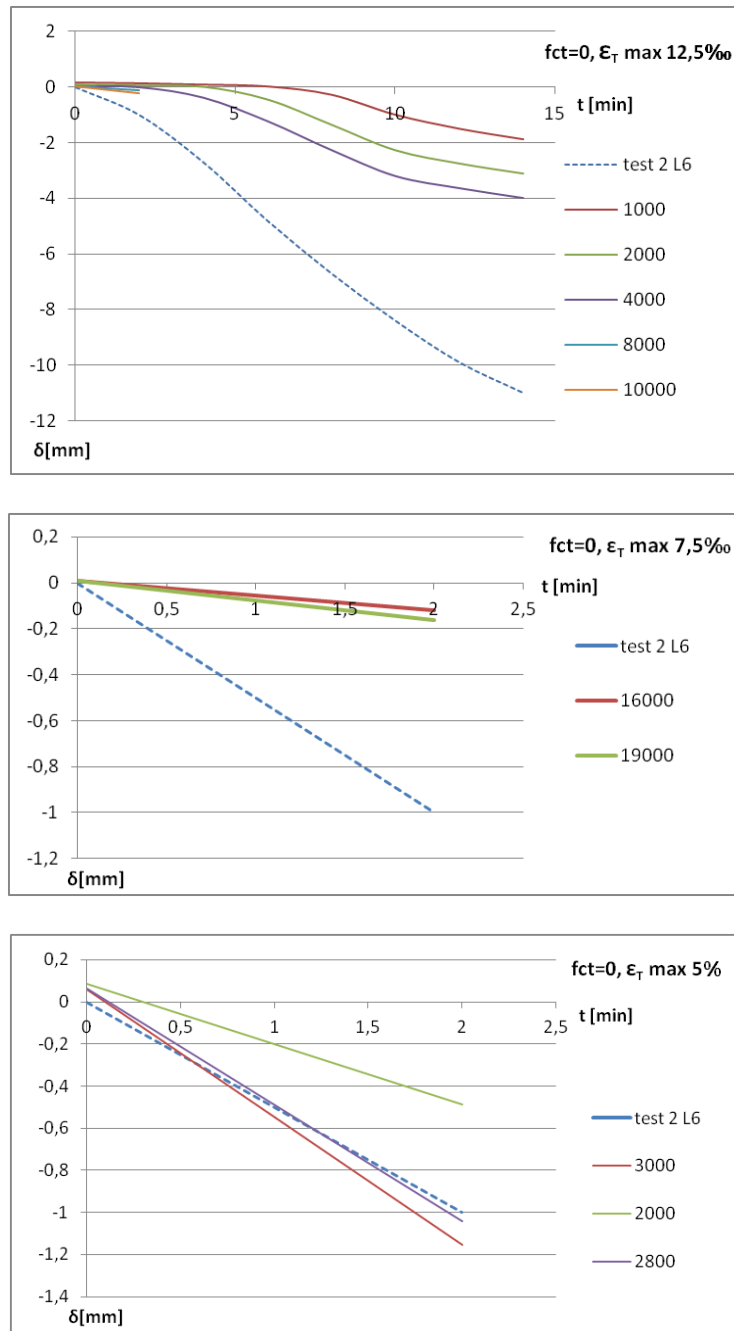


Figure 78 - Numerical results compared to test 2 outputs.

### 5.3 Experimental and numerical comparison

#### Temperatures comparison:

- Validation at keystone, considering TMC 43-44 (intrados) and 55-57 (extrados). The following graph has been obtained by plotting the first row (which represent numerical temperatures in time on intrados) and the last one (numerical temperatures in time on extrados) of the attachment 2. Data are overlapped to average experimental records to appreciate differences (Figure 79).

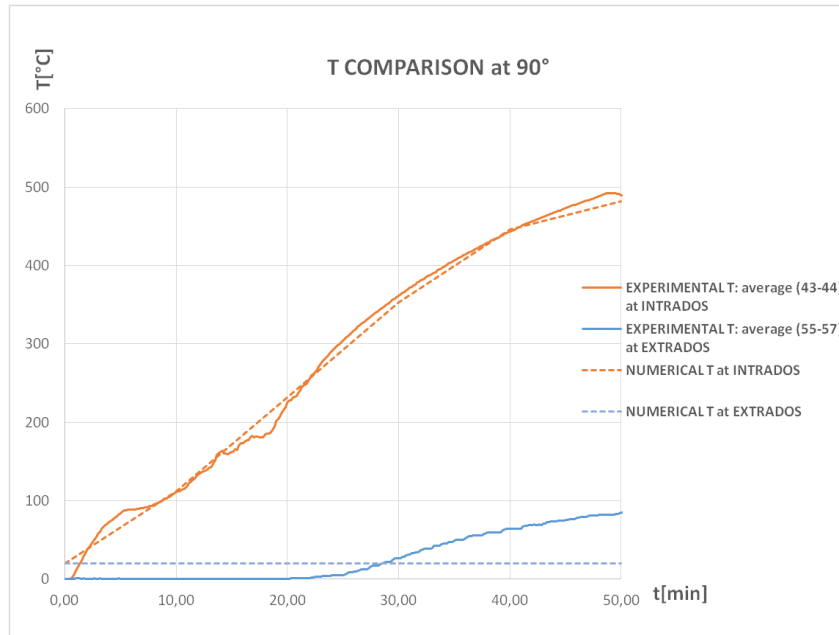


Figure 79 - Temperatures comparison at keystone.

Temperatures described by the numerical model fit very tightly experimental records at the intrados (orange lines). However they are almost never on the safe side since temperatures assumed by the code are often slightly lower than experimental results. It can be observed that, numerical model measures the absolute temperature at intrados and extrados, while experimental records describe the increment in temperature. In fact as the oven is switched on, temperature is 0°C, not the room temperature, 13°C. However this discrepancy

between actual and experimental temperatures can be neglected considering the order of magnitude of temperatures reached during the test. Hence the initial gap between temperatures on extrados is only graphical while, starting from the minute 30, the difference starts to be higher. This is due to the fact that model response is slower compared to the real heat transfer.

2. Validation at  $\pm 70^\circ$ , considering TMC 47-48 and 49-50. Experimental temperatures profiles at middle line are described in clay units and mortar respectively. Numerical values at 60 mm are considered (attachment 2).

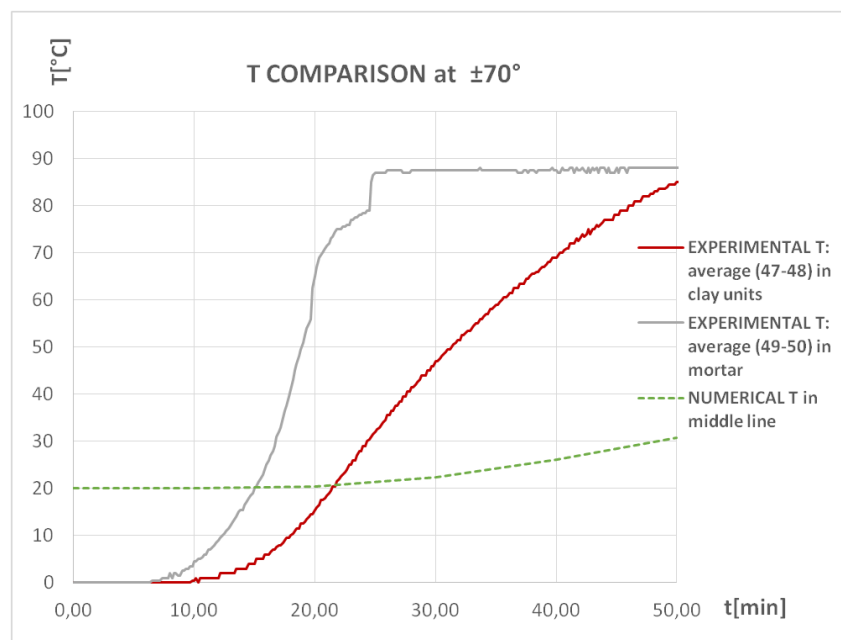


Figure 80 - Temperatures comparison at arch axis.

It is clear that numerical model does not describe properly temperatures changing within the cross section, neither the heterogeneity of the material. Model estimates quite correctly the instant at which temperature starts changing, however the increment should be faster: average values recorded in clay units and in mortar can be adopted to describe the global behaviour. Also this comparison shows the slower estimation of heat transfer speed.

3. Validation at  $\pm 55^\circ$ , considering TMC 41-42-45-46 (intrados) and 51-52-53-54 (extrados). Same observations referred to Picture 79 apply.

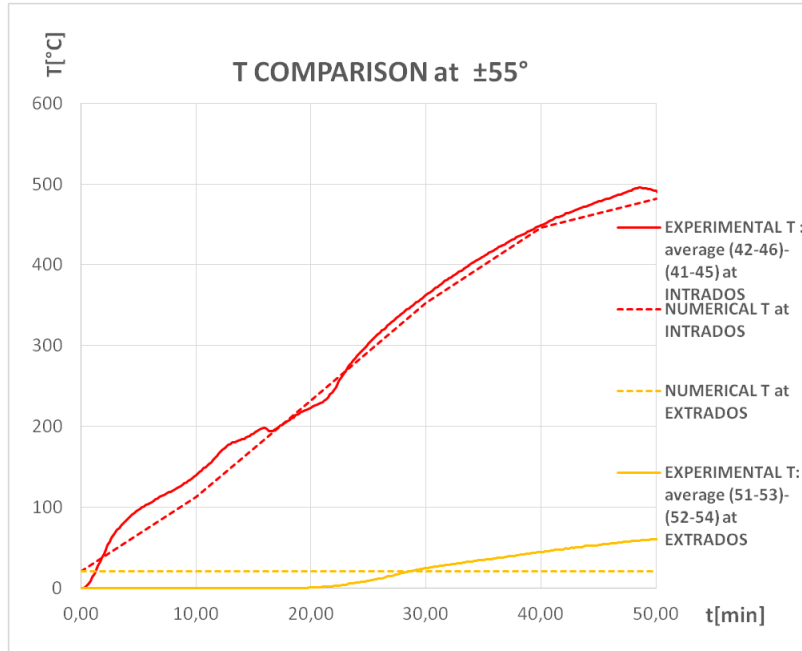


Figure 81 - Temperatures comparison near springings.

In conclusion it can be stated that some hypothesis assumed in the implementation of the numerical model meet experimental observations. In fact both at the keystone and at reins, intrados and extrados, numerical trends fit experimental results. The hypothesis to adopt constant thermal map along the arch axis z is consistent with the reality too. On the other hand the heat transfer within the arch thickness described by the numerical model shows a great delay. Therefore numerical temperatures can be considered reliable at intrados and extrados, while they should be considered carefully at middle line.

## *Chapter 6*

# *Conclusions*

---

It is possible to summarize most important steps about the process of analysis and validation and most significant results achieved. This paper studies the calibration of the numerical model FireArm by means of experimental tests carried out on arches in fire conditions, cast on site at Vigili del Fuoco laboratory in Roma Capannelle, precisely at “Laboratorio di Resistenza al Fuoco dell’Area di Protezione Passiva della Direzione Centrale per la Prevenzione e la Sicurezza Tecnica (DCPST)” .

This work starts from the analysis and the study of the assumptions and results previously stated in “Archi in muratura soggetti a elevati gradienti termici” written by Nicholas Sergio Burello, where two experimental tests described have been carried out at room temperature and applying concentrated vertical loads in fire conditions.

This paper offers new results which can be added to the outputs already available. The aim is to know strengths and weaknesses of the numerical model in order to understand which conditions it is actually able to describe. Where great differences between numerical and experimental results are shown, the goal is to improve the code, making this gap as small as possible.

Two tests performed in fire conditions and applying distributed vertical loads on the arch extrados are studied. Experimental results are commented and the arch is assessed in REI terms, no collapse is reached during both tests, therefore all requirements are satisfied. Since loadings applied on the arch during tests 1 and 2 are different, different displacements are expected. In practice this is not the results obtained: the arch behavior is almost the same, the voussoir at the keystone cracks changing the static configuration of the structure. This result can be explained considering that the strength of the material is not affected by the increment of load applied at the extrados. Maybe by increasing a lot vertical mechanical load a different behavior could be achieved, leading to lower displacements.

Model outputs are studied by means of the following procedure. Several parameters have been tested during the validation process: the influence of the tensile strength of the masonry, the importance of constitutive laws and thermal strain-temperature relationship used, the role of the Young Modulus of the material, the time step set in the numerical code.

Initial inputs set are referred to Italian and European Rules. It is verified that Young modulus of the order of magnitude of 10,000 MPa do not allow the model to reach the convergence. However it has been observed that by increasing maxima thermal strains and decreasing the Young Modulus the numerical model reach the convergence for higher number of loading increments. However strength parameters set should be as closer as possible to real ones, therefore constitutive laws are modified.

Some suggestions in literature are given by Sassu at al., who describe a linear elastic relationship between stresses and strains without any plastic branch; and Heyman, who

suggests a constitutive law which is indefinitely elastic therefore the yield strength cannot be reached, both in compression and in tension. By using constitutive laws proposed by Heyman better results in terms of displacements are achieved, although gap between experimental and numerical outputs remains quite important.

By setting smaller time steps, as one minute or less, the model reach the convergence for higher number of loading increments since less iterations are required to adjust the result in narrow time steps.

In this contest tensile strength set plays a secondary role, it quite affects results but the great part is governed by constitutive laws and thermal strains-temperature relationship.

In conclusion it has been verified that model is not able to describe behavior shown by the arch during the experimental tests. In fact the new static configuration grown as a consequence of high temperatures applied at intrados and low stabilizing effects at extrados, prevents the model to reach the convergence and this situation remains hard to describe numerically. However this validation procedure leads to the detection of conditions for which numerical outputs can be considered reliable and laws which are able to better describe experimental results.

# *References*

---

- [1] UNI EN 1996-1-2: “Eurocode 6: *Design of masonry structures - Part 1-2: General Rules – Structural fire design*”, 2005.
- [2] G. Guglielmini C. Pisoni, *Elementi di trasmissione del calore*, 2004.
- [3] Consiglio Superiore dei Lavori Pubblici, *Norme Tecniche per le Costruzioni; Parte 3.6 Azioni eccezionali (3.6.1.2, 3.6.1.3, 3.6.1.5)*, Italia, 2018.
- [4] Consiglio Superiore dei Lavori Pubblici, *Norme Tecniche per le Costruzioni; Parte 11.10.3.1.1 Determinazione sperimentale della resistenza a compressione*, Italia, 2008.
- [5] A2C Consulenza Tecnica Specialistica, *Le curve di incendio per le verifiche strutturali*, 2015. [Online] <http://www.a2c.it/News-Antincendio/le-curve-di-incendio-per-le-verifiche-strutturali.html>
- [6] Servizi di progettazione, protezione incendi, [Online]: [http://www.dding.it/prevenzione\\_incendi.htm](http://www.dding.it/prevenzione_incendi.htm)
- [7] [Online] [https://en.wikipedia.org/wiki/Heat\\_transfer](https://en.wikipedia.org/wiki/Heat_transfer)
- [8] UNI EN 1363-1:2012 “Fire resistance tests – Part 1: general requirements”.
- [9] [Online] <http://www.poroton.it/news/ntc-2018-resistenza-meccanica-murature.aspx>
- [10] [Online] [https://www.fassabotolo.it/documents/10179/536414/FASSA\\_STE\\_IT\\_MM-30\\_2019-09.pdf/987bf994-2058-49fd-a221-20ae662d66e9](https://www.fassabotolo.it/documents/10179/536414/FASSA_STE_IT_MM-30_2019-09.pdf/987bf994-2058-49fd-a221-20ae662d66e9)

- [11] [Online] <https://globepanels.com/difference-between-reaction-resistance-to-fire-euroclassand-rei-ei/>
- [12] Nicholas Sergio Burello Tesi di Laurea Magistrale in Ingegneria Edile, *Archi in muratura soggetti a elevati gradienti termici*. Politecnico di Torino, 2018
- [13] Fantilli, A.P.; *Relazione gara Proof of Concept*, Politecnico di Torino, 2020.
- [14] Ministero dell'interno, Dipartimento dei Vigili del Fuoco, del Soccorso Pubblico e della Difesa Civile, Direzione Centrale per la Prevenzione e la Sicurezza Tecnica – Area Protezione Passiva – Settore Resistenza al Fuoco, *Prova di resistenza al fuoco su una volta a botte in muratura*; Italia, 2015
- [15] Zavanella V.; Leti E.; Veggetti P.; *Progettazione, costruzioni e impianti per costruzioni, ambiente e territorio*, 2012. [Online]: [https://online.scuola.zanichelli.it/cannarozzozavanella-files/Costruzioni/Approfondimenti/Zanichelli\\_Costruzioni\\_UnitaL3\\_Par6.pdf](https://online.scuola.zanichelli.it/cannarozzozavanella-files/Costruzioni/Approfondimenti/Zanichelli_Costruzioni_UnitaL3_Par6.pdf)
- [16] Andreini, M.; De Falco, A.; Sassu, M.; *Stress-strain curves for masonry materials exposed to fire actions*. Fire Safety Journal, 2014.
- [17] [Online] Energy methods in structural analysis, <https://nptel.ac.in/content/storage2/courses/105105109/pdf/m115.pdf>
- [18] Carpinteri A.; *Scienza delle Costruzioni, volume II*. Ingegneria strutturale, 1995.

# *List of Figures*

Figure 1 - Nominal and natural (real) fire curves.....	15
Figure 2 - Figure 0.1: Design procedures. (Source Eurocode 6, part 1-2 pag 8).....	17
Figure 3 - Temperature in function of time, thickness and units type. (Source Eurocode 6, part 1-2, p 68).....	19
Figure 4 - Areas of masonry element divided in function of temperature profile. (Source Eurocode 6, part 1-2, annex C p66). .....	19
Figure 5 - Temperature distribution in different areas. (Source Eurocode 6, part 1-2, annex C, p67).....	20
Figure 6 - Normalized parameters on respective room temperature values for temperatures from 0°C to 1200°C. (Source Eurocode 6, part 1-2, p73).....	21
Figure 7 - Thermal strains (on the left) and stress-strain constitutive laws (on the right) in function of temperature for clay units with a normalized compressive strength range 12-20 N/mm <sup>2</sup> , gross dry density 900-1200 kg/m <sup>3</sup> (Source Eurocode 6, part 1-2, p76).....	22
Figure 8 - Fire development stages in time-temperature graph: ignition, growth stage, fully developed, decay.....	25
Figure 9 - Heat release rate (HRR) during fire development stages.....	25
Figure 10 - Actual and considered heat transfer.....	27
Figure 11 - Euler forward method example. Points involved in the calculation of temperature in point (i+1, j): temperatures at the previous instant in nearest fibers. ....	27
Figure 12 - Thermal map T(t,x) of six fibers of a generic cross section. ....	29

Figure 13 - Constitutive laws as a function of temperature. Gross dry density range 900-1200 kg/m <sup>3</sup> (clay units) is considered. (Source: Nicholas Sergio Burello master thesis, 2018, p79).....	31
Figure 14 - Peak and maximum strains, pre-peak and post-peak Young Modula as functions of temperature (Source: Nicholas Sergio Burello master thesis, 2018).....	32
Figure 15 - Reference system. One-dimensional model. ....	33
Figure 16 - Temperature distribution at the beginning of the fire and some instants later. .	34
Figure 17 - Qualitative representation of temperature, strains and stresses. ....	34
Figure 18 - Segmental arch geometry. ....	37
Figure 19 - Three hinges collapse mechanism due to dead loads. ....	38
Figure 20 - Resultants on semi-arch. ....	38
Figure 21 - Arch and oven section. ....	41
Figure 22 - Arch built for experimental test 1. Photo has been taken on the ceiling of the oven. ....	42
Figure 23 - Thermocouples devices. Device on the left collects data at the outer surface, on the right at the inner surfaces (median axis and intrados).....	44
Figure 24 - Devices positioning (1). ....	44
Figure 25 - Devices positioning (2). ....	45
Figure 26 - Cross and plan views of thermocouples and extensometers positioning. ....	46
Figure 27 - Model of test 1. ....	47
Figure 28 - Top, lateral, bottom views of arch and confinement for filler material and thermal insulation.....	48
Figure 29 - Model of test 2. ....	49

Figure 30 - Samples tested. ....	52
Figure 31 - Compressive test apparatus (DCPST laboratory). ....	52
Figure 32 - Characteristic value according to Gaussian distribution. ....	56
Figure 33 - Comparison between design and experimental temperature curves in time. ....	59
Figure 34 - Absolute difference between design and experimental temperature curves in time.....	60
Figure 35 - Acceptance criterion of temperatures applied during test 1A. ....	60
Figure 36 - Thermal devices positioning and definition. Blue devices are at intrados, black ones at extrados.....	62
Figure 37 - Thermocouples positioning at 55°, 70°, 90°. (Relazione Poc 2019, Fantilli). ..	62
Figure 38 - Experimental temperatures at intrados.....	63
Figure 39 - Experimental temperatures at extrados. ....	63
Figure 40 - Experimental temperatures at cross sections midline. ....	64
Figure 41 - Average temperatures recorded at intrados and extrados.....	65
Figure 42 - Extensometers positioning and definition. ....	66
Figure 43 - Extensometers records.....	67
Figure 44 - Experimental and numerical displacements directions. ....	69
Figure 45 - Crack at crown. ....	70
Figure 46 - Ignition of supporting structure. ....	70
Figure 47 - Temperatures recorded at intrados during test 1B. ....	71
Figure 48 - Temperatures recorded at middle line during test 1B. ....	72
Figure 49 - Temperatures recorded at extrados during test 1B. ....	72
Figure 50 - Experimental displacements at 90°, test 1B. ....	73

Figure 51 - Experimental displacements at 70°, test 1B. ....	73
Figure 52 - Experimental displacements at 55°, test 1B. ....	74
Figure 53 - Temperatures at intrados, test 2. ....	75
Figure 54 - Temperatures at extrados, test 2. ....	76
Figure 55 – Temperatures at middle line, test 2. ....	76
Figure 56 - Experimental displacements at 90°, test 2.....	77
Figure 57 - Experimental displacements at 70°, test 2.....	78
Figure 58 – Experimental displacements, test 2. ....	78
Figure 59 - Displacements comparison at 55°.....	80
Figure 60 - Displacements comparison at 70°.....	80
Figure 61 - Displacements comparison at 90°.....	81
Figure 62 - "N" points discretization, function of input data. ....	86
Figure 63 - Imposed displacements at constraints. ....	86
Figure 64 - Thermal map example till minute 50, test 1A (attachment 2). ....	87
Figure 65 - Eurocode 6 constitutive laws. ....	89
Figure 66 - Eurocode 6 thermal strain-temperature graph. ....	90
Figure 67 - Numerical results assuming relationships suggested by Eurocode 6.....	91
Figure 68 - Thermal strains - temperatures graphs related to data in table 16. ....	92
Figure 69 – Numerical results assuming alternative thermal strains – temperature graphs. ....	93
Figure 70 - Sassu et al. constitutive laws. ....	94
Figure 71 - Numerical results assuming Sassu at al. constitutive law, by changing tensile strength. ....	95

Figure 72 - Numerical results assuming Sassu et al. constitutive law, by changing tensile strength (2).....	96
Figure 73 - New static scheme after the failure at the crown. ....	97
Figure 74 - Principle of virtual works applied to cantilever semi arch subject to constant thermal variation along transversal cross section and longitudinal axis. .....	99
Figure 75 - Principle of virtual works applied to cantilever semi-arch subject to linear thermal variation along transversal cross section and longitudinal axis. ....	100
Figure 76 - Coefficient of thermal expansion in time. ....	101
Figure 77 - Coefficient of thermal expansion comparison. ....	102
Figure 78 - Numerical results compared to test 2 outputs.....	103
Figure 79 - Temperatures comparison at keystone. ....	104
Figure 80 - Temperatures comparison at arch axis. ....	105
Figure 81 - Temperatures comparison near springings. ....	106

# *List of Tables*

Table 1 - Performance levels of buildings in fire. ....	15
Table 2 - Part of Table N.B.1.2 Minimum thickness of loadbearing partition walls (criteria REI) for fire resistance classification. (Source Eurocode 6, part 1-2, annex B, p32).....	18
Table 3 - Values of temperatures linked to a change of performance under fire for clay masonry blocks and constant c obtained from stress strain tests at high temperatures. (Source Eurocode 6, part 1-2, p67). ....	20
Table 4 - Summary of hypothesis adopted in the numerical procedure.....	39
Table 5 - Solid units clay technical data.....	42
Table 6 - High strength cement mortar technical data. ....	42
Table 7 - Compressive tests results.....	54
Table 8 - Masonry compressive strength. ....	54
Table 9 - Compressive strength values for masonry of solid units and 5-15 mm lime plaster joints thickness.....	55
Table 10 - Partial coefficient for masonry.....	55
Table 11 - Graphic computation of k(3) by means of third order polynomial regression. ..	56
Table 12 - Summary of masonry mechanical parameters. ....	57
Table 13 - Displacement speed in test 1B. ....	74
Table 14 - Displacement speed in test 2.....	79
Table 15 - Input data. ....	85
Table 16 - Part of attachment 1, test 1A, function of input data.....	86

Table 17 - Thermal strains - temperatures laws according to Eurocode 6 and two possible alternatives.....	92
Table 18 - Average records of thermocouples at crown. ....	97
Table 19 - Constant and linear temperature variations. .....	98
Table 20 - Adjusted thermal variations. ....	98
Table 21 - Coefficient of thermal expansion computation. ....	101
Table 22 - Coefficient of thermal expansion in thermal strains-temperatures graphs. ....	102



# Attachments

Geometria arco	Geometria dei conci			Carichi impliciti		Carichi esplicativi
	ascisse dei punti	ordinate dei punti	altezza della sezione	lambda imp	mu imp	concentrati verticali
Num. Conci	Z (mm)	Y(mm)	H(mm)	(1/mm)	(1/mm)	(N)
0	0,00	0,00	120,00	0,00	0,00	0,00
1	14,58	15,69	120,00	0,00	0,00	0,00
2	29,37	31,17	120,00	0,00	0,00	0,00
3	44,38	46,44	120,00	0,00	0,00	0,00
4	59,60	61,51	120,00	0,00	0,00	0,00
5	75,02	76,37	120,00	0,00	0,00	0,00
6	90,64	91,01	120,00	0,00	0,00	0,00
7	106,47	105,43	120,00	0,00	0,00	0,00
8	122,50	119,64	120,00	0,00	0,00	0,00
9	138,72	133,62	120,00	0,00	0,00	0,00
10	155,13	147,38	120,00	0,00	0,00	0,00
11	171,73	160,90	120,00	0,00	0,00	0,00
12	188,51	174,20	120,00	0,00	0,00	0,00
13	205,48	187,27	120,00	0,00	0,00	0,00
14	222,63	200,10	120,00	0,00	0,00	0,00
15	239,95	212,69	120,00	0,00	0,00	0,00
16	257,44	225,04	120,00	0,00	0,00	0,00
17	275,11	237,14	120,00	0,00	0,00	0,00
18	292,93	249,01	120,00	0,00	0,00	0,00
19	310,93	260,62	120,00	0,00	0,00	0,00
20	329,08	271,98	120,00	0,00	0,00	0,00
21	347,38	283,10	120,00	0,00	0,00	0,00
22	365,84	293,96	120,00	0,00	0,00	0,00
23	384,44	304,56	120,00	0,00	0,00	0,00
24	403,19	314,91	120,00	0,00	0,00	0,00
25	422,08	324,99	120,00	0,00	0,00	0,00
26	441,11	334,81	120,00	0,00	0,00	0,00
27	460,27	344,37	120,00	0,00	0,00	0,00
28	479,56	353,67	120,00	0,00	0,00	0,00
29	498,98	362,69	120,00	0,00	0,00	0,00
30	518,53	371,45	120,00	0,00	0,00	0,00
31	538,19	379,94	120,00	0,00	0,00	0,00
32	557,96	388,15	120,00	0,00	0,00	0,00
33	577,85	396,09	120,00	0,00	0,00	0,00
34	597,85	403,75	120,00	0,00	0,00	0,00
35	617,95	411,14	120,00	0,00	0,00	0,00
36	638,15	418,25	120,00	0,00	0,00	0,00
37	658,44	425,08	120,00	0,00	0,00	0,00
38	678,83	431,63	120,00	0,00	0,00	0,00
39	699,31	437,89	120,00	0,00	0,00	0,00
40	719,87	443,88	120,00	0,00	0,00	0,00
41	740,51	449,57	120,00	0,00	0,00	0,00
42	761,23	454,99	120,00	0,00	0,00	0,00
43	782,02	460,11	120,00	0,00	0,00	0,00
44	802,88	464,95	120,00	0,00	0,00	0,00
45	823,81	469,50	120,00	0,00	0,00	0,00
46	844,79	473,76	120,00	0,00	0,00	0,00
47	865,84	477,73	120,00	0,00	0,00	0,00
48	886,93	481,41	120,00	0,00	0,00	0,00
49	908,08	484,79	120,00	0,00	0,00	0,00
50	929,27	487,89	120,00	0,00	0,00	0,00

51	950,50	490,69	120,00	0,00	0,00	0,00
52	971,76	493,19	120,00	0,00	0,00	0,00
53	993,06	495,41	120,00	0,00	0,00	0,00
54	1.014,39	497,32	120,00	0,00	0,00	0,00
55	1.035,75	498,95	120,00	0,00	0,00	0,00
56	1.057,12	500,28	120,00	0,00	0,00	0,00
57	1.078,51	501,31	120,00	0,00	0,00	0,00
58	1.099,91	502,05	120,00	0,00	0,00	0,00
59	1.121,32	502,49	120,00	0,00	0,00	0,00
60	1.142,73	502,64	120,00	0,00	0,00	0,00
61	1.164,15	502,49	120,00	0,00	0,00	0,00
62	1.185,56	502,04	120,00	0,00	0,00	0,00
63	1.206,96	501,30	120,00	0,00	0,00	0,00
64	1.228,35	500,26	120,00	0,00	0,00	0,00
65	1.249,72	498,93	120,00	0,00	0,00	0,00
66	1.271,07	497,30	120,00	0,00	0,00	0,00
67	1.292,40	495,38	120,00	0,00	0,00	0,00
68	1.313,70	493,16	120,00	0,00	0,00	0,00
69	1.334,96	490,65	120,00	0,00	0,00	0,00
70	1.356,19	487,85	120,00	0,00	0,00	0,00
71	1.377,38	484,75	120,00	0,00	0,00	0,00
72	1.398,53	481,36	120,00	0,00	0,00	0,00
73	1.419,62	477,68	120,00	0,00	0,00	0,00
74	1.440,67	473,71	120,00	0,00	0,00	0,00
75	1.461,65	469,44	120,00	0,00	0,00	0,00
76	1.482,58	464,89	120,00	0,00	0,00	0,00
77	1.503,44	460,05	120,00	0,00	0,00	0,00
78	1.524,23	454,92	120,00	0,00	0,00	0,00
79	1.544,94	449,50	120,00	0,00	0,00	0,00
80	1.565,59	443,80	120,00	0,00	0,00	0,00
81	1.586,15	437,82	120,00	0,00	0,00	0,00
82	1.606,62	431,55	120,00	0,00	0,00	0,00
83	1.627,01	425,00	120,00	0,00	0,00	0,00
84	1.647,30	418,16	120,00	0,00	0,00	0,00
85	1.667,50	411,05	120,00	0,00	0,00	0,00
86	1.687,60	403,66	120,00	0,00	0,00	0,00
87	1.707,60	395,99	120,00	0,00	0,00	0,00
88	1.727,48	388,05	120,00	0,00	0,00	0,00
89	1.747,26	379,83	120,00	0,00	0,00	0,00
90	1.766,92	371,34	120,00	0,00	0,00	0,00
91	1.786,46	362,58	120,00	0,00	0,00	0,00
92	1.805,87	353,55	120,00	0,00	0,00	0,00
93	1.825,16	344,25	120,00	0,00	0,00	0,00
94	1.844,33	334,69	120,00	0,00	0,00	0,00
95	1.863,35	324,86	120,00	0,00	0,00	0,00
96	1.882,24	314,78	120,00	0,00	0,00	0,00
97	1.900,99	304,43	120,00	0,00	0,00	0,00
98	1.919,59	293,82	120,00	0,00	0,00	0,00
99	1.938,05	282,96	120,00	0,00	0,00	0,00
100	1.956,35	271,84	120,00	0,00	0,00	0,00
101	1.974,50	260,47	120,00	0,00	0,00	0,00
102	1.992,49	248,86	120,00	0,00	0,00	0,00
103	2.010,31	236,99	120,00	0,00	0,00	0,00
104	2.027,97	224,88	120,00	0,00	0,00	0,00
105	2.045,47	212,53	120,00	0,00	0,00	0,00
106	2.062,78	199,93	120,00	0,00	0,00	0,00
107	2.079,93	187,10	120,00	0,00	0,00	0,00
108	2.096,89	174,04	120,00	0,00	0,00	0,00
109	2.113,68	160,74	120,00	0,00	0,00	0,00
110	2.130,27	147,20	120,00	0,00	0,00	0,00

111	2.146,68	133,45	120,00	0,00	0,00	0,00
112	2.162,90	119,46	120,00	0,00	0,00	0,00
113	2.178,92	105,25	120,00	0,00	0,00	0,00
114	2.194,75	90,83	120,00	0,00	0,00	0,00
115	2.210,37	76,18	120,00	0,00	0,00	0,00
116	2.225,79	61,32	120,00	0,00	0,00	0,00
117	2.241,01	46,25	120,00	0,00	0,00	0,00
118	2.256,01	30,97	120,00	0,00	0,00	0,00
119	2.270,80	15,49	120,00	0,00	0,00	0,00
120	2.285,38	-0,20	120,00	0,00	0,00	0,00

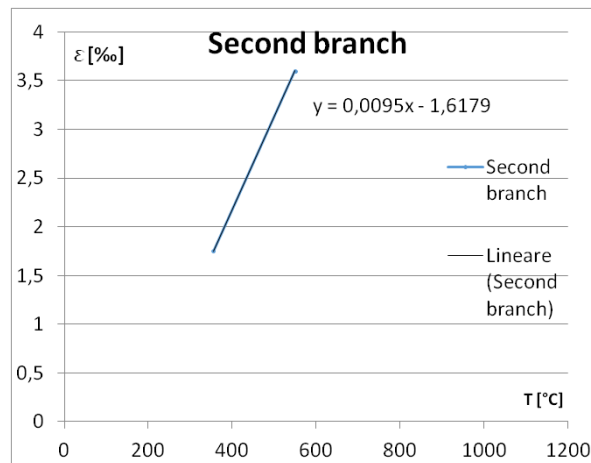
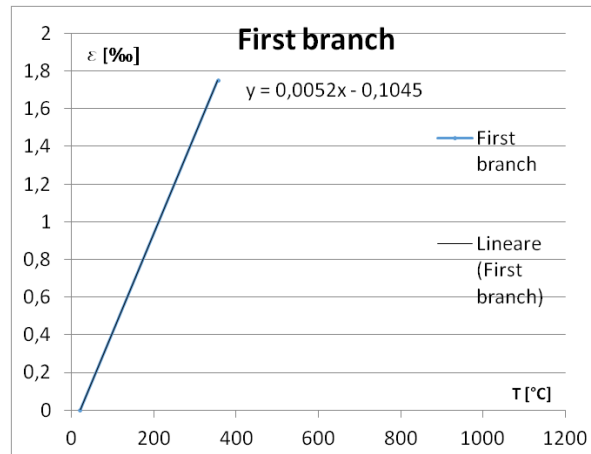
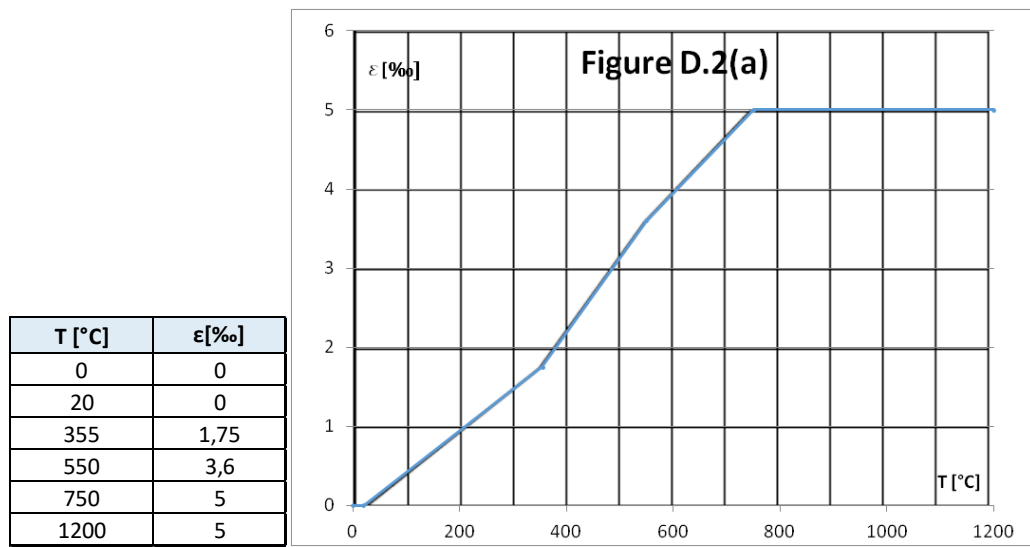
Attachment 1.

	0	10	20	30	40	50	60
0,00	20,00	112,52	231,57	352,86	446,38	482,15	430,16
0,60	20,00	101,27	195,53	316,02	411,65	453,27	411,91
1,20	20,00	98,15	160,75	279,89	377,30	424,42	393,18
1,80	20,00	95,05	131,42	244,51	343,38	395,63	374,02
2,40	20,00	91,97	112,65	209,93	309,95	366,95	354,48
3,00	20,00	88,93	103,77	176,18	277,03	338,42	334,61
3,60	20,00	85,92	100,31	145,25	244,69	310,09	314,47
4,20	20,00	82,95	98,51	121,83	212,97	282,02	294,12
4,80	20,00	80,02	96,72	108,48	181,91	254,24	273,62
5,40	20,00	77,13	94,93	102,47	152,66	226,82	253,03
6,00	20,00	74,30	93,15	100,13	128,57	199,80	232,39
6,60	20,00	71,51	91,37	98,69	112,82	173,24	211,79
7,20	20,00	68,78	89,60	97,26	104,69	148,49	191,28
7,80	20,00	66,12	87,84	95,82	101,08	127,93	171,01
8,40	20,00	63,52	86,09	94,40	99,80	113,72	151,59
9,00	20,00	60,99	84,35	92,97	98,53	105,69	134,13
9,60	20,00	58,54	82,62	91,55	97,26	101,80	120,09
10,20	20,00	56,16	80,90	90,14	95,99	100,09	110,37
10,80	20,00	53,87	79,19	88,73	94,74	98,98	104,58
11,40	20,00	51,66	77,49	87,32	93,49	97,87	101,54
12,00	20,00	49,54	75,80	85,92	92,24	96,76	100,08
12,60	20,00	47,51	74,14	84,53	91,01	95,65	99,06
13,20	20,00	45,57	72,48	83,14	89,77	94,54	98,05
13,80	20,00	43,73	70,84	81,77	88,55	93,44	97,04
14,40	20,00	41,98	69,22	80,40	87,33	92,34	96,03
15,00	20,00	40,32	67,62	79,03	86,12	91,24	95,02
15,60	20,00	38,75	66,04	77,68	84,91	90,15	94,01
16,20	20,00	37,28	64,47	76,34	83,71	89,06	93,01
16,80	20,00	35,90	62,93	75,00	82,52	87,97	92,01
17,40	20,00	34,60	61,41	73,68	81,33	86,88	91,01
18,00	20,00	33,39	59,91	72,36	80,15	85,80	90,01
18,60	20,00	32,26	58,43	71,06	78,98	84,73	89,02
19,20	20,00	31,21	56,98	69,77	77,82	83,66	88,03
19,80	20,00	30,24	55,56	68,49	76,66	82,59	87,04
20,40	20,00	29,34	54,16	67,22	75,51	81,53	86,05
21,00	20,00	28,50	52,79	65,97	74,37	80,47	85,07
21,60	20,00	27,74	51,44	64,73	73,23	79,42	84,09
22,20	20,00	27,03	50,13	63,50	72,11	78,38	83,12
22,80	20,00	26,38	48,84	62,28	70,99	77,34	82,15
23,40	20,00	25,79	47,58	61,08	69,88	76,30	81,18
24,00	20,00	25,25	46,36	59,90	68,78	75,27	80,22
24,60	20,00	24,75	45,16	58,73	67,69	74,25	79,27
25,20	20,00	24,30	44,00	57,58	66,61	73,24	78,31
25,80	20,00	23,89	42,86	56,44	65,54	72,23	77,37
26,40	20,00	23,51	41,76	55,32	64,47	71,23	76,42
27,00	20,00	23,17	40,70	54,21	63,42	70,23	75,49
27,60	20,00	22,86	39,66	53,12	62,38	69,25	74,55
28,20	20,00	22,58	38,66	52,05	61,35	68,27	73,63
28,80	20,00	22,32	37,69	51,00	60,33	67,29	72,71
29,40	20,00	22,09	36,76	49,96	59,32	66,33	71,79
30,00	20,00	21,88	35,86	48,95	58,32	65,37	70,88
30,60	20,00	21,69	34,99	47,95	57,33	64,42	69,98
31,20	20,00	21,52	34,16	46,97	56,36	63,48	69,08
31,80	20,00	21,36	33,36	46,01	55,40	62,55	68,19
32,40	20,00	21,22	32,59	45,07	54,45	61,63	67,30
33,00	20,00	21,09	31,86	44,15	53,51	60,71	66,42
33,60	20,00	20,98	31,15	43,25	52,58	59,81	65,55
34,20	20,00	20,87	30,48	42,37	51,67	58,91	64,68
34,80	20,00	20,78	29,84	41,51	50,77	58,03	63,82
35,40	20,00	20,70	29,23	40,66	49,89	57,15	62,97
36,00	20,00	20,62	28,65	39,85	49,01	56,28	62,13
36,60	20,00	20,55	28,10	39,05	48,16	55,42	61,29
37,20	20,00	20,49	27,58	38,27	47,31	54,57	60,46
37,80	20,00	20,44	27,09	37,51	46,48	53,73	59,63
38,40	20,00	20,39	26,62	36,77	45,66	52,90	58,82
39,00	20,00	20,35	26,18	36,06	44,86	52,09	58,01
39,60	20,00	20,31	25,76	35,36	44,08	51,28	57,21
40,20	20,00	20,27	25,37	34,69	43,30	50,48	56,42
40,80	20,00	20,24	25,00	34,04	42,55	49,70	55,63

41,40	20,00	20,21	24,65	33,40	41,80	48,92	54,86
42,00	20,00	20,19	24,32	32,79	41,08	48,16	54,09
42,60	20,00	20,17	24,02	32,20	40,37	47,40	53,33
43,20	20,00	20,15	23,73	31,63	39,67	46,66	52,58
43,80	20,00	20,13	23,46	31,08	38,99	45,93	51,84
44,40	20,00	20,11	23,21	30,55	38,32	45,21	51,10
45,00	20,00	20,10	22,98	30,03	37,67	44,50	50,38
45,60	20,00	20,09	22,76	29,54	37,03	43,81	49,66
46,20	20,00	20,08	22,55	29,07	36,41	43,12	48,96
46,80	20,00	20,07	22,36	28,61	35,81	42,45	48,26
47,40	20,00	20,06	22,18	28,17	35,22	41,79	47,57
48,00	20,00	20,05	22,02	27,75	34,65	41,14	46,89
48,60	20,00	20,04	21,86	27,35	34,09	40,51	46,22
49,20	20,00	20,04	21,72	26,96	33,54	39,88	45,56
49,80	20,00	20,03	21,59	26,60	33,01	39,27	44,91
50,40	20,00	20,03	21,46	26,24	32,50	38,67	44,27
51,00	20,00	20,03	21,35	25,91	32,00	38,08	43,64
51,60	20,00	20,02	21,24	25,59	31,52	37,51	43,02
52,20	20,00	20,02	21,14	25,28	31,05	36,95	42,41
52,80	20,00	20,02	21,05	24,99	30,59	36,39	41,81
53,40	20,00	20,01	20,96	24,71	30,15	35,86	41,22
54,00	20,00	20,01	20,88	24,45	29,72	35,33	40,63
54,60	20,00	20,01	20,81	24,19	29,31	34,81	40,06
55,20	20,00	20,01	20,74	23,96	28,91	34,31	39,50
55,80	20,00	20,01	20,68	23,73	28,53	33,82	38,95
56,40	20,00	20,01	20,62	23,51	28,15	33,34	38,41
57,00	20,00	20,01	20,57	23,31	27,79	32,88	37,88
57,60	20,00	20,01	20,52	23,11	27,45	32,42	37,36
58,20	20,00	20,00	20,48	22,93	27,11	31,98	36,85
58,80	20,00	20,00	20,44	22,76	26,79	31,55	36,35
59,40	20,00	20,00	20,40	22,59	26,48	31,13	35,86
60,00	20,00	20,00	20,36	22,43	26,18	30,72	35,38
60,60	20,00	20,00	20,33	22,29	25,90	30,33	34,91
61,20	20,00	20,00	20,30	22,15	25,62	29,94	34,45
61,80	20,00	20,00	20,28	22,01	25,36	29,57	34,00
62,40	20,00	20,00	20,25	21,89	25,10	29,20	33,56
63,00	20,00	20,00	20,23	21,77	24,86	28,85	33,13
63,60	20,00	20,00	20,21	21,66	24,63	28,51	32,71
64,20	20,00	20,00	20,19	21,56	24,40	28,18	32,30
64,80	20,00	20,00	20,17	21,46	24,19	27,86	31,90
65,40	20,00	20,00	20,16	21,36	23,98	27,55	31,51
66,00	20,00	20,00	20,14	21,28	23,79	27,24	31,13
66,60	20,00	20,00	20,13	21,19	23,60	26,95	30,75
67,20	20,00	20,00	20,12	21,11	23,42	26,67	30,39
67,80	20,00	20,00	20,11	21,04	23,25	26,40	30,04
68,40	20,00	20,00	20,10	20,97	23,09	26,14	29,69
69,00	20,00	20,00	20,09	20,91	22,93	25,88	29,36
69,60	20,00	20,00	20,08	20,85	22,78	25,64	29,03
70,20	20,00	20,00	20,07	20,79	22,64	25,40	28,72
70,80	20,00	20,00	20,06	20,74	22,50	25,18	28,41
71,40	20,00	20,00	20,06	20,69	22,37	24,96	28,11
72,00	20,00	20,00	20,05	20,64	22,25	24,74	27,82
72,60	20,00	20,00	20,05	20,59	22,13	24,54	27,54
73,20	20,00	20,00	20,04	20,55	22,01	24,35	27,26
73,80	20,00	20,00	20,04	20,51	21,91	24,16	27,00
74,40	20,00	20,00	20,03	20,48	21,80	23,98	26,74
75,00	20,00	20,00	20,03	20,44	21,71	23,80	26,49
75,60	20,00	20,00	20,03	20,41	21,61	23,63	26,25
76,20	20,00	20,00	20,02	20,38	21,53	23,47	26,01
76,80	20,00	20,00	20,02	20,36	21,44	23,32	25,78
77,40	20,00	20,00	20,02	20,33	21,36	23,17	25,56
78,00	20,00	20,00	20,02	20,31	21,29	23,03	25,35
78,60	20,00	20,00	20,02	20,28	21,22	22,89	25,15
79,20	20,00	20,00	20,01	20,26	21,15	22,76	24,95
79,80	20,00	20,00	20,01	20,24	21,08	22,63	24,75
80,40	20,00	20,00	20,01	20,23	21,02	22,51	24,57

81,00	20,00	20,00	20,01	20,21	20,96	22,39	24,39
81,60	20,00	20,00	20,01	20,19	20,91	22,28	24,21
82,20	20,00	20,00	20,01	20,18	20,85	22,17	24,05
82,80	20,00	20,00	20,01	20,16	20,81	22,07	23,88
83,40	20,00	20,00	20,01	20,15	20,76	21,97	23,73
84,00	20,00	20,00	20,01	20,14	20,71	21,88	23,58
84,60	20,00	20,00	20,01	20,13	20,67	21,79	23,43
85,20	20,00	20,00	20,00	20,12	20,63	21,70	23,29
85,80	20,00	20,00	20,00	20,11	20,59	21,62	23,16
86,40	20,00	20,00	20,00	20,10	20,56	21,54	23,03
87,00	20,00	20,00	20,00	20,09	20,52	21,47	22,90
87,60	20,00	20,00	20,00	20,09	20,49	21,39	22,78
88,20	20,00	20,00	20,00	20,08	20,46	21,32	22,66
88,80	20,00	20,00	20,00	20,07	20,43	21,26	22,55
89,40	20,00	20,00	20,00	20,07	20,41	21,20	22,44
90,00	20,00	20,00	20,00	20,06	20,38	21,14	22,34
90,60	20,00	20,00	20,00	20,06	20,36	21,08	22,24
91,20	20,00	20,00	20,00	20,05	20,34	21,02	22,14
91,80	20,00	20,00	20,00	20,05	20,32	20,97	22,05
92,40	20,00	20,00	20,00	20,04	20,30	20,92	21,96
93,00	20,00	20,00	20,00	20,04	20,28	20,87	21,87
93,60	20,00	20,00	20,00	20,04	20,26	20,83	21,79
94,20	20,00	20,00	20,00	20,03	20,24	20,78	21,71
94,80	20,00	20,00	20,00	20,03	20,23	20,74	21,63
95,40	20,00	20,00	20,00	20,03	20,21	20,70	21,56
96,00	20,00	20,00	20,00	20,03	20,20	20,67	21,48
96,60	20,00	20,00	20,00	20,02	20,19	20,63	21,42
97,20	20,00	20,00	20,00	20,02	20,17	20,60	21,35
97,80	20,00	20,00	20,00	20,02	20,16	20,56	21,29
98,40	20,00	20,00	20,00	20,02	20,15	20,53	21,23
99,00	20,00	20,00	20,00	20,02	20,14	20,50	21,17
99,60	20,00	20,00	20,00	20,02	20,13	20,48	21,11
100,20	20,00	20,00	20,00	20,01	20,12	20,45	21,06
100,80	20,00	20,00	20,00	20,01	20,11	20,42	21,01
101,40	20,00	20,00	20,00	20,01	20,11	20,40	20,96
102,00	20,00	20,00	20,00	20,01	20,10	20,38	20,91
102,60	20,00	20,00	20,00	20,01	20,09	20,35	20,86
103,20	20,00	20,00	20,00	20,01	20,09	20,33	20,82
103,80	20,00	20,00	20,00	20,01	20,08	20,31	20,77
104,40	20,00	20,00	20,00	20,01	20,07	20,30	20,73
105,00	20,00	20,00	20,00	20,01	20,07	20,28	20,69
105,60	20,00	20,00	20,00	20,01	20,06	20,26	20,65
106,20	20,00	20,00	20,00	20,01	20,06	20,24	20,62
106,80	20,00	20,00	20,00	20,00	20,05	20,23	20,58
107,40	20,00	20,00	20,00	20,00	20,05	20,21	20,55
108,00	20,00	20,00	20,00	20,00	20,05	20,20	20,51
108,60	20,00	20,00	20,00	20,00	20,04	20,19	20,48
109,20	20,00	20,00	20,00	20,00	20,04	20,17	20,45
109,80	20,00	20,00	20,00	20,00	20,04	20,16	20,42
110,40	20,00	20,00	20,00	20,00	20,03	20,15	20,39
111,00	20,00	20,00	20,00	20,00	20,03	20,14	20,36
111,60	20,00	20,00	20,00	20,00	20,03	20,13	20,33
112,20	20,00	20,00	20,00	20,00	20,03	20,11	20,31
112,80	20,00	20,00	20,00	20,00	20,02	20,10	20,28
113,40	20,00	20,00	20,00	20,00	20,02	20,09	20,26
114,00	20,00	20,00	20,00	20,00	20,02	20,08	20,23
114,60	20,00	20,00	20,00	20,00	20,02	20,08	20,21
115,20	20,00	20,00	20,00	20,00	20,01	20,07	20,18
115,80	20,00	20,00	20,00	20,00	20,01	20,06	20,16
116,40	20,00	20,00	20,00	20,00	20,01	20,05	20,13
117,00	20,00	20,00	20,00	20,00	20,01	20,04	20,11
117,60	20,00	20,00	20,00	20,00	20,01	20,03	20,09
118,20	20,00	20,00	20,00	20,00	20,01	20,02	20,07
118,80	20,00	20,00	20,00	20,00	20,00	20,02	20,04
119,40	20,00	20,00	20,00	20,00	20,00	20,01	20,02
120,00	20,00	20,00	20,00	20,00	20,00	20,00	20,00

#### Attachment 2.



Attachment 3.

*	NUMERICAL DISPLACEMENT	z [mm]	0	1	2	3	4	5	6	7	8	9	10	11	12	13	14	15
	0	0	0	0	0	0	0	0	0	0	0	0	0	0	0	0	0	
1	14,57869	0,000175	0,000151	0,000124	8,98E-05	3,97E-05	-2,3E-05	-0,00011	-0,00023	-0,00037	-0,00053	-0,00064	-0,00073	-0,00079	-0,00085	-0,00091	-0,00096	
2	29,37269	0,000558	0,000498	0,000396	0,000288	0,000126	-6,1E-05	-0,00029	-0,00058	-0,00094	-0,00133	-0,00163	-0,00184	-0,00201	-0,00216	-0,00223	-0,00243	
3	44,37917	0,001011	0,00087	0,000719	0,000528	0,000229	-7,9E-05	-0,00037	-0,00073	-0,00115	-0,00163	-0,00198	-0,00224	-0,00244	-0,00262	-0,00279	-0,00295	
4	59,59527	0,001528	0,001316	0,001089	0,000804	0,000345	-7,6E-05	-0,00035	-0,00065	-0,001	-0,00139	-0,00168	-0,0019	-0,00206	-0,00221	-0,00235	-0,00248	
5	75,01809	0,002106	0,001814	0,001501	0,00112	0,000473	-4,8E-05	-0,00022	-0,00034	-0,00046	-0,00058	-0,00069	-0,00079	-0,00084	-0,0009	-0,00094	-0,00099	
6	90,64467	0,002739	0,002368	0,001952	0,00147	0,00061	5,37E-06	2,36E-05	0,00022	0,000486	0,000799	0,001008	0,001131	0,001254	0,001363	0,00147	0,001569	
7	106,472	0,003423	0,002948	0,002437	0,001805	0,000752	8,71E-05	0,000393	0,001042	0,001854	0,002789	0,003449	0,003883	0,004259	0,004597	0,004917	0,005227	
8	122,4972	0,004152	0,003574	0,002952	0,002183	0,000898	0,0002	0,000893	0,002135	0,003662	0,005407	0,006655	0,007495	0,008201	0,008838	0,009436	0,010021	
9	138,717	0,004923	0,004234	0,003492	0,002575	0,001044	0,000345	0,00153	0,003511	0,005925	0,008677	0,010655	0,011998	0,013112	0,014118	0,015061	0,015986	
10	155,1285	0,005729	0,004922	0,004054	0,002979	0,001188	0,000526	0,002313	0,005182	0,008661	0,012619	0,015472	0,01742	0,019021	0,02047	0,021825	0,023158	
11	171,7284	0,006565	0,005634	0,004632	0,00339	0,001329	0,000744	0,003247	0,00716	0,011887	0,017258	0,021133	0,023787	0,025957	0,027924	0,029761	0,03157	
12	188,5137	0,007427	0,006366	0,005223	0,003805	0,001463	0,001004	0,00434	0,009456	0,01562	0,022613	0,027662	0,03127	0,033949	0,036508	0,038898	0,041256	
13	205,481	0,008311	0,007113	0,005823	0,004219	0,001589	0,001308	0,005599	0,012083	0,019875	0,028707	0,035082	0,039463	0,043021	0,046251	0,049265	0,052244	
14	222,6273	0,00929	0,00787	0,006427	0,004631	0,001706	0,001659	0,007033	0,015051	0,024668	0,035585	0,043415	0,04882	0,053197	0,057174	0,060885	0,064557	
15	239,9491	0,01012	0,008633	0,007031	0,005035	0,001812	0,00206	0,008646	0,018371	0,030014	0,043186	0,05268	0,059206	0,06326	0,066898	0,070672	0,074801	
16	257,4432	0,011038	0,009398	0,007633	0,00543	0,001905	0,002514	0,01044	0,020555	0,035926	0,051601	0,060021	0,065725	0,068691	0,071379	0,074553	0,078317	
55	17	275,1063	0,011958	0,010162	0,008228	0,005811	0,001986	0,003027	0,012444	0,026111	0,041458	0,055218	0,06112	0,06509	0,066389	0,067576	0,069581	0,072461
18	292,9349	0,012876	0,010919	0,008813	0,006177	0,002052	0,0036	0,014642	0,029787	0,042374	0,051947	0,053769	0,054745	0,053736	0,052848	0,053118	0,054498	
19	310,9257	0,013784	0,011668	0,009388	0,006528	0,002105	0,004237	0,017045	0,029631	0,037153	0,039421	0,035844	0,032894	0,029085	0,025631	0,023366	0,022467	
20	329,0753	0,014693	0,012405	0,009941	0,006852	0,002143	0,004943	0,017965	0,02506	0,024138	0,01664	0,006628	0,00089	-0,00792	-0,01429	-0,01957	-0,02382	
21	347,3801	0,015585	0,013126	0,010479	0,007157	0,002167	0,005721	0,016039	0,016462	0,020926	-0,01602	-0,03299	-0,04528	-0,05569	-0,06518	-0,07388	-0,08205	
22	365,8367	0,01646	0,013829	0,010997	0,007438	0,002178	0,006574	0,010881	-0,00154	-0,0253	-0,0565	-0,08063	-0,09779	-0,11177	-0,12455	-0,13659	-0,14858	
23	384,4416	0,017317	0,014512	0,011491	0,007693	0,002176	0,006749	0,01932	-0,02256	-0,0584	-0,1017	-0,13331	-0,15559	-0,17332	-0,18959	-0,20508	-0,22088	
24	403,1912	0,018153	0,015171	0,011961	0,007922	0,002162	0,005316	-0,01043	-0,04665	-0,09494	-0,15026	-0,18946	-0,21661	-0,23794	-0,25751	-0,27639	-0,29576	
25	422,0819	0,018965	0,015806	0,012405	0,008123	0,002138	0,002234	-0,02517	-0,07309	-0,13196	-0,19816	-0,24409	-0,27568	-0,30053	-0,32341	-0,34545	-0,36807	
26	441,1102	0,019751	0,016144	0,012822	0,008295	0,002106	-0,0276	-0,04177	-0,09947	-0,16559	-0,24153	-0,29396	-0,33015	-0,35868	-0,38494	-0,41005	-0,4356	
27	460,2723	0,020501	0,016995	0,013211	0,008438	0,002066	-0,00938	-0,0582	-0,12328	-0,19882	-0,28334	-0,34219	-0,38278	-0,41472	-0,44414	-0,47223	-0,50082	
28	479,5647	0,021239	0,017546	0,01357	0,008553	0,002021	-0,01705	-0,07365	-0,1462	-0,23053	-0,32442	-0,38956	-0,43445	-0,46972	-0,50223	-0,53234	-0,56481	
70	29	498,9837	0,021937	0,018067	0,013901	0,008639	0,001971	-0,02506	-0,08826	-0,16874	-0,26168	-0,36474	-0,43603	-0,48513	-0,52365	-0,55916	-0,59304	-0,62752
30	518,5254	0,022604	0,018558	0,014201	0,008696	0,00158	-0,03326	-0,10265	-0,19088	-0,29223	-0,40426	-0,48155	-0,53475	-0,57644	-0,6149	-0,65157	-0,6889	
31	538,1863	0,023239	0,019017	0,014472	0,008726	0,002084	-0,0406	-0,11679	-0,2126	-0,32216	-0,44294	-0,52608	-0,58327	-0,62806	-0,66938	-0,70787	-0,74888	
32	557,9626	0,023841	0,019446	0,014714	0,008729	0,002034	-0,04783	-0,13067	-0,23387	-0,35143	-0,48073	-0,56957	-0,63065	-0,67845	-0,72256	-0,76461	-0,80741	
33	577,8505	0,02441	0,019843	0,014927	0,008706	0,002019	-0,05495	-0,14427	-0,25467	-0,38002	-0,51761	-0,61197	-0,67683	-0,72756	-0,77438	-0,81901	-0,86443	
34	597,8461	0,024945	0,020201	0,015112	0,008658	0,00375	-0,06194	-0,15758	-0,27497	-0,40788	-0,55352	-0,65326	-0,72178	-0,77535	-0,8248	-0,87193	-0,9199	
35	617,9457	0,025447	0,020547	0,01527	0,008587	0,003568	-0,06879	-0,17056	-0,29474	-0,43499	-0,58844	-0,69338	-0,76545	-0,82176	-0,87376	-0,92331	-0,97376	
36	638,1455	0,025917	0,020854	0,015402	0,008495	0,00376	-0,07548	-0,18321	-0,31397	-0,46132	-0,62232	-0,73229	-0,80779	-0,86676	-0,92122	-0,97312	-1,02596	
37	658,4416	0,026354	0,021132	0,01551	0,008383	0,003941	-0,08202	-0,1955	-0,33262	-0,46864	-0,65513	-0,76995	-0,84876	-0,9103	-0,96714	-1,0213	-1,07644	
38	678,83	0,02676	0,021383	0,015594	0,008253	0,00312	-0,08838	-0,20743	-0,35068	-0,51151	-0,68684	-0,80633	-0,88833	-0,95233	-1,01146	-1,0678	-1,12517	
39	699,307	0,027135	0,021608	0,015656	0,008108	0,01295	-0,09456	-0,21896	-0,36812	-0,53532	-0,7174	-0,84138	-0,92644	-0,99282	-1,05414	-1,11258	-1,17208	
40	719,8686	0,027481	0,021807	0,015699	0,007949	0,01467	-0,10054	-0,23009	-0,38491	-0,55822	-0,74679	-0,87057	-0,96307	-1,03171	-1,09515	-1,15559	-1,21715	
41	740,5109	0,027798	0,021983	0,015723	0,007778	0,01635	-0,1063	-0,24079	-0,40410	-0,58019	-0,77497	-0,90736	-0,99816	-1,06898	-1,13443	-1,19679	-1,26031	
42	761,2299	0,028087	0,022137	0,015731	0,007598	0,01798	-0,11185	-0,25106	-0,41649	-0,60122	-0,80191	-0,93823	-1,0317	-1,10458	-1,17195	-1,23615	-1,30154	
43	782,0217	0,02835	0,022277	0,015724	0,007411	0,01956	-0,11717	-0,26087	-0,43123	-0,62126	-0,82758	-0,96762	-1,06363	-1,13848	-1,20767	-1,27361	-1,34078	
44	802,8824	0,028589	0,022384	0,015705	0,00722	0,02108	-0,12225	-0,27021	-0,44524	-0,6403	-0,85195	-0,99552	-1,09394	-1,17065	-1,24156	-1,30915	-1,37801	
45	823,8079	0,028804	0,022481	0,015675	0,007027	0,02254	-0,12708	-0,27906	-0,45851	-0,65831	-0,875	-1,02189	-1,12527	-1,20104	-1,27358	-1,34273	-1,41317	
46	844,7942	0,028997	0,022563	0,015636	0,006833	0,02393	-0,13164	-0,28742	-0,47101	-0,67572	-0,89669	-1,0467	-1,14951	-1,22962	-1,3037	-1,37432	-1,44624	
47	865,8374	0,029169	0,022623	0,015159	0,00535	0,03319	-0,16112	-0,34089	-0,55069	-0,78309	-0,9349	-1,06993	-1,17472	-1,25637	-1,33188	-1,40385	-1,47718	
48	886,9334	0,029322	0,022685	0,015536	0,006455	0,02649	-0,13995	-0,30257	-0,49365	-0,67056	-0,9359	-1,09154	-1,19819	-1,28126	-1,35809	-1,43133	-1,50596	
49	908,0782	0,029458	0,022729	0,015485	0,006275	0,02766	-0,14368	-0										

	71	1377,383	0,029499	0,022763	0,01551	0,006289	-0,02765	-0,14371	-0,3094	-0,50384	-0,71977	-0,95356	-1,11174	-1,22012	-1,3045	-1,38258	-1,457	-1,53284
	72	1398,528	0,029368	0,022722	0,015566	0,006471	-0,02649	-0,13998	-0,30263	-0,49374	-0,70609	-0,9361	-1,09178	-1,19846	-1,28153	-1,35838	-1,43163	-1,50628
	73	1419,623	0,029218	0,02267	0,015619	0,006659	-0,02524	-0,13597	-0,29532	-0,48283	-0,69131	-0,91722	-1,07018	-1,17502	-1,25666	-1,33219	-1,40417	-1,47752
	74	1440,665	0,029049	0,022605	0,015667	0,006851	-0,02392	-0,13167	-0,28748	-0,47111	-0,67543	-0,89692	-1,04698	-1,14983	-1,22993	-1,30403	-1,37464	-1,4466
	75	1461,651	0,02886	0,022527	0,015708	0,007046	-0,02253	-0,12711	-0,27913	-0,45862	-0,65848	-0,87525	-1,02218	-1,12291	-1,20137	-1,27394	-1,34309	-1,41356
	76	1482,576	0,028649	0,022433	0,015741	0,007241	-0,02107	-0,12228	-0,27028	-0,44536	-0,64048	-0,85223	-0,99583	-1,0943	-1,171	-1,24195	-1,30954	-1,37842
	77	1503,436	0,028414	0,022321	0,015762	0,007433	-0,01954	-0,11721	-0,26095	-0,43135	-0,62145	-0,82787	-0,96795	-1,06402	-1,13886	-1,20808	-1,27403	-1,34123
	78	1524,226	0,028154	0,022191	0,015771	0,007621	-0,01796	-0,11189	-0,25114	-0,41662	-0,60141	-0,80222	-0,93858	-1,03211	-1,10499	-1,17239	-1,23659	-1,30201
	79	1544,945	0,027868	0,02204	0,015765	0,007802	-0,01633	-0,10634	-0,24088	-0,40118	-0,58004	-0,77529	-0,90774	-0,9986	-1,06941	-1,13489	-1,19726	-1,26081
	80	1565,586	0,027555	0,021867	0,015743	0,007973	-0,01465	-0,10057	-0,23018	-0,38505	-0,55844	-0,74713	-0,87546	-0,96352	-1,03216	-1,09563	-1,15608	-1,21768
	81	1586,146	0,027213	0,02167	0,015703	0,008134	-0,01293	-0,0946	-0,21905	-0,36827	-0,53555	-0,71776	-0,84179	-0,92697	-0,99329	-1,05465	-1,1131	-1,17264
	82	1606,622	0,026841	0,021448	0,015642	0,00828	-0,01118	-0,08842	-0,20752	-0,35083	-0,51175	-0,68721	-0,80676	-0,88883	-0,95283	-1,012	-1,06835	-1,12575
	83	1627,01	0,026439	0,0212	0,01556	0,008411	-0,00939	-0,08206	-0,1956	-0,33278	-0,48709	-0,65552	-0,7704	-0,84929	-0,91082	-0,9677	-1,02187	-1,07706
	84	1647,304	0,026005	0,020924	0,015455	0,008524	-0,00758	-0,07553	-0,18331	-0,31414	-0,46159	-0,62273	-0,73276	-0,80834	-0,86731	-0,92182	-0,97372	-1,0266
	85	1667,503	0,025539	0,02062	0,015325	0,008618	-0,00575	-0,06883	-0,17067	-0,29492	-0,43527	-0,58887	-0,69387	-0,76602	-0,82233	-0,87438	-0,92394	-0,97443
	86	1687,601	0,02504	0,020286	0,015169	0,00869	-0,00393	-0,06198	-0,15769	-0,27515	-0,40817	-0,55397	-0,65378	-0,72238	-0,77594	-0,82545	-0,87259	-0,9206
	87	1707,596	0,024508	0,019923	0,014986	0,008738	-0,00221	-0,055	-0,14439	-0,25486	-0,38032	-0,51807	-0,61251	-0,67746	-0,72818	-0,77506	-0,8197	-0,86517
	88	1727,482	0,023943	0,019528	0,014775	0,008763	-0,0007	-0,04788	-0,13079	-0,23407	-0,35174	-0,48122	-0,57013	-0,6313	-0,6791	-0,72327	-0,76533	-0,80817
	89	1747,257	0,023345	0,019102	0,014535	0,008761	0,000498	-0,04063	-0,11692	-0,21281	-0,32248	-0,44344	-0,52666	-0,58395	-0,62874	-0,67012	-0,70953	-0,74967
	90	1766,916	0,022714	0,018646	0,014266	0,008733	0,001327	-0,03332	-0,10278	-0,1911	-0,29257	-0,40478	-0,48216	-0,53546	-0,57715	-0,61567	-0,65235	-0,68973
70	91	1786,457	0,02205	0,018158	0,013968	0,008676	0,001807	-0,0259	-0,0884	-0,16896	-0,26202	-0,36528	-0,43667	-0,48586	-0,52438	-0,55996	-0,59385	-0,62839
	92	1805,874	0,021355	0,01764	0,01364	0,008592	0,002033	-0,0183	-0,07379	-0,14643	-0,23089	-0,32498	-0,39022	-0,43522	-0,47049	-0,50306	-0,53409	-0,56571
	93	1825,165	0,02063	0,017092	0,013283	0,008479	0,00208	-0,01123	-0,05898	-0,12352	-0,1992	-0,28392	-0,34287	-0,38358	-0,41551	-0,445	-0,47311	-0,50176
	94	1844,325	0,019875	0,016514	0,012897	0,008337	0,00212	-0,00496	-0,04385	-0,10027	-0,16699	-0,24213	-0,29467	-0,33098	-0,35951	-0,38586	-0,41097	-0,43658
	95	1863,352	0,019093	0,012482	0,018066	0,002153	4,15E-05	-0,02864	-0,07657	-0,13428	-0,19967	-0,24565	-0,27749	-0,30254	-0,32567	-0,34774	-0,37025	
	96	1882,241	0,018285	0,015278	0,012041	0,007967	0,002178	0,003492	-0,01488	-0,0523	-0,1006	-0,15633	-0,19564	-0,22288	-0,24434	-0,26415	-0,28311	-0,3025
	97	1900,989	0,017453	0,014622	0,011573	0,00774	0,002192	0,005372	-0,0307	-0,02946	-0,06679	-0,11172	-0,14419	-0,16688	-0,18486	-0,20142	-0,2172	-0,23326
	98	1919,592	0,0166	0,013943	0,011081	0,007487	0,002194	0,005983	0,006098	-0,00968	-0,03579	-0,06903	-0,09432	-0,11227	-0,12676	-0,1401	-0,15264	-0,16519
	99	1938,046	0,015729	0,013243	0,010567	0,007208	0,00218	0,005566	0,01214	0,006405	-0,00895	-0,03112	-0,0493	-0,06272	-0,07375	-0,0839	-0,0932	-0,10221
	100	1956,349	0,014842	0,012525	0,010032	0,006905	0,00216	0,004793	0,01507	0,017792	0,012393	0,000755	-0,0112	-0,02	-0,02779	-0,03497	-0,04124	-0,04685
	101	1974,497	0,013942	0,011793	0,009479	0,00658	0,002123	0,00409	0,015619	0,024247	0,027105	0,024702	0,018687	0,014019	0,00920	0,004753	0,01367	-0,00106
	102	1992,486	0,013033	0,011048	0,00891	0,006234	0,002071	0,003457	0,014238	0,026196	0,034946	0,039866	0,039018	0,038039	0,035894	0,033889	0,032924	0,030348
55	103	2010,312	0,01212	0,010294	0,008328	0,005871	0,002005	0,002888	0,012047	0,024944	0,036793	0,046684	0,049882	0,051855	0,051926	0,051947	0,052889	0,05468
	104	2027,973	0,011204	0,009534	0,007737	0,005492	0,001925	0,00238	0,010055	0,021338	0,034271	0,046564	0,052527	0,056532	0,058302	0,05986	0,062032	0,064833
	105	2045,465	0,010292	0,008874	0,007139	0,005101	0,001833	0,001929	0,008258	0,017658	0,028926	0,041687	0,049057	0,054052	0,056926	0,059489	0,062381	0,065669
	106	2062,785	0,009386	0,008015	0,006538	0,004699	0,001728	0,001531	0,006648	0,01434	0,023582	0,03406	0,041615	0,046803	0,050242	0,053313	0,056442	0,059779
	107	2079,929	0,008493	0,007262	0,005938	0,004291	0,001612	0,001185	0,00522	0,011375	0,018789	0,027206	0,033278	0,037447	0,040836	0,043914	0,046787	0,049626
	108	2096,894	0,007615	0,006521	0,005343	0,00388	0,001487	0,000885	0,003965	0,008752	0,014534	0,021108	0,025852	0,029102	0,031755	0,034162	0,036409	0,038628
	109	2113,677	0,006758	0,005794	0,004756	0,003469	0,000629	0,002876	0,006459	0,010802	0,015749	0,019316	0,021754	0,023754	0,025565	0,027258	0,028927	
	110	2130,274	0,005927	0,005087	0,004182	0,003061	0,001216	0,000414	0,001946	0,004484	0,007576	0,011106	0,013648	0,015377	0,016806	0,018098	0,019308	0,020498
	111	2146,683	0,005127	0,004404	0,003625	0,002661	0,001073	0,000237	0,001169	0,002816	0,004841	0,00716	0,008824	0,010945	0,011733	0,012529	0,013309	
	112	2162,901	0,004363	0,00375	0,00309	0,002273	0,000929	9,61E-05	0,000536	0,001444	0,002579	0,003888	0,004817	0,005433	0,005963	0,006439	0,006889	0,007326
	113	2178,923	0,00364	0,00313	0,00258	0,0019	0,000786	-1,2E-05	4,12E-05	0,000355	0,000773	0,001267	0,001604	0,001811	0,002009	0,002185	0,002355	0,002516
	114	2194,748	0,002963	0,002547	0,0021	0,001546	0,000646	-9E-05	-0,00032	-0,00046	-0,00059	-0,00073	-0,00084	-0,00095	-0,00101	-0,0011	-0,00111	
	115	2210,372	0,002336	0,002008	0,001655	0,0003126	0,000512	-0,00014	-0,00056	-0,00102	-0,00154	-0,00211	-0,00255	-0,00288	-0,00311	-0,00333	-0,00353	-0,00373
	116	2225,792	0,001765	0,001516	0,001248	0,000913	0,000387	-0,00016	-0,00069	-0,00133	-0,00208	-0,00291	-0,00354	-0,004	-0,00435	-0,00466	-0,00495	-0,00524
	117	2241,006	0,001255	0,001077	0,000885	0,000641	0,000273	-0,00016	-0,00007	-0,0014	-0,00223	-0,00316	-0,00385	-0,00435	-0,00473	-0,00508	-0,0054	-0,00572
	118	2256,01	0,00081	0,000693	0,000568	0,000406	0,000173	-0,00014	-0,00061	-0,00125	-0,00201	-0,00286	-0,0035	-0,00395	-0,00431	-0,00463	-0,00492	-0,00522
	119	2270,801	0,000434	0,000371	0,000303	0,000212	9,06E-05	-9,4E-05	-0,00043	-0,00089</								

# ***Ringraziamenti***

*Desidero ringraziare tutti coloro che hanno contribuito allo svolgimento di questa tesi. In particolare ringrazio il mio relatore, Professore Alessandro Pasquale Fantilli, per la disponibilità e per avermi dato la possibilità di affrontare un argomento interessante e di notevole importanza. Ringrazio l'Ingegnere Nicholas Sergio Burello per la pazienza e l'aiuto fornito durante la stesura dell'elaborato.*

*Ringrazio i Tecnici e tutto il Personale del Corpo Nazionale dei Vigili del Fuoco di Roma Capannelle, Area Protezione Passiva della D.C.P.S.T., senza il loro contributo tutta la parte sperimentale di questa tesi non sarebbe mai stata possibile. In modo particolare ringrazio il Dirigente Vigili del Fuoco Ing. Marcello Lombardini, il Responsabile dell'acquisizione dei dati sperimentali, Claudio Cicchetti e il Responsabile dell'esecuzione delle lavorazioni, Giuseppe Cirasella.*

*Per ultimi, ma non per importanza, ringrazio la mia famiglia e i miei amici per avermi sostenuto durante questo biennio. Un ringraziamento particolare va a mia sorella Claudia, grazie per l'incoraggiamento costante che mi fornisci, i miei traguardi sono dovuti anche a questo.*